Vector Based Control for Power Electronics Dominated AC Power Grid

Haris Bin Ashraf

Thesis submitted to the faculty of the Virginia Polytechnic Institute and State University in partial fulfillment of the requirements for the degree of

Master of Science
In
Electrical Engineering

Richard Zhang (Chair)
Dushan Boroyevich
Boran Fan

December 8th 2023
Arlington, Virginia

Keywords: *Grid Forming Control, Grid Connected Power Converters, Power Electronics based grid, Microgrid*

Vector Based Control for Power Electronics Dominated AC Power Grid

Haris Bin Ashraf

ABSTRACT

The global trend towards electrifying the grid has positioned power electronics at the forefront of modern power systems. To control power electronics in grid-connected applications, Grid Forming (GFM) control has become a focal point of research. GFM control utilizes control laws derived from steady-state relationships in the phasor domain. Although these control methods have historically performed well in traditional power systems dominated by electrical machines, they exhibit unexpected control issues in power electronics-dominant power systems. The root of these unexpected behaviors lies in the foundational assumptions of these control methods (Droop control and Virtual Synchronous Machine) i.e. frequency is considered to be a steady state quantity which is constant within the fundamental line cycle. This thesis critically examines these assumptions and elucidates their potential inapplicability in power electronics-dominated power systems.

This thesis also introduces vectors as an alternative representation of voltages and currents. Unlike phasors, vectors are instantaneous and time-varying representation of electrical quantities at any point in time, defined by three time-varying values: Magnitude, Polar angle, and Azimuthal angle, using the spherical coordinate system. An initial attempt to demonstrate the capability of using these vectors to control the active and reactive power in inverters connected to the grid has also been presented in this thesis. The proposed vector-based control is able to track the commanded power setpoints within a fraction of the fundamental AC voltage cycle.

Vector Based Control for Power Electronics Dominated AC Power Grid

Haris Bin Ashraf

GENERAL AUDIENCE ABSTRACT

As the world moves towards cleaner, greener energy, power electronics have become a key technology in modern electrical grids. One of the main ways to control power converters in grid-connected systems is through a method called Grid Forming (GFM) control. GFM control has been effective in traditional grids with large rotating machines, but it faces unexpected problems in grids that rely more on power electronics. This is because the basic assumptions of GFM control, such as treating frequency as a steady value, do not always hold true in power electronics-driven systems. This thesis explores these issues and proposes a new approach to improve control. Instead of using traditional methods based on steady-state values, it introduces the idea of using vectors to represent electrical quantities like voltage and current. Unlike traditional methods, vectors can describe electrical signals at any moment in time. The thesis demonstrates how this vector-based approach can be used to control important parameters of power converters in the grid, like active and reactive power, in a way that responds quickly and accurately to changes and disturbances. This new method could help make power systems more reliable and efficient as they evolve to incorporate more power electronics.

ACKNOWLEDGEMENTS

I'm very grateful to my advisor Dr. Richard Zhang, who has been an excellent guide throughout my graduate studies. I am lucky to have learned from him a lot on technical storytelling, depth of technical understanding, and critical thinking. This work could not have been done without his support and wise guidance throughout my research. I am also very thankful to my committee members Dr. Dushan Boroyevich and Dr. Boran Fan for their challenging questions and insightful discussions.

I want to express my sincere gratitude to Dr. Igor Cvetkovic, who was my advisor when I initially joined CPES. He provided me with the pathway and opportunity to start my graduate education at Virginia Tech.

I want to thank all faculty, students, and visiting scholars who guided me and worked with me in the lab, especially Dr. Eric Hsieh, Mr. Vladimir Mitrovic, Mr. Arash Nazari, Mr. Xinliang Yang, Mr. Taha Moaz, Mr. Narayan Rajagopal, Mr. Jack Knoll, and Mr. Mark Cairnie. I enjoyed working with them and learned a lot from them. Special thanks to my colleagues, Mr. Jiaxiong Yu, Ms. Shivani Nair, Mr. William Chong, and Mr. Xiaotian, for the long and enlightening group meetings with Dr. Zhang every week. This work could also not have been complete without the support of you all.

Finally, I would like to thank my family – my parents Ashraf Azim and Rizwana Ashraf for supporting me in my decision to pursue graduate education, my siblings Bilal Ashraf, Sana Ashraf, and Samra Ashraf for their valuable care and affection, and finally my wife Bisma Shaikh who has been an exceptional support system for me throughout all my thick and thin moments.

Table of Contents

List of Figures

Chapter 1: Introduction

1.1 Research Motivation and Challenges

The electrical grid, considered in its entirety, is the most complex machine mankind has ever built [1]. It is the greatest engineering achievement of the 20th century, according to the National Academy of Engineering [2]. For more than 140 years, the grid has served as a means to provide electrical energy everywhere – from big urban metropolitan cities, to small rural villages. The abundant availability of electrical energy drastically transformed human civilization, making electricity a commodity in our daily lives.

From a technological standpoint, the revolutionary creation of the grid 140+ years ago was followed by a long period of relatively slow evolution. The fundamental concept has remained the same – rotating machinery is used to generate AC voltage, which is then transmitted and distributed over long distances to provide energy wherever required. However, this fundamental concept is beginning to change as the grid is now undergoing a massive transformation, and power electronics is at the forefront of this transformation [3], [4].

Figure 1: Overview of the transformation of the electrical grid

Figure 1 represents the transformation of the electrical grid [3]. Grid 1.0 represents the first generation of the grid that was the result of a long saga of collaboration and competition among the giants – Thomas Edison, Nikola Tesla, George Westinghouse, and Samuel Insull. Grid 1.0 was primarily based on passive components – rotating machines generated AC voltage at 50/60 Hz, which was used to supply energy to loads such as incandescent bulbs and induction motors), over long distances through transmission lines. Grid 2.0 represents the second generation in which Information Technology (IT) was introduced to the grid. Communication technologies, better computing resources, and sensors were used to monitor and control the existing power flow infrastructure (generation, transmission, consumption). Grid 3.0 represents the third generation in which the power flow infrastructure is also undergoing a massive transformation, due to the pervasive penetration of power electronics-based equipment and systems on the grid. With the

integration of wind turbines and solar farms, HVDC stations, flexible AC transmission system (FACTS) devices, and a variety of small and large industrial loads, the power flow infrastructure can now possess an unprecedented level of intelligence and control bandwidth through power electronics. Together with the overlaid IT infrastructure, grid 3.0 can have embedded intelligence, with power electronics serving as intelligent interfaces between energy sources and loads.

1.1.1 Transformation Towards a Power Electronics based Electrical Grid

The transformation of the grid is driven by several reasons. Some of the most important reasons are listed as follows:

- **GROWTH OF RENEWABLE ENERGY:**

  Energy from renewable sources such as wind, solar, geothermal, etc. is growing due to the imminent threat posed by climate change and global warming. Energy derived from fossil fuels generates a massive carbon footprint and greenhouse gases in the atmosphere of the Earth, that is causing environmental conditions to deteriorate significantly, and it is projected to have further adverse consequences if remedial measures are not undertaken [5]. This has prompted the growth of renewable energy resources [6]. As shown in Figure 2, energy generated from renewables is expected to increase to 45% of the total energy mix of the United States in the next 10 years [7]. Integration of these renewable energy resources in the grid is enabled by power electronics, which acts as an interface between the DC or varying frequency AC produced by renewables, and the fixed frequency AC grid. In the ideal case of 100% renewable energy generation, the grid will need to be established completely by power electronics.

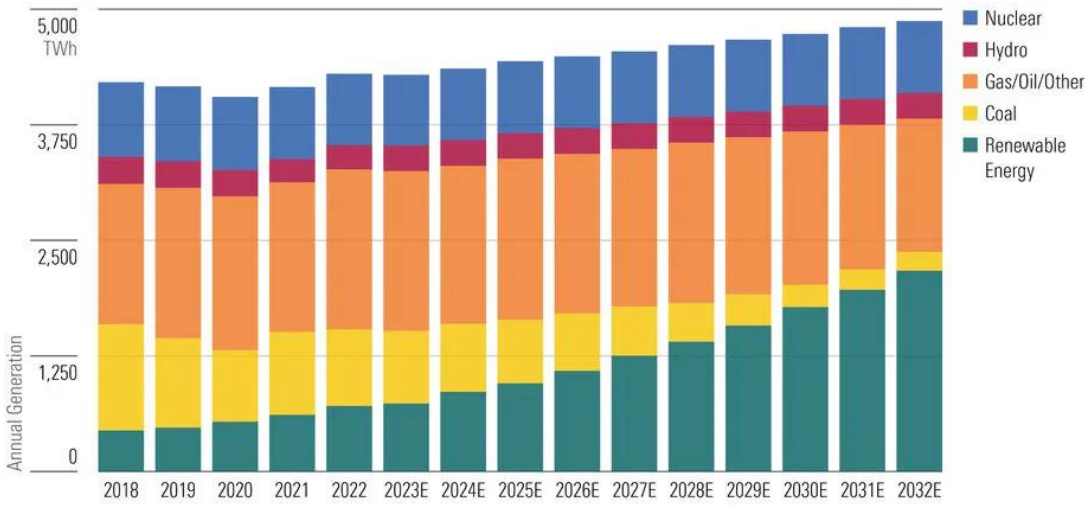

Figure 2: 10-year outlook for power generation sources in the U.S.

- **INTEGRATION OF ENERGY STORAGE:**

  Renewable energy is intermittent in nature, because the amount of solar irradiation and wind velocity varies based on geographical location, weather, time of day, etc. Energy storage is used to account for this intermittency. Therefore, Battery Energy Storage Systems (BESS) are also deployed along with renewable resources. The charging and discharging of BESS, and the power interface between the battery DC and fixed frequency AC grid requires power electronics.

- **DISTRIBUTED POWER SYSTEMS WITH VARIOUS ENERGY RESOURCES:**

  The increase in frequency of extreme weather events has underscored the significance of resiliency in the electrical grid, which leads towards distributed power systems comprising of a variety of energy sources. Historically, the grid has been operating in a centralized fashion – where power generation is physically located far away from the loads. In the face of storms, cyclones, tornadoes, etc., a

large population is impacted as a result of power system blackouts. A recent example of this is the snowstorm in Texas that impacted 4.5 Million homes [8]. Therefore, a more distributed power system with Distributed Energy Resources (DERs) offers a sustainable and long-term solution for resilient operation. Similar to any power system, these DERs can be renewable and/or fossil fuel based. The integration of renewable DERs requires power electronics.

Power electronics serves as the interface between different kinds of energy resources and loads, to provide efficient power conversion and control of energy flow. Therefore, Inverter Based Resources (IBRs) are at the forefront of modern and future power systems. As a result, the penetration of power electronics in the grid is growing higher. Looking into the future, if renewable energy is used to meet 100% energy needs, electrical grids comprised of 100% Power Electronics will be required to establish the grid.

1.1.2 Challenges from high penetration of Power Electronics in the grid

The high penetration of power electronics in the grid gives rise to several challenges [9]. The grid was designed to operate with electrical machines having low control bandwidth and slow dynamics. In contrast, power electronics converters exhibit fast dynamics due to high control bandwidth, and fast switching of the power semiconductor switches. Some of the prominent challenges due to high penetration of power electronics in the grid are listed below:

- When electrical machines and power electronics are operating in the same power system, the difference in their dynamic response may trigger dynamic and transient instability. The fast dynamic behavior of power converters is dictated by the converter's control system, while the slow dynamics of electrical machines are dictated by the physical construction of the machine.

- There is no generic control system and set of operation principles / rules for grid-connected power converters. There are several control schemes in the literature for grid-connected power converters, with each one having different dynamic responses. When these converters operate together in a power system, the different dynamic responses may trigger instability.
- Protection schemes in the grid were designed for electrical machines. Under fault conditions, machines react slowly and are able to supply a large current. In contrast, power converters have lower fault currents, which are unable to trip the circuit breakers designed for the legacy grid. Moreover, protection is designed for unidirectional flow of power from generation to load. However, with the integration of energy storage through power converters, power flow in the system is bidirectional, which is not accounted for in the protection schemes.

1.2 Thesis Outline

The main objectives of this thesis are:

- To articulate the challenges arising from existing control methods of grid-connected power converters.
- To introduce the concept of vector representation of electrical quantities that can be used to design new control schemes for power converters in grid applications.

These objectives are crucial stepping stones towards answering the following grand question:

"How do we establish a grid with 100% Power Electronics?"

This thesis consists of 9 chapters in total. Chapter 1 is an introduction that describes why power electronics is at the forefront of modern power systems and what are the challenges associated with this. Chapter 2 traces the origins of power systems and describes the evolution to explain the past, present, and future of power systems.

Chapter 3 introduces the two most commonly deployed control methods for Grid-connected converters: 'Grid Following (GFL)' and 'Grid Forming (GFM)' control, along with the required framework to establish a 100% power electronics-based grid. Chapter 4 elaborates the state-of-the-art GFM control schemes that are used in scientific literature today. The origins, design example, and working principles are described in detail. Chapter 5 probes into the GFM control schemes to analyze the conditions in which these control laws exhibit unexpected results, thereby underscoring the need to explore a new control method.

Chapter 6 provides insight into why the phasor-based control methods are not suitable to be used in power electronics-based systems. Chapter 7 introduces the vector-based representation as an alternative to phasors. It compares the phasor and vector-based representation to lay the foundation for developing a control method based on rotating vectors. Chapter 8 introduces a method using the vector-based representation to develop a control scheme. As an initial attempt, the control objective is designed to follow a reference power setpoint delivered to the grid by the inverter. The performance of this vector-based control is compared with existing GFM control methods. Simulation results are presented to show that the vector-based control tracks the reference power setpoint within a fraction of the fundamental AC cycle, as opposed to several cycles required by existing GFM control methods to reach steady state.

Finally, Chapter 9 describes the conclusion and future work of this research effort.

Chapter 2: Evolution of Power Systems

2.1 Introduction

The origins of the electrical grid can be traced back to 1882, when the first centralized power generation plant in the US was built at Pearl Street Station to generate electricity and supply energy to customers for lamps [10]. After the success of this initial system architecture configuration, the generation, transmission, and consumption of electrical energy continued to evolve. This chapter explains the evolution of power system architecture, progressing from centralized power generation to distributed. This evolution also entails moving from solely electrical machine-based resources to a combination of machines and power electronics-based resources, due to the integration of multiple energy sources into the grid. This chapter also introduces a real world power system architecture example – the Lanai microgrid. The purpose of this example is to create an equivalent test circuit for evaluating existing and new control schemes for power converters in grid applications.

2.2 Technological Evolution of Power System Architectures

A representation of the evolution of power system architectures is shown in Figure 3. Initially, power systems were comprised of electrical machines as sources. The earliest system architecture of the grid was simply an electrical machine that fed a grid bus serving multiple loads, similar to the Pearl Street Station power generation plant [10]. Due to the increase in electrical energy demand over the years, the system was scaled up. Rotating machines operating in parallel formed the bulk grid bus, transmitting and distributing electrical energy over long distances. This is an example of centralized power generation, because power is generated at one location, and the loads are located at multiple locations. Afterwards, the concept of distributed generation was

introduced to reduce dependence on the bulk grid and provide a backup energy source for loads. In distributed power generation, power is generated at multiple locations and therefore, multiple sources serve the loads. This architecture provides resiliency because power delivery to the loads is not halted if any one of the sources fails.

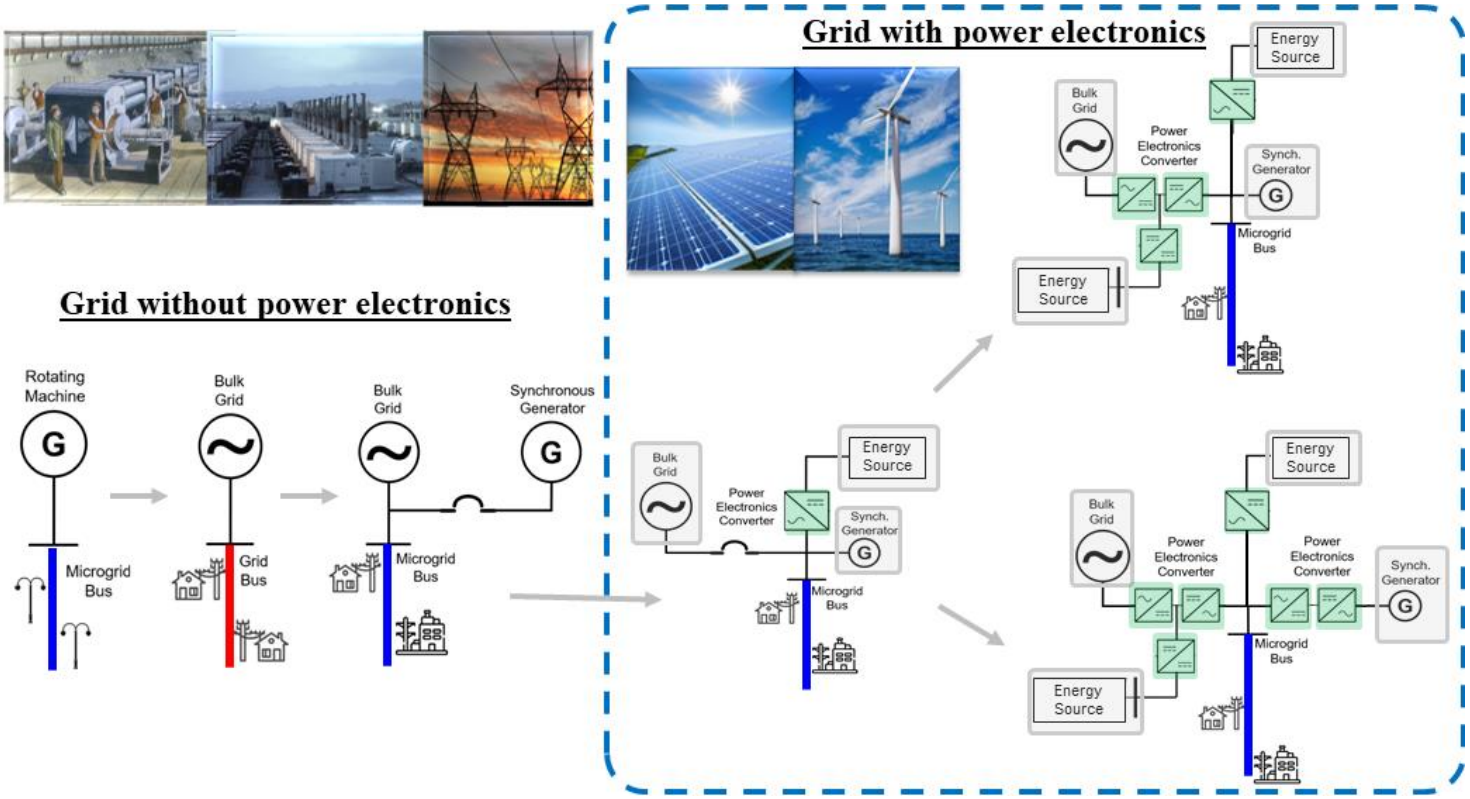

Figure 3: Evolution of the grid system architectures

Figure 3 also shows the grid architecture after the advent of power electronics. Owing to the growth of renewable energy, power converters started becoming a mainstream component of power systems. The penetration of power electronics in the grid started because power converters were required to serve as a power interface between the fixed frequency AC grid, and energy sources with DC and varying frequency AC. The penetration of power electronics in the grid

increased further over the period of time, because of the integration of multiple renewable energy sources. Due to the intermittent nature of renewables, the integration of energy storage was also introduced. As shown in Figure 3, the system architecture evolved to a configuration in which the grid bus is formed by electrical machines and power converters together, due to the integration of multiple energy sources and storage.

In future power system architectures, the penetration of power electronics may increase to an extent that the grid could be formed completely by 100% power electronics. Figure 3 shows such a configuration in which the grid bus is completely formed by power converters, that establish the grid bus by serving as the power interface between several energy sources. However, such a system architecture leads to questions about how exactly the energy flow, establishment of voltage and frequency on the grid bus, dynamic behaviors, and protection can be managed.

2.3 Real World Power System Architecture Example

In order to assess the challenges of current and future power systems, it is important to consider application scenarios in a physical system that is practical enough to be implemented in the real world. The purpose of selecting this real-world power system architecture is to evaluate the challenges of existing power converter control schemes, and validate the proposed vector-based control method for power converters in grid applications This test system should be generic enough to reveal insights from all converter control schemes, while also being simple enough to enable easy understanding and implementation. Therefore, the electrical grid in Lanai island of Hawaii has been selected as the test system. The Lanai grid is actually a remote microgrid. The U.S. Department of Energy defines a microgrid as follows [11]:

"A microgrid is a group of ***interconnected loads*** *and* ***distributed energy resources*** *within clearly defined electrical boundaries that acts as a* ***single controllable entity*** *with respect to the (bulk) grid. A microgrid can connect and disconnect from the grid to enable it to operate in both* ***grid-connected*** *or* ***island-mode****. A* ***remote microgrid*** *is a variation of a microgrid that operates in* ***islanded conditions****."*

The future electrical grid could consist of multiple microgrids physically connected together and functionally interoperable i.e. the energy flow is coordinated among them to serve multiple loads. This concept is known as networked microgrids [12]. This concept also gives rise to the future electronic power distribution system, in which microgrids represent a hierarchical level in the grid. Several microgrids clustered together can form a milligrid, and several milligrids combined together form the grid [13]. In such a hierarchical architecture, power electronics serve as the interface between each level in the electronic power distribution system. Therefore, in order to proceed towards the future electrical grid, it is critical to answer fundamental questions about microgrids – how is the microgrid bus formed, supplied, controlled, and protected? The Lanai microgrid can be used as a test system to evaluate existing and new power converter control schemes as an initial step towards answering these fundamental questions.

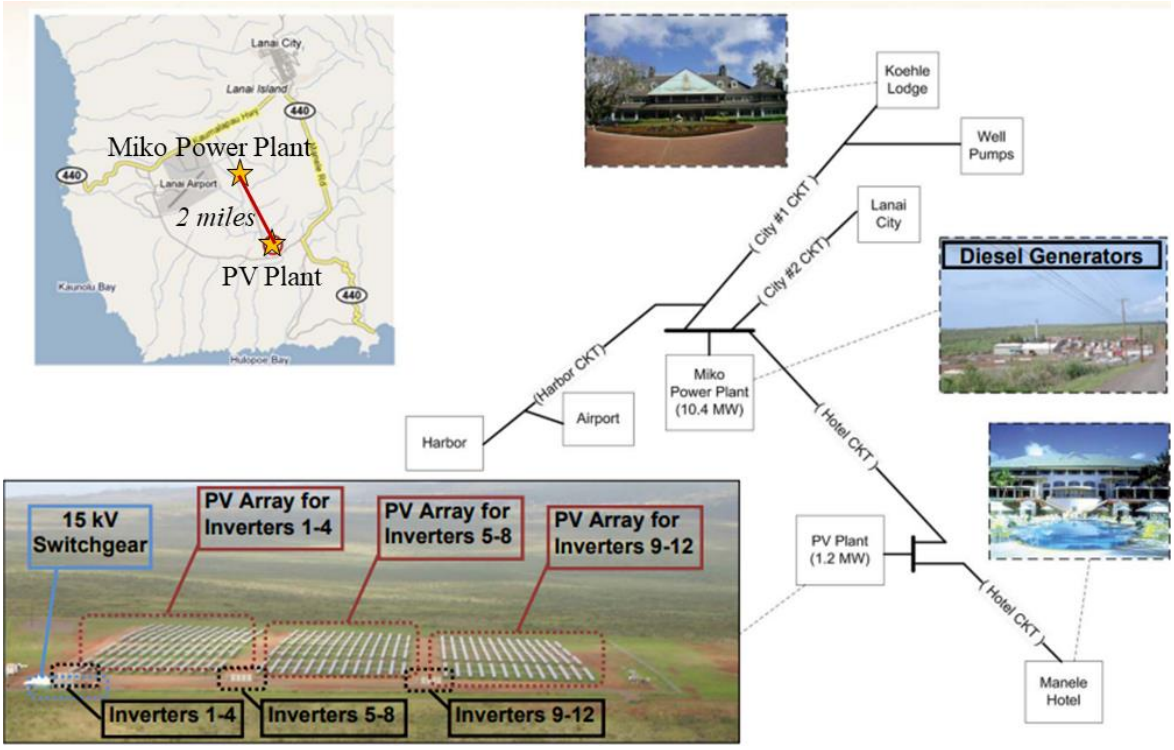

Figure 4: Lanai Grid system architecture

The Lanai grid consists of a central power plant with diesel engine generators having a combined capacity of 10.4 MW, and a PV power plant with a power rating of 1.2 MW [14]. Figure 4 shows the layout, geographical location, and representative system diagram of the Lanai grid. There are also several loads geographically dispersed within the island, as shown in Figure 5 (a). Figure 5 (b) shows the simplified Lanai grid in which both the sources are retained and the load is lumped to one node close to the central power generation plant. As a result of this simplification, the lumped load is effectively in parallel with the central power generation plant. Figure 6 shows the resulting equivalent circuit. v_i and i_i represent the PV inverter voltages and currents, v_g represents the central power plant voltages, the equivalent load is shown as Z_L, and the lumped transmission line resistance and inductance is represented by R and L respectively.

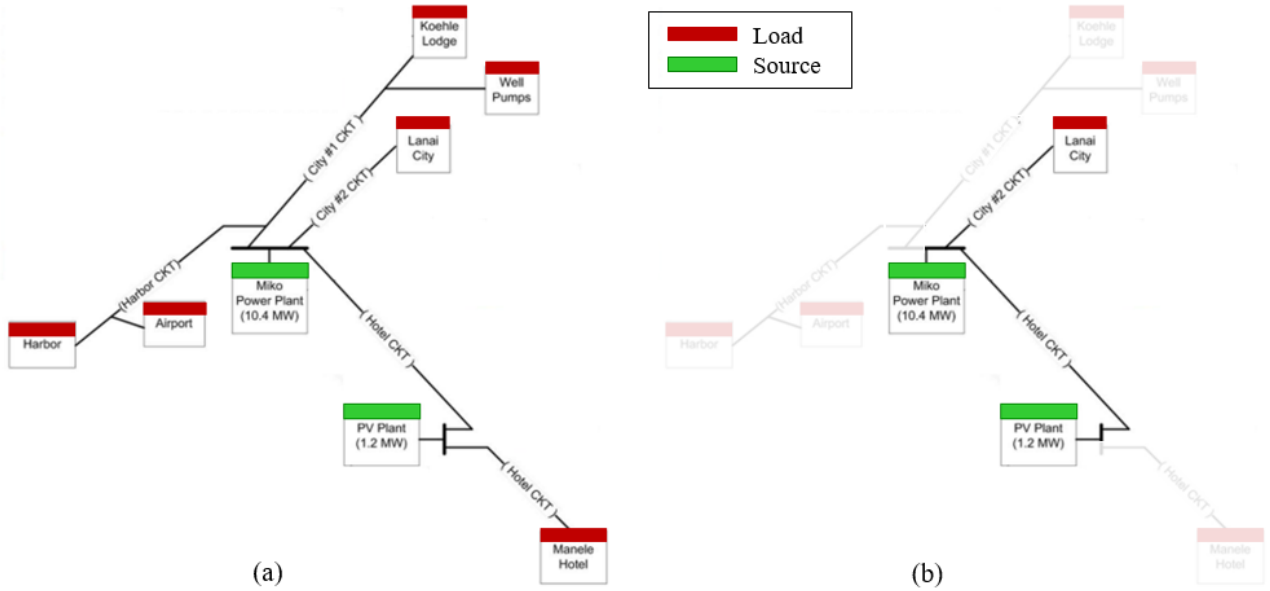

Figure 5: (a) Single Line Diagram of Lanai Grid (b) Single Line Diagram of selected part of Lanai Grid

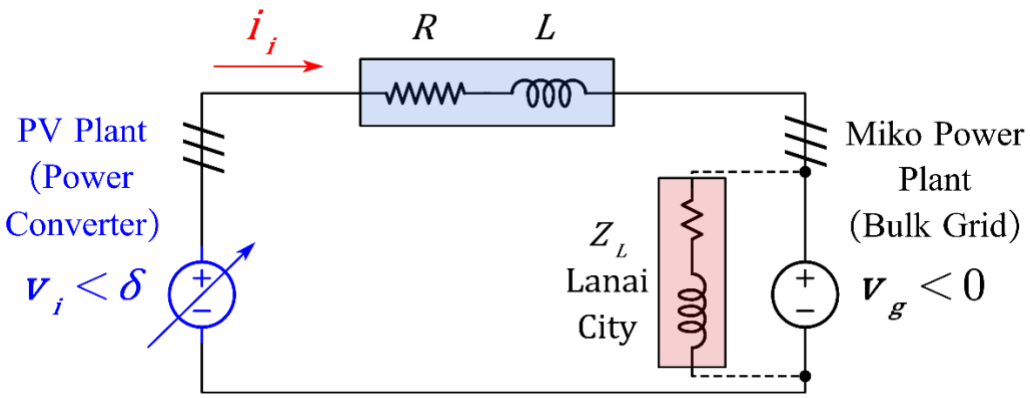

Figure 6: Equivalent circuit of selected part of Lanai Grid

The nominal system voltage is 12.47 kV. The values of R and L are not specified in the design documents, hence these values are estimated based on the typical reactance to resistance X/R ratio in distribution systems. It is assumed that aluminum cables are used as the transmission line. The

selected parameters are based on IEEE Application Guide for AC High-Voltage Circuit Breakers for approximated equivalent system X/R ratios as observed from remote locations connected to synchronous machines through transformers rated 10 MVA or less, transmission lines, distribution feeders etc. [15]. The selected ratio is also consistent with the reactance and resistance values defined by the characteristics of Aluminum Cable Steel Reinforced Conductors (ACSR) [16]. The given per kilometer values of resistance and reactance are used to estimate R and L for the 2 mile transmission line between the central power plant and the PV plant. Table 1 lists the final estimated system parameters.

Table 1: Test system specifications

Parameter	Value
Power System X/R ratio $\left(\frac{X}{R}\right)$	~10
Transmission Line Distance ($miles$)	~2
Transmission Line Resistance (R)	~0.1 Ω
Transmission Line Reactance at 60 Hz (X)	~1 Ω
Transmission Line Inductance (L)	~2.7 mH
System Nominal Line-Line Voltage (v_{LL})	12.47 kV
System Nominal Line-Neutral Voltage (v_P)	7.2 kV
Power Rating of Miko Power Plant (P_{grid_max})	10.4 MW
Power Rating of PV Plant (P_{i_max})	1.3 MW

2.4 Summary

- The evolution of the electrical grid reveals that there is a trend of moving from centralized power generation to distributed power systems. By having multiple energy sources serving the loads, resiliency is increased and dependence on only one energy resource is reduced.
- In earlier power system architectures, the grid was formed by electrical machine-based sources. However, due to the growth of renewable energy sources, power electronics became a requirement in modern power system architectures because it serves as the power interface between the fixed frequency AC grid and energy sources with DC or varying frequency AC. In future power system architectures,

the penetration of power electronics may increase to the extent that the grid could be formed by 100% power electronics.

- To evaluate the challenges of existing power converter control schemes in grid connected applications, and validate new control methods, a real-world example microgrid is considered and simplified to an equivalent circuit. The circuit is parametrized using physical system characteristics, such as distance between the sources, impedance per unit length of transmission lines, etc.

Chapter 3: Power Electronics Control for Grid-Connected Applications

3.1 Introduction

This chapter explains the two most commonly used control techniques for Power Electronics in grid connected applications – Grid Following (GFL) and Grid Forming (GFM) control. Initially, GFL was widely used in grid connected power converters. Recently, however, GFM has stimulated a lot of research activities due to the instability of GFL controls under circumstances such as weak grid conditions. In this chapter, the meaning of GFM is described in the light of definitions available in today's literature. Based on these definitions, the control behavior of GFM and GFL has been described in open circuit, short circuit, and transient conditions to show the limitations of these control techniques. Finally, the framework of control functionalities required to establish a 100% Power Electronics based grid is described.

3.2 Grid Forming and Grid Following Control in Power Electronics

GFL and GFM are the most commonly deployed control techniques for power converters connected to the grid. As the name suggests, GFL control refers to following the grid voltage, and GFM control refers to forming the voltage and frequency at the terminals of the inverter. An explanation of both these control techniques is presented as follows:

3.2.1 Grid Following Control

In GFL control, inverter follows the voltage and frequency of an external voltage source. The voltage and frequency are not controlled, as it relies on the external source. Typically, a Phase Locked Loop (PLL) is used to generate the voltage and frequency references, as shown in Figure

7. In GFL, it is not possible to operate as a standalone inverter, since there are no voltage and frequency references from an external source. GFL exhibits current source behavior because the converter's inner control loop tracks the current reference $i_{dq}{}^{*}$. The current reference may be generated by active and reactive power setpoints P_{set} and Q_{set}. These setpoints could be defined as constants, or generated by an outer control loop, such as droop control, as highlighted in Figure 7.

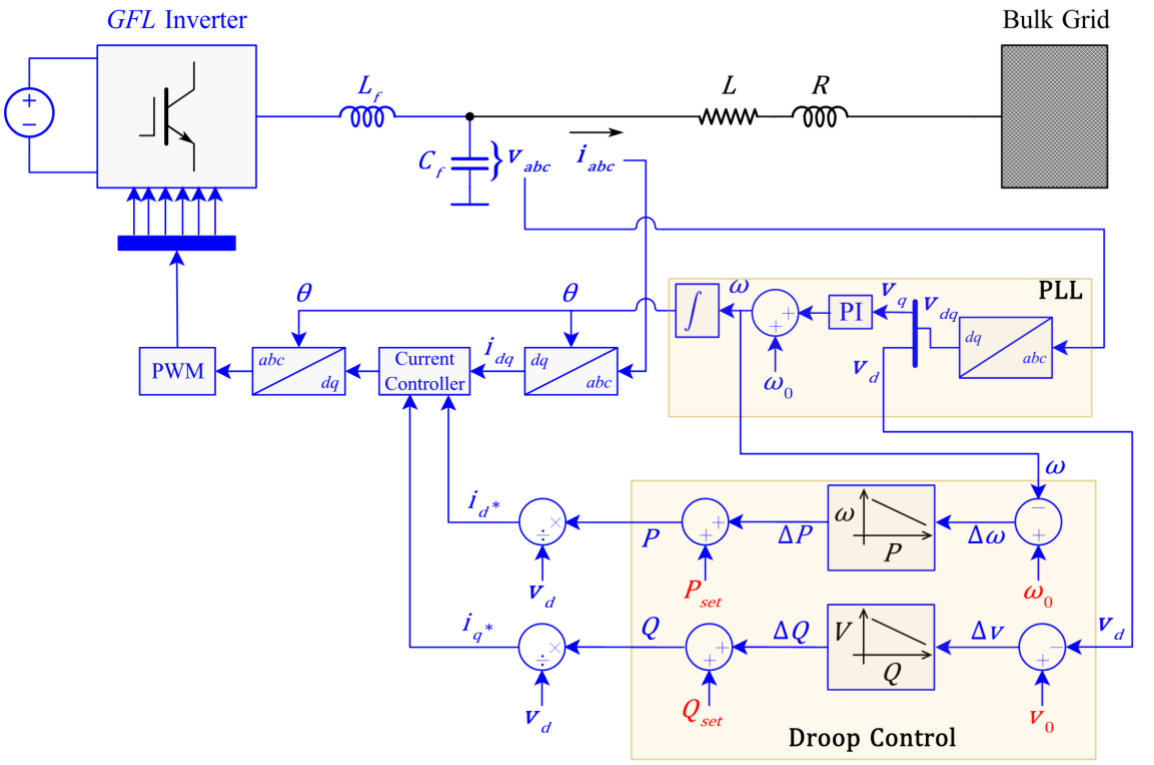

Figure 7: Power Converter with typical Grid Following control loop

3.2.2 The Push Towards GFM

GFL control has been widely used in power converters connected to the grid, to achieve fast control of the inverter's output currents. However, due to the inability of GFL inverters to

operate without an external voltage source, and instability caused by high penetration of GFL inverters in the grid, GFM inverters are now being promoted, through initiatives such as the UNIFI consortium [17].

GFL control has a weakness – it causes system instability in conditions such as weak grid. The impedance-based stability of the GFL inverter (represented as a current source) shown in Figure 8, can be determined using the Generalized Nyquist Criterion. The plot of the product of small signal output admittance of the inverter $Y_s(s)$ and small signal impedance of the grid $Z_g(s)$ in the complex plane can be used to determine the stability. The plot of $Z_g(s).Y_s(s)$ must not encircle -1 for the system to be stable [18], as shown in Figure 9.

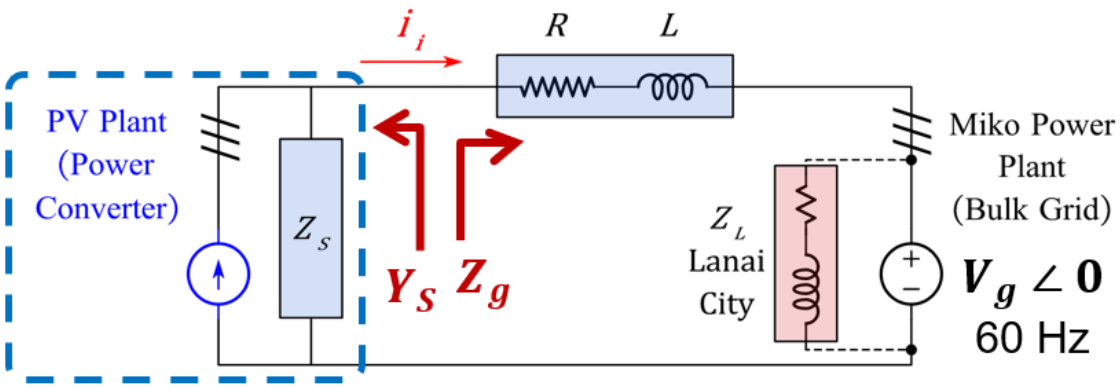

Figure 8: Small Signal Impedance for checking stability in the system

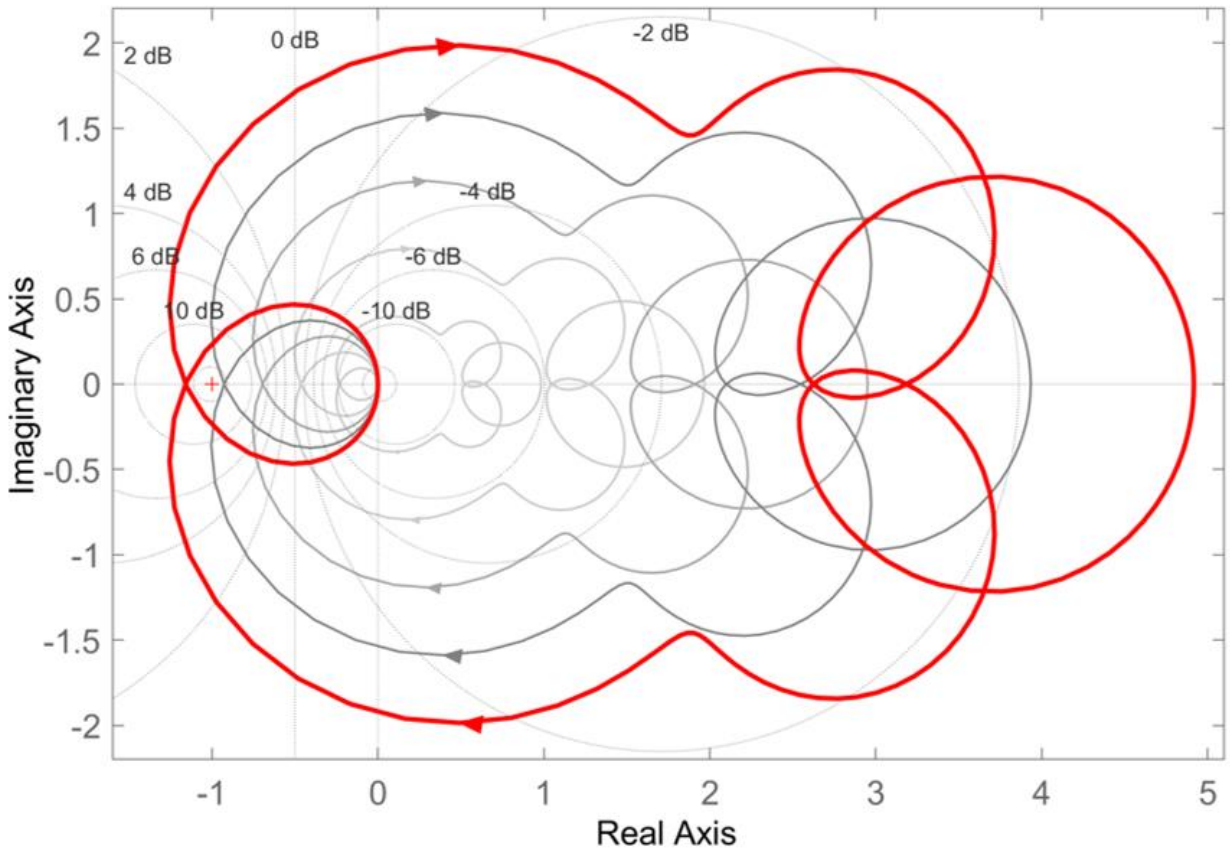

Figure 9: Nyquist diagram to show determine system stability using small signal impedance

In weak grid conditions, the value of $Z_g(s)$ is high. As a result, the plot of $Z_g(s).Y_s(s)$ may encircle -1, which causes the system to become unstable. Due to the system instability, the inverter's output voltage and frequency cannot be maintained. This gives rise to the idea of using inverter controls to regulate the voltage and frequency – hence, the idea of Grid 'Forming' was introduced.

In GFM, the voltage V_{dq} and frequency ω are regulated by the converter's voltage control loop, as shown in Figure 10. The converter's nominal voltage V_0 and frequency ω_0 are defined internally. Outer control loops such as droop control are used to change the voltage and frequency by ΔV and $\Delta\omega$ respectively, to regulate the active and reactive power setpoints P_{set} and Q_{set}.

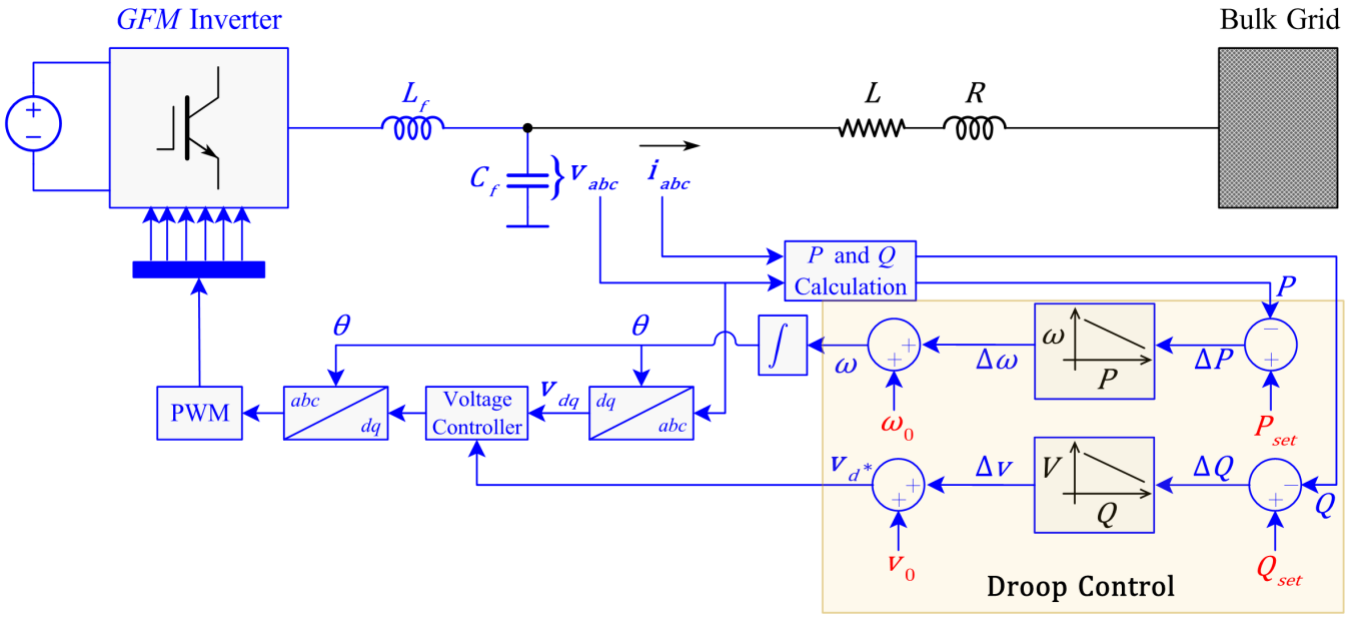

Figure 10: Power Converter with typical Grid Forming control loop

3.2.3 Definition of GFM

There is no universally accepted definition at the time of writing of this thesis. Grid Forming (GFM) Control can mean different things for different people. Available definitions from reputed organizations have been compiled and listed as under.

CIGRE Task Force (September 2019) defines GFM as follows [19]: *"The basic idea of a Grid Forming converter is that it can create an* ***AC voltage with a controlled magnitude and frequency*** *at its AC terminals in the absence of another source of AC voltage; hence, it can supply a passive load. A Grid-Forming converter is one that can regulate both instantaneous AC frequency and AC voltage. Such a converter is also able to provide reactive current equal to the steady-state rated current during AC faults. A Synchronous Grid-Forming converter is a Grid-Forming converter that is also* ***able to operate in parallel with other AC frequency regulating***

equipment *and converters."* The first part of this definition implies that a GFM inverter may simply be a UPS, that produces controlled AC voltage from a DC source. However, the second part that defines synchronous GFM is inspired by the functionality of synchronous generators that are capable of operating in parallel with other machines.

The U.S Department of Energy (November 2020) defines GFM as follows [20]: "*We use the term grid-forming as an umbrella for any inverter controller that* ***regulates instantaneous terminal voltages*** *and can* ***coexist with other grid-following and grid-forming inverters*** *and* ***synchronous generation*** *on the same system. We further restrict our definition to inverter controls that do not require a PLL. This contrasts with grid-following units that act as current sources, require a PLL, and cannot function without an externally regulated voltage. Our use of the term grid-forming also excludes single-inverter stand-alone systems or multi-inverter systems that require communications to operate. In principle, grid-forming inverters should allow for the realization of scalable and decentralized AC power systems where system voltages and frequency are regulated by the collective interactions of the grid-forming units themselves."* This definition again talks about coexistence with other sources in the grid by regulating instantaneous voltages. The focus is on decentralized systems, similar to how synchronous generators work together to form the grid.

North American Electric Reliability Corporation – NERC (December 2021) defines GFM as follows [17]: *"GFM IBR controls maintain an* ***internal voltage phasor that is constant or nearly constant in the sub-transient to transient time frame****. This allows the IBR to immediately respond to changes in the external system and maintain IBR control stability during challenging network conditions. The voltage phasor must be controlled to maintain synchronism with other devices in the grid and must also regulate active and reactive power appropriately to support the*

grid." This is an interesting definition that talks about the control behavior of GFM in transient conditions. Holding the voltage phasor constant in the transient time frame is analogous to inertia in synchronous generators. Therefore, this definition is also inspired by the behavior of the rotating machine dominated grid.

The Energy Systems Integration Group – ESIG (March 2022) defines GFM as follows [21]: "*A GFM IBR maintains an* ***internal voltage phasor in the transient time frame****, with the magnitude and frequency set locally at each inverter. GFM IBRs can be controlled to operate in an electrical island ("forming" the grid voltage and frequency). They can also be controlled to synchronize to an external grid. This allows GFM IBRs to immediately respond to changes in the external system phase angle, providing additional active and reactive power in the transient time frame as necessary."* This definition describes the transient behavior of GFM and also mentions synchronization to an external grid as a feature. However, the method of synchronization is not specified clearly.

IEEE Standard 2800-2022 (April 2022) defines GFM as follows [22]: *"In research literature, these modified IBRs that are capable of operating in a stable fashion in weak ac systems or in an islanded electrical grid have been given the name of "grid-forming" inverters. Historically, "grid forming" inverters have simply been* ***inverters that independently regulate voltage and frequency****, and thus could be used for off-grid operation (i.e., they can form their own grids). However, as of this writing, the precise meaning of "grid forming" is still in some flux. Thus, caution should be exercised when using this terminology: use of terms such as "grid following" and "grid forming" should be accompanied by context that describes the reasonable expected performance required from the IBR by the bulk power system."* This definition recognizes

the fact that GFM can mean different things for different people. Therefore, it is important to specify the functionality that the control method delivers.

The Australian Energy Market Operator – AEMO (June 2023) defines GFM as follows [23]: *"A grid-forming (GFM) inverter maintains a* ***constant internal voltage phasor in a short time frame****, with magnitude and frequency set locally by the inverter, thereby allowing immediate response to a change in the external grid. On a longer timescale, the internal voltage phasor may vary to achieve desired performance. In this document, the term 'inverter' is used in a general sense and is intended to also cover non-generating power electronic devices, such as AC-to-DC converters and STATCOMs."* This definition describes not only the transient timescale, but also goes on to mention that the steady state response can be different from the transient response. This leads the way to a more generic control method in which the steady state control law can be changed depending on performance requirements.

All of the above-mentioned definitions have a common thread – Grid Forming inverters establish the Voltage Magnitude and Frequency at their output terminals. Some definitions mention that GFM inverters should be able to operate with other sources (synchronous generators and inverters) in the AC power grid.

3.3 Grid Forming vs. Grid Following Control Behaviors

3.3.1 GFM and GFL Control Behavior Approximated as Voltage and Current Sources

GFM and GFL are considered to be controlled voltage and current sources respectively. Figure 11 represents the test circuit in which a power converter is connected to the grid through an impedance. If the converter is controlled with GFL, it can be considered as a current source with

equivalent parallel admittance Y. In the case of GFM control, the converter can be considered as a voltage source with an equivalent series impedance Z.

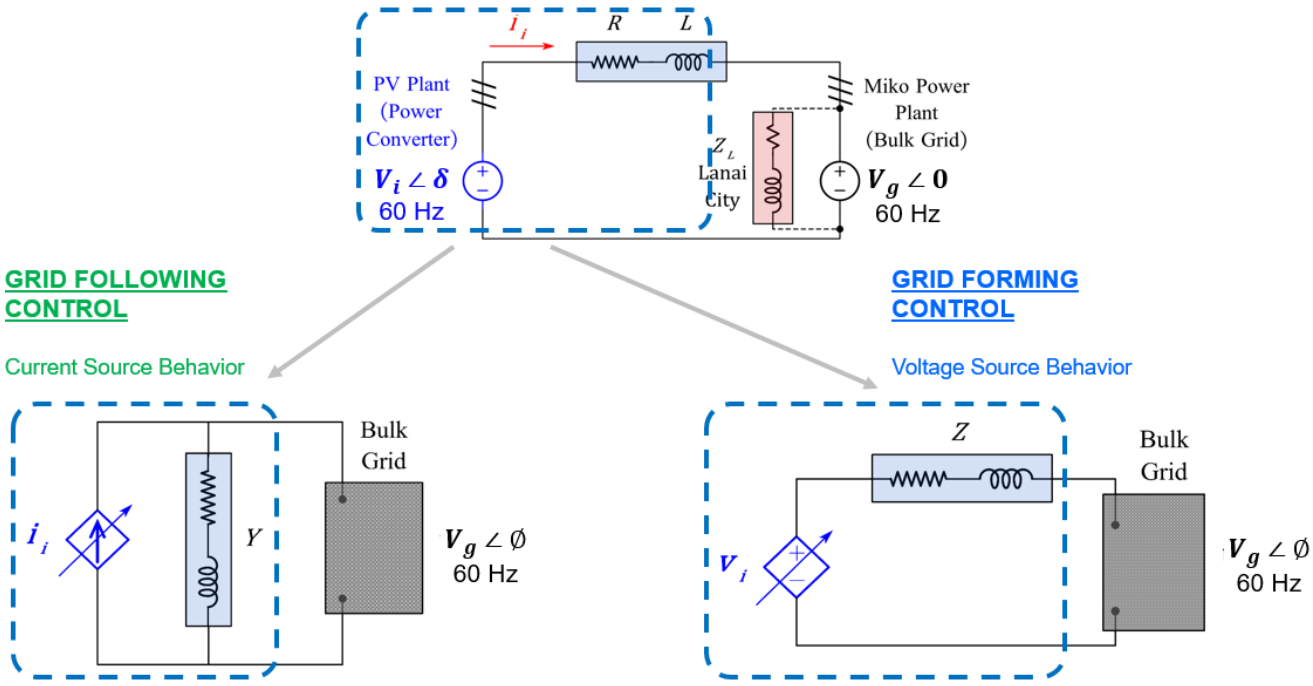

Figure 11: Grid Following and Grid Forming controls represented as current and voltage sources respectively

GFM and GFL control methods are not entirely opposite control concepts. The conventional classification of GFM and GFL as voltage and current sources may not be enough to identify the subtleties of these methods. Caution should be exercised when using this classification, as it does not provide insight into the control dynamics of these methods. According to the techniques of circuit analysis, every Thevenin equivalent circuit can be transformed into its Norton equivalent circuit, and vice versa, as shown in Figure 13, Figure 14, and Figure 15. This basic understanding suggests that GFM and GFL are not two entirely different control concepts. Rather, it may be possible to have an overlap between the two. This idea has previously been presented in [24], where the duality of GFM and GFL has been challenged. The concept of voltage and

frequency ‘stiffness’ has been presented as shown in Figure 12. In this context, stiffness refers to the rigidity of the source to maintain its own voltage and frequency.

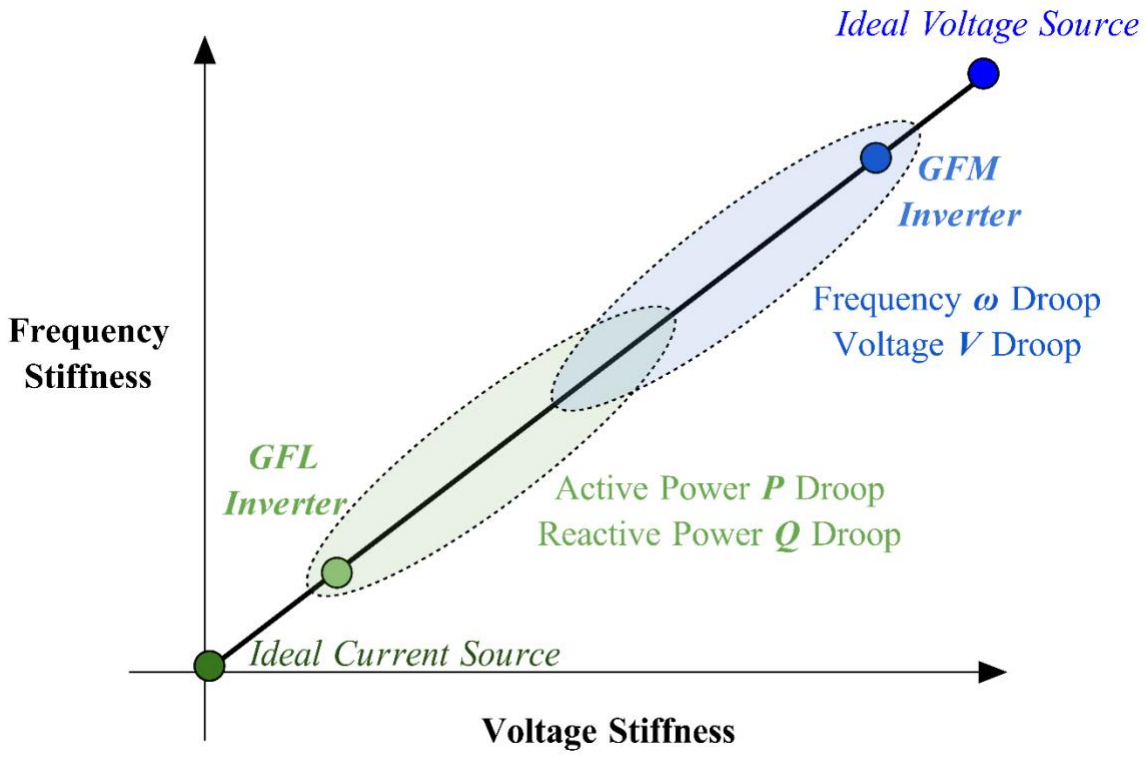

Figure 12: Voltage and Frequency Stiffness in GFM and GFL control

At one extreme end of the chart, there is an ideal voltage source, which exhibits constant voltage magnitude and frequency, regardless of the load conditions. A GFM inverter which maintains voltage magnitude and frequency is similar to the ideal voltage source, but as the voltage and frequency are drooped according to active and reactive power respectively, the frequency and voltage becomes flexible, therefore the GFM inverter becomes ‘less stiff’. On the other extreme end of the line, there is an ideal current source that exhibits zero voltage and frequency stiffness as it simply follows the voltage of an external voltage source and injects current. A GFL inverter with a PLL and current reference is similar to the ideal current source, but as the active and reactive

power follow the droop curves for frequency and voltage respectively, the frequency and voltage become ‘more stiff’. Considering the voltage and frequency stiffness in GFM and GFL leads to the idea that a single unified control method can be developed in which the voltage and frequency stiffness can be a tunable parameter, because of which the inverter can move along the line from one end of the stiffness chart to the other [24].

3.3.2 GFM and GFL Control Behaviors Under Different Grid Conditions

Inverters with GFM and GFL control methods respond to different grid conditions based on their inner control loops – voltage and current control loops respectively. Both control methods can maintain active and reactive power setpoints in the steady state. As described previously, Figure 10 and Figure 7 represent the basic control structure of GFM and GFL.

These inner control loop objectives of these control methods give rise to the notion that GFM and GFL inverters can be considered as voltage and current sources respectively. When subjected to extreme grid conditions such as short circuit and open circuit, the controlled voltage and current source representations reveal inherent issues. These conditions and the control behaviors are explained as follows:

1. **<u>In Short Circuit Condition:</u>**

   If the GFM inverter is represented as a voltage source, a short circuit condition at the output, as shown in Figure 13 (a), will cause the inverter to exceed overcurrent limits. In this case, the GFM inverter will be unable to maintain the voltage and frequency setpoints at its output terminals. Meanwhile, the GFL inverter represented as a current source, can maintain the current setpoint if there is a short circuit condition at the output, as shown in Figure 13 (b).

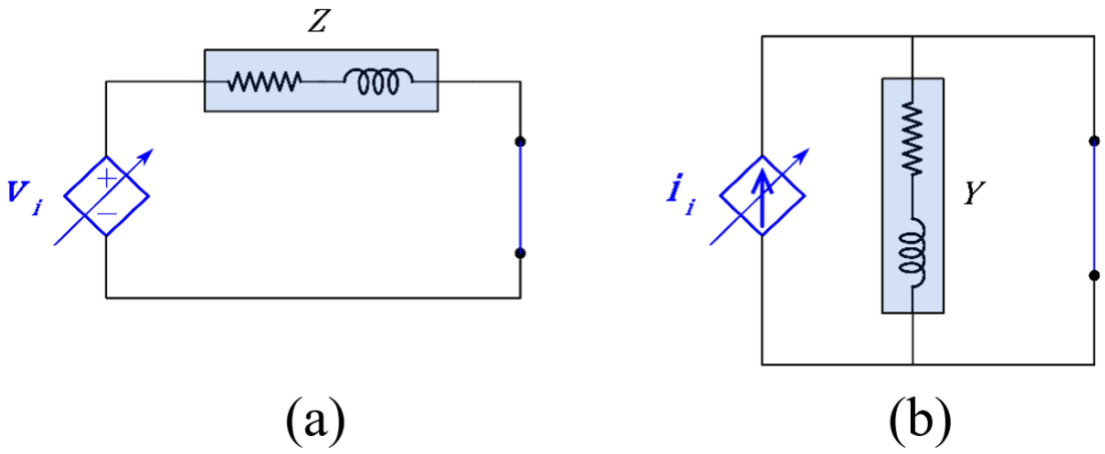

Figure 13: (a) GFM and (b) GFL in short circuit conditions

2. In Open Circuit Condition:

GFM inverter, represented as a voltage source, is subjected to open circuit condition, as shown in Figure 14 (a). The output current of the GFM inverter is zero, therefore the inverter will be able to maintain the voltage and frequency setpoints at its output terminals. Meanwhile, the GFL inverter, represented as a current source, as shown in Figure 14 (b) will be unable to maintain the current setpoint due to a lack of current flow path. The inverter will trip due to overvoltage limits.

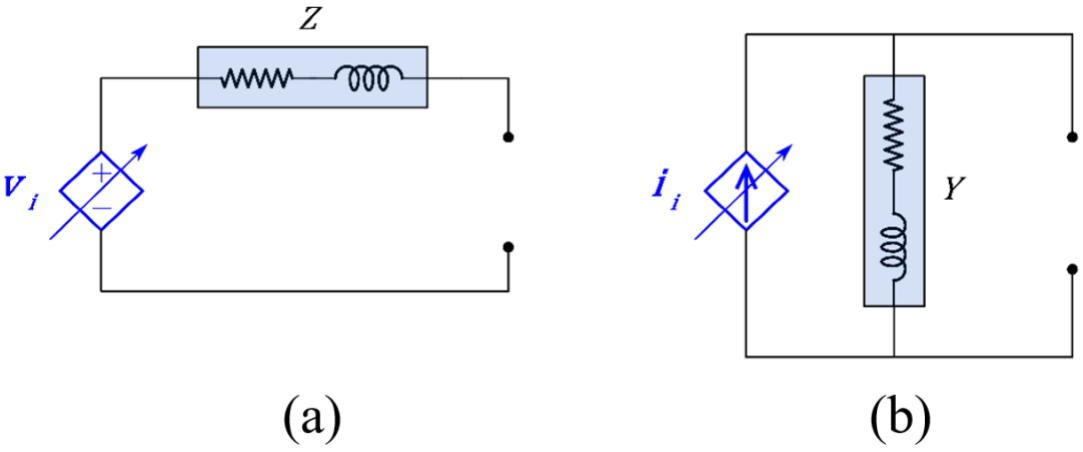

Figure 14: (a) GFM and (b) GFL in open circuit conditions

3. **During Transients:**

The control behavior of GFM and GFL during transients can be distinguished by observing how the inverter phase δ changes when the grid phase $\emptyset$ changes suddenly due to a disturbance, in the circuit shown in Figure 15. The inverter (having voltage magnitude V_i and phase δ) is connected to the grid (having voltage magnitude V_g and phase $\emptyset$) and the system is initially at a steady state value. When there is a disturbance, the GFM inverter holds its phasor constant in the sub-transient time frame, and eventually transitions to the new steady state after a period of time. As a result, there is an increase in power in the sub-transient time frame due to the difference between $\emptyset$ and δ, as represented in Figure 16 (b). On the contrary, the GFL inverter phase δ responds to the disturbance by following the grid voltage phase $\emptyset$. Eventually, δ transitions to the new steady state due to droop control. As a result, the power is constant in the sub-transient time frame, immediately after the disturbance due to close alignment of $\emptyset$ and δ, as shown in Figure 16 (a).

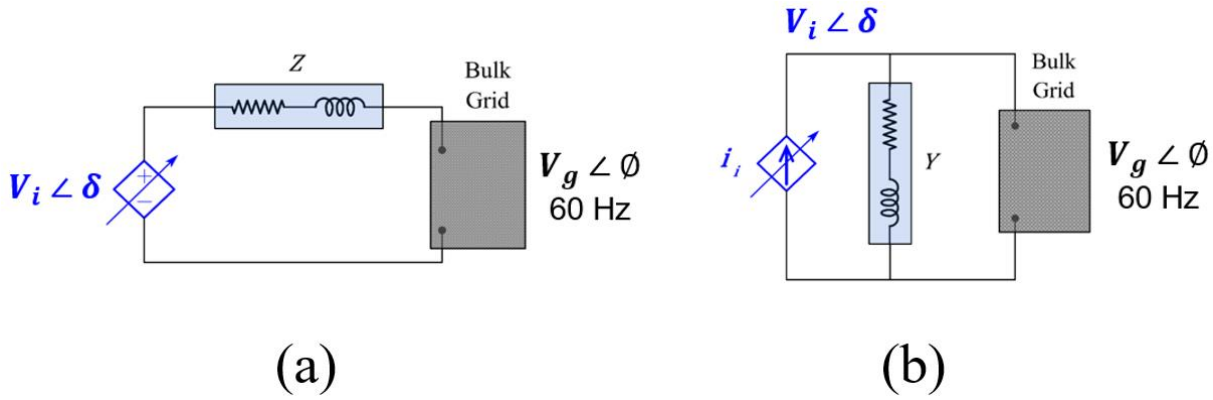

Figure 15: (a) GFM and (b) GFL in transient conditions

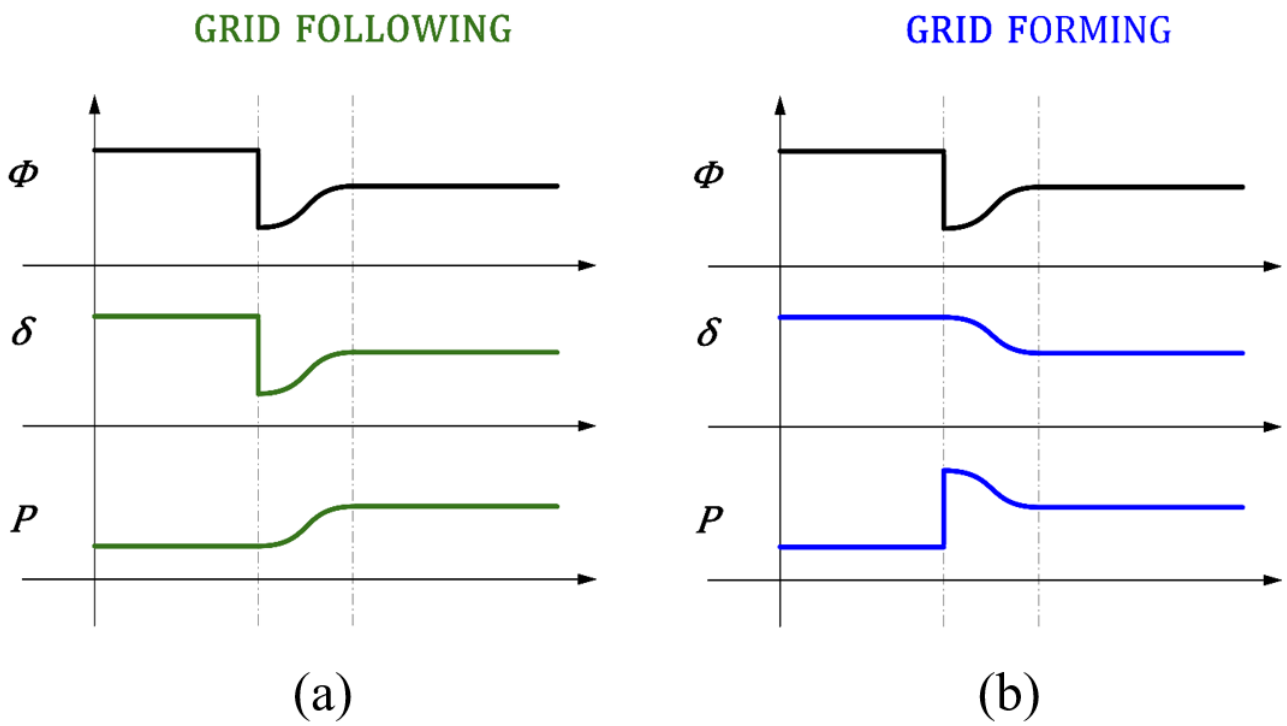

Figure 16: (a) GFL and (b) GFM response to grid disturbance

3.4 Framework for establishing a 100% Power Electronics Based Grid

In order to establish a 100% power electronics-based grid, specifying the control functionality is crucial for power electronics converters in grid connected applications. In general, control for power converters in the AC power grid must ensure the grid bus integrity i.e. the grid must be robust and resilient, so that the loads are served with uninterrupted power supply. Bus integrity can be achieved if the control for power electronics has the following design considerations, as presented in Figure 17:

1. **Power Flow and Energy Balance:** Power flow must be controlled to maintain net energy balance amongst all sources and loads in the system.
2. **Establishment of Voltage and Frequency:** Voltage magnitude and frequency must to be established that is capable of operating as a standalone system or as a part of a larger system consisting of other sources (synchronous generators and/or inverters)
3. **Small Signal Transients:** Inverter control must be able to maintain small signal stability.
4. **Large Signal Transients:** Inverter control must accommodate changes in required mode of operation (for example, Blackstart).
5. **Protection:** Control behavior under different kinds of fault conditions must be designed to protect the integrity of the AC power grid.

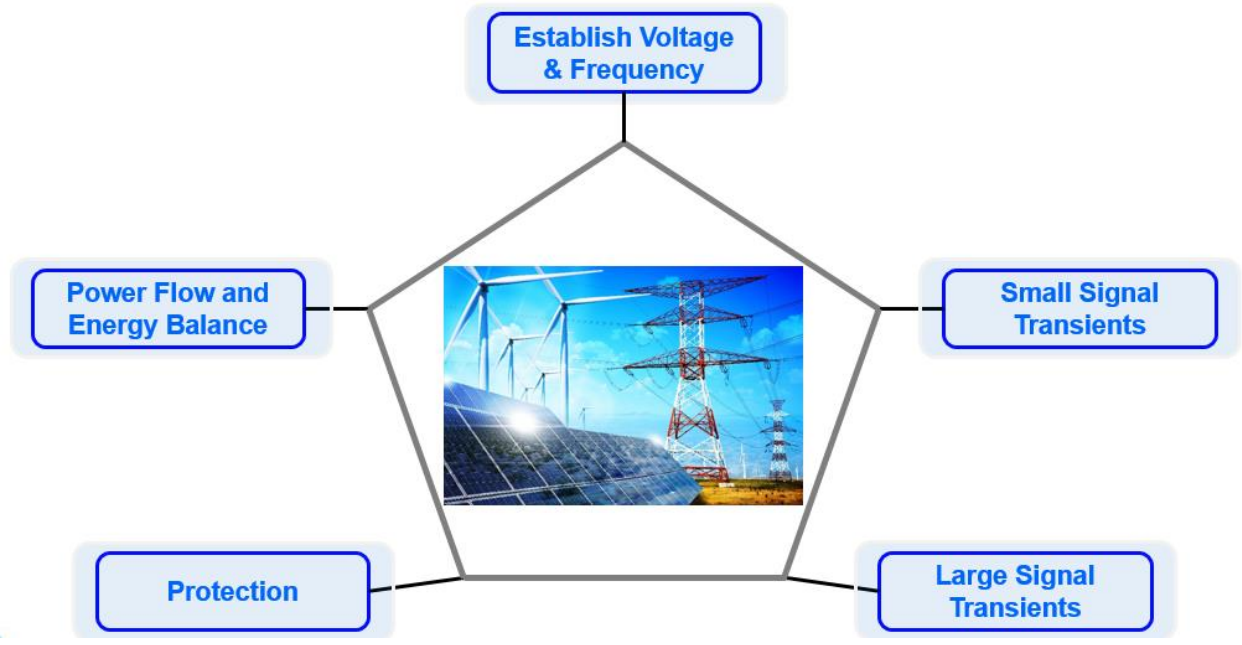

Figure 17: Required functionality for Power Electronics Based Grid

Summary

- GFL control has widely been used in grid connected power converters. However, due to the inability of GFL inverters to operate in standalone/islanded mode, and instability caused by high penetration of GFL inverters, recently GFM control has stimulated a lot of research activities.
- The precise meaning of GFM is still in flux. Most of the definitions available today are inspired by the old grid dominated by rotating machines.
- Even though GFL and GFM are considered different, it can be possible to develop a single unified control method [24], by looking at the voltage and frequency stiffness in both of these control methods. The voltage and frequency stiffness can be a tunable parameter which could be set according to the grid conditions.
- The framework for the establishment of a 100% Power Electronics based grid has been described which leads to the five desired control functionalities defined in this chapter.

Chapter 4: State-of-The-Art Grid Forming Control Methods

4.1 Introduction

This chapter describes the origins, assumptions, and working principles of State-of-the-art GFM control methods. GFM control schemes can be traced long before the term of 'Grid Forming' was even coined, because the concept of controlling the voltage and frequency of inverters is not new. All control schemes that satisfy the definitions presented in Chapter 3 may be categorized as GFM. Three popular types of Grid Forming control can be found in the literature [25], presented as follows, and also shown in Figure 18.

1. Droop based control: Active power and Frequency (P-ω) and Reactive power and Voltage (Q-V) Droop control
2. Emulation of synchronous machine: Virtual Synchronous Machine (VSM)
3. Nonlinear control: Virtual Oscillator Control

Droop-based control and Virtual Synchronous Machine (VSM) are linear control systems that draw inspiration from the control of electric machines in power systems. These control laws, derived from steady-state phasor-based relationships, are applied to power converters. The assumption is that the control laws effective for grid systems based on rotating machines remain applicable to grid connected power converters.

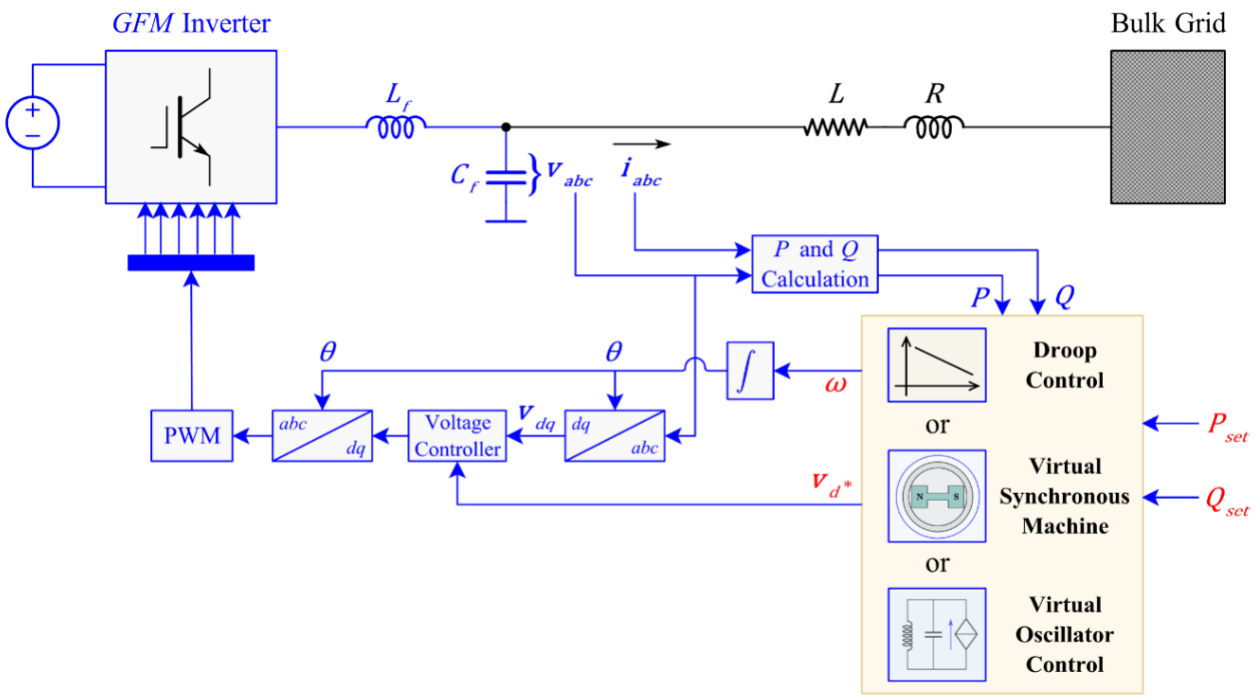

Figure 18: Common types of Grid Forming Control

Droop control in Power Electronics was first introduced in 1993 [26] to share power and achieve synchronization among parallel connected voltage source inverters. The concept of VSM was introduced in 2007 [27], inspired by the operation of synchronous machines in the legacy power system. Several variations of these control methods exist in the literature today, but the fundamental principles revolve around the same idea. These two methods and their equivalence is discussed in further detail in this chapter.

The Virtual Oscillator Control (VOC) concept was introduced more recently in 2014 [28]. It is a type of non-linear control that is inspired by the operation of non-linear oscillators. The details of this type of control are not included in this thesis.

4.2 Droop Control

4.2.1 Origins and adoption in Power Electronics

Droop control is originated from the control of synchronous generators in the grid [29]. These control laws determine the relationship between active power and rotating speed (frequency), and reactive power and voltage magnitude.

The legacy power system was dominated by synchronous generators. The dynamic behavior in these machines is governed by their physical properties/construction. In machines, the rotating speed ω is inversely proportional to the load P on the machine's rotating shaft. As the load P_1 increases to P_2, the speed ω_1 of the rotating shaft of the machine slows down to ω_2 linearly, with a linear coefficient k_p, called the droop coefficient, as represented in the following equation:

$$\omega_2 = \omega_1 + k_p(P_2 - P_1) \quad (1)$$

The rotating speed of the machines is controlled to achieve the nominal value of the power system's electrical frequency through a 'Governor', by regulating the flow of fuel. The Power-Frequency droop curve of the machine, as shown in Figure 19, is enforced by the governor. The maximum frequency ω_{max} is obtained at minimum load condition, and the minimum frequency corresponds to the full load condition P_{max}.

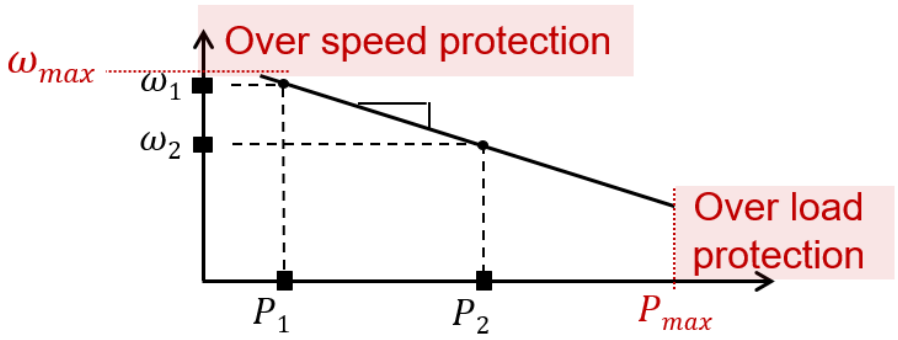

Figure 19: Power-Frequency Droop Curve

Different machines have their own droop curves, according to their power ratings. Machines with higher power ratings have a droop curve with lower linear droop coefficient. Figure 20 shows the droop curves of two machines having full load power ratings of P_1 and P_2. The difference $\Delta\omega$ between no load frequency ω_{max} and full load frequency ω_{min} is designed to be minimal, usually 2 – 4 % of the rated frequency [30].

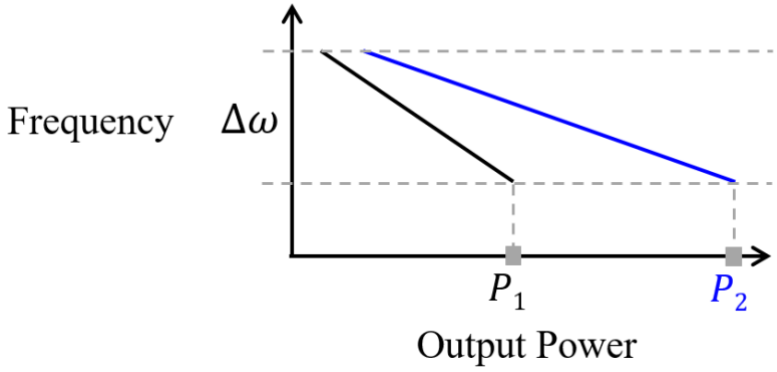

Figure 20: Droop curves of different machines

If multiple machines whose frequency is controlled according to their respective droop curves are connected together, each machine delivers power in proportion to its rating. As shown

in Figure 21, the machines coupled together (either mechanically or electrically) cannot have different rotating speeds, so the required power demand is delivered according to the droop curves. In this case, Generator B has a higher power rating than Generator A as depicted in the droop curves. As a result, the power delivered by Generator B P_b is greater than the power delivered by Generator A P_a at any frequency of operation ω.

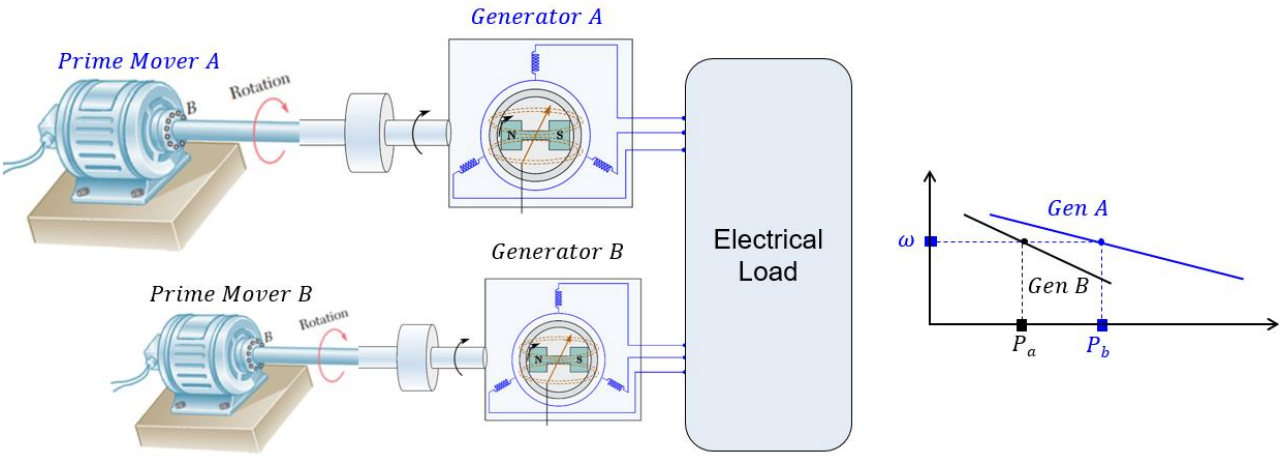

Figure 21: Operation of coupled rotating machines and their droop curves

As power systems evolved and power electronics converters also started making their way into power systems, this principle of droop control was also applied to power electronics. The first use of droop control for standalone AC inverters connected together in parallel was demonstrated in 1993 [26]. Droop control was used for synchronization and power sharing among parallel connected inverters, by utilizing the droop curves to control the active power P and reactive power Q.

4.2.2 Steady State Power Flow Analysis

To understand the synchronization and power sharing in a droop-controlled inverter, the steady state power flow can be analyzed for the test circuit introduced in Chapter 2, as shown in

Figure 22. One of these sources is considered to be a droop-controlled power converter, while the other is considered to be the bulk grid. Load Z_L is connected in parallel with the bulk grid v_g, and the power converter v_i is required to share the power demand of load Z_L.

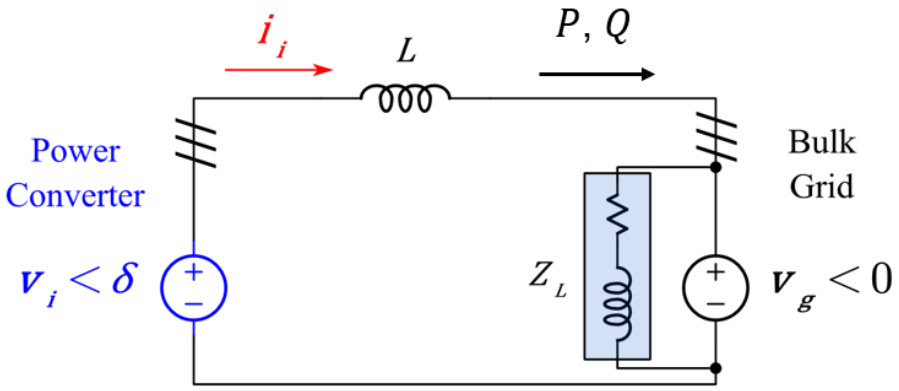

Figure 22: Power converter connected to the bulk grid through an inductor

The steady state active and reactive power flow P and Q in this circuit can be calculated by considering the phasor diagrams of the voltages and currents in the circuit, represented by Figure 23. The phasor diagram represents single phase, but the same technique is valid for three phase system. v_g and v_i have an angle difference of δ, causing current i_i to flow in the circuit. The voltage across the inductor is $i_i.X_L$.

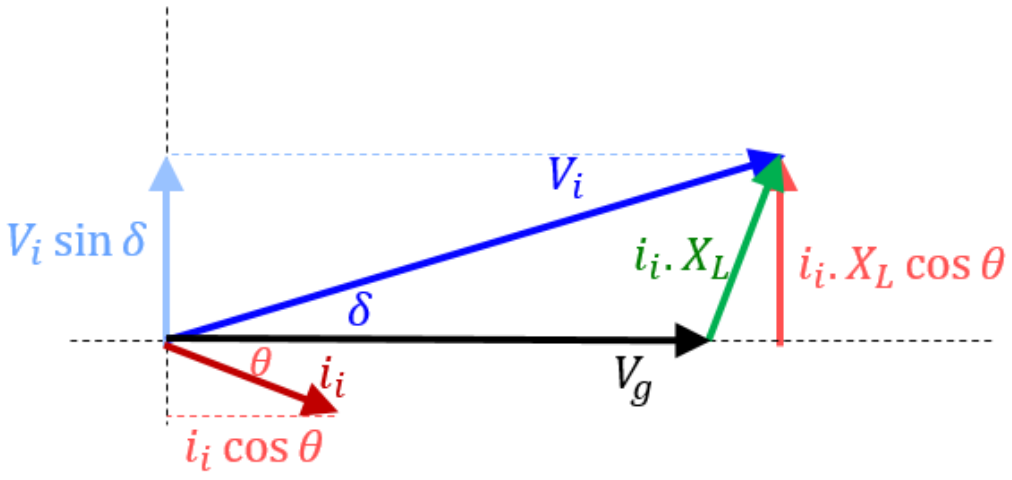

Figure 23: Phasor diagrams of voltages and currents for an inverter connected to the bulk grid through an inductance

The steady state active power is the product of the RMS values of of v_g and the component of i_i in parallel with v_g.

$$P = V_g i_i \cos \theta \tag{2}$$

From the phasor diagram, it can be observed that:

$$i_i . X_L \cos \theta = V_i \sin \delta$$

The above equations yield the steady state active power as follows:

$$\boldsymbol{P = \frac{V_g V_i \sin \delta}{X_L}} \tag{3}$$

Similarly, the reactive power Q is the product of RMS values of v_g and the component of the current perpendicular to v_g. Equation 4 is derived from the phasor diagram, which leads to the conclusion that the inverter voltage V_i can be used to control the reactive power Q. Even though this relationship is not linear, it provides a control variable that can be used to regulate Q.

$$\boldsymbol{Q = \frac{V_g\{V_g - V_i \cos \delta\}}{X_L}} \quad (\mathbf{4})$$

Equations 3 and 4 form the basis of the droop control laws. The relationship between active power P and angle difference δ between the voltage sources v_i and v_g in equation 3 is further examined in detail. It leads to the conclusion that P can be controlled using δ, also commonly referred to as the 'power angle', shown as follows:

$$P \propto \sin \delta$$

When δ is small enough, $\sin \delta \approx \delta$. The assumption of small δ is true for synchronous generators-based power system. After a machine is synchronized with the grid, δ can only change slightly, due to the rotating mass of the machine. If there is a sudden or large change in δ, the rotating shaft may break due to the huge torque. However, in a power electronics-based power system, this assumption may not always be true because the output sine wave is created through controls, and the control command can cause δ to have a large value at any instant of time. With the assumption of small δ, the control law becomes:

$$\boldsymbol{P \propto \delta} \quad (\mathbf{5})$$

It is always assumed in the literature that this relationship can be extended to say that the active power P is dependent on the frequency ω [31]. The underlying assumption here is that the frequency ω can be utilized to control P in a manner similar to how δ can be used to control P.

4.2.3 Reason of using Power-Frequency Droop instead of Power-Angle Relationship

According to the steady state power flow equation, the power angle δ can be used to control the steady state active power P. However, the GFM control methods use frequency as the control variable. The question arises, why is the frequency used to control the power and not the angle? This question can be answered by observing how the power angle changes in electrical machines. As shown in Figure 24, when the machine is at an initial steady state, the power angle causes a time difference of Δt_1 between the two voltages. For a new steady state with a higher power angle, the required time difference is Δt_2. This change cannot happen instantaneously because the rotor of the machine cannot jump from one position to another. As shown in Figure 25, the only way is to create a change $\Delta\omega$ in the frequency, which causes the time difference to become Δt_2.

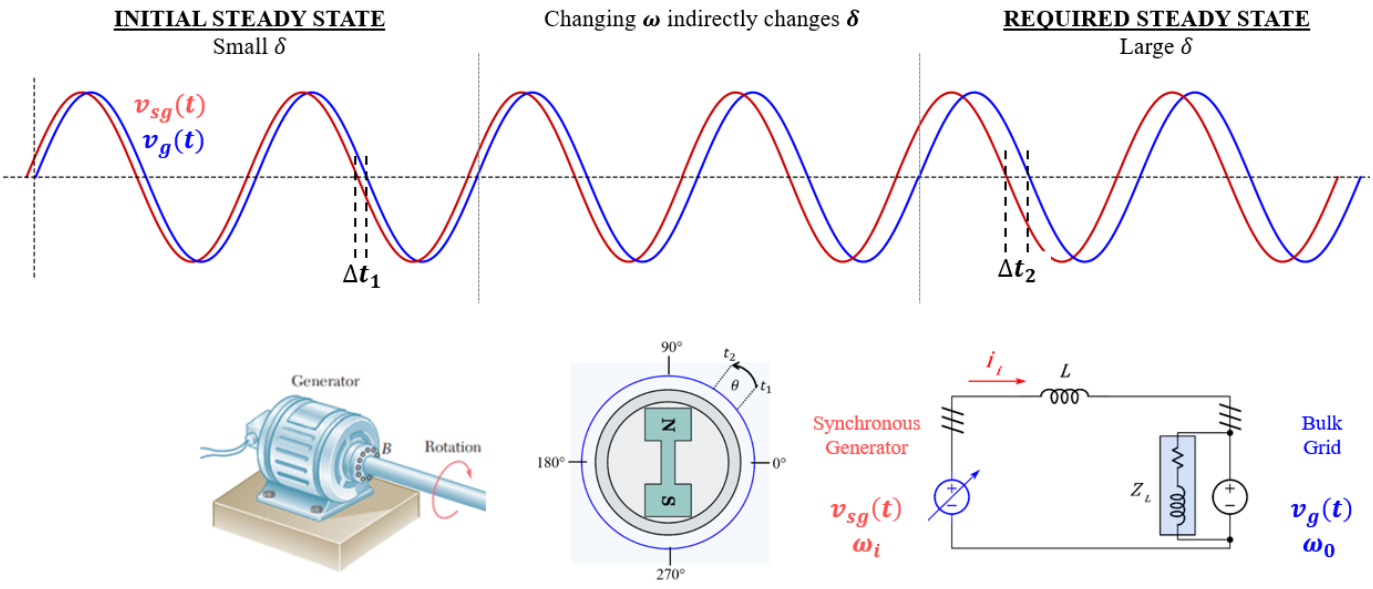

Figure 24: Change in power angle by changing rotating speed of a generator

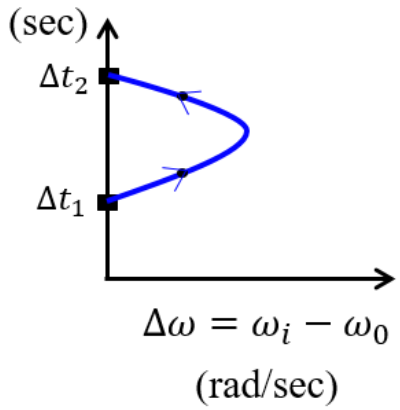

Figure 25: Gradual change in rotor angle of synchronous generator

In the legacy power systems with electrical machines, using frequency to control the active power P was inevitable due to the rotating mass of the machines. However, in the modern power system with power electronics, there is no such restriction. With high bandwidth voltage and current control loops, the voltage can almost instantaneously be regulated to any value within the range of $+V_{DC}$ and $-V_{DC}$, as shown in Figure 26. As presented in Figure 27, the power angle δ can be changed by instantaneously going from Δt_1 to Δt_2.

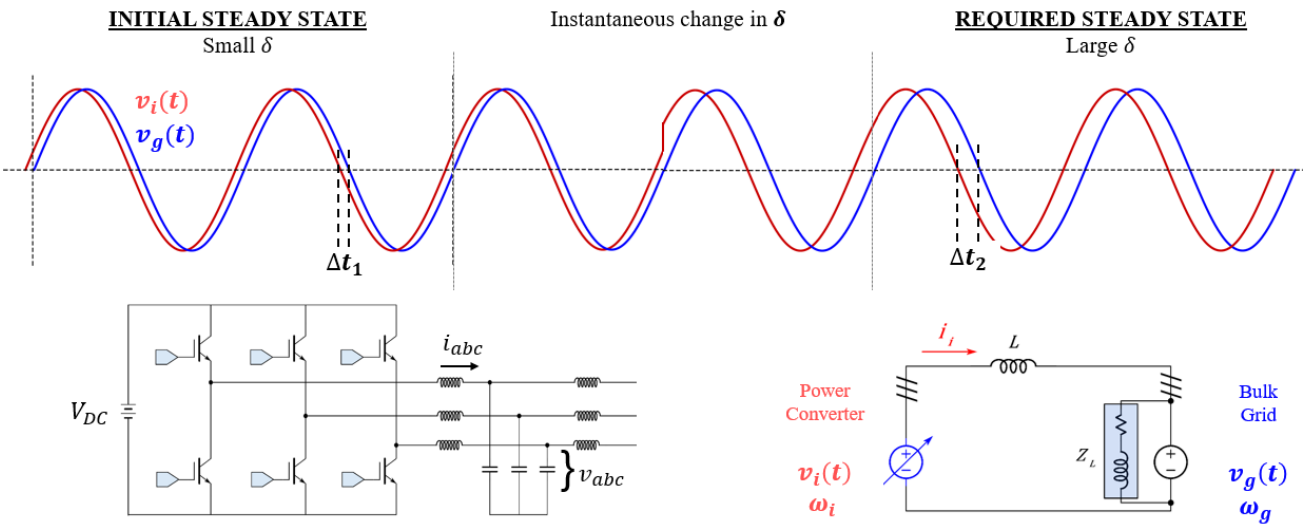

Figure 26: Change in power angle by instantaneously changing the angle of sine wave produced by the inverter

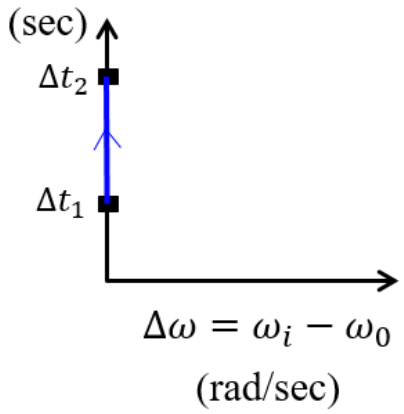

Figure 27: Instantaneous change in electrical angle of power electronics

4.2.4 Control Loop Design Example

The Power-Frequency droop control loop generates the frequency of the inverter's output voltage sine wave, based on the output active power P measurement. The objective of this control loop is to implement a power setpoint P_{set}, by varying ω. The value of the droop

coefficient k_p dictates the change in frequency $\Delta\omega$ required to track P_{set}. k_p is designed by considering the allowable range of frequency deviation $\Delta\omega$ from the nominal frequency ω_0. Figure 28 shows the Power-Frequency droop control loop.

As a design example, the droop control loop is designed for the equivalent circuit of Lanai grid. It is assumed that both sources have three-phase balanced voltages with linear balanced load, hence the instantaneous value of P will be a constant. P is calculated as the product of the inverter's instantaneous voltage v_i and current i_i. The error between the desired power P_{set} and measured power P is used to multiplied by the droop coefficient k_p to calculate the difference in frequency $\Delta\omega$ required to implement the droop curve, as shown in Figure 28. Finally, the required difference in frequency $\Delta\omega$ is subtracted from the nominal frequency ω_0 and integrated to obtain the angle of the inverter.

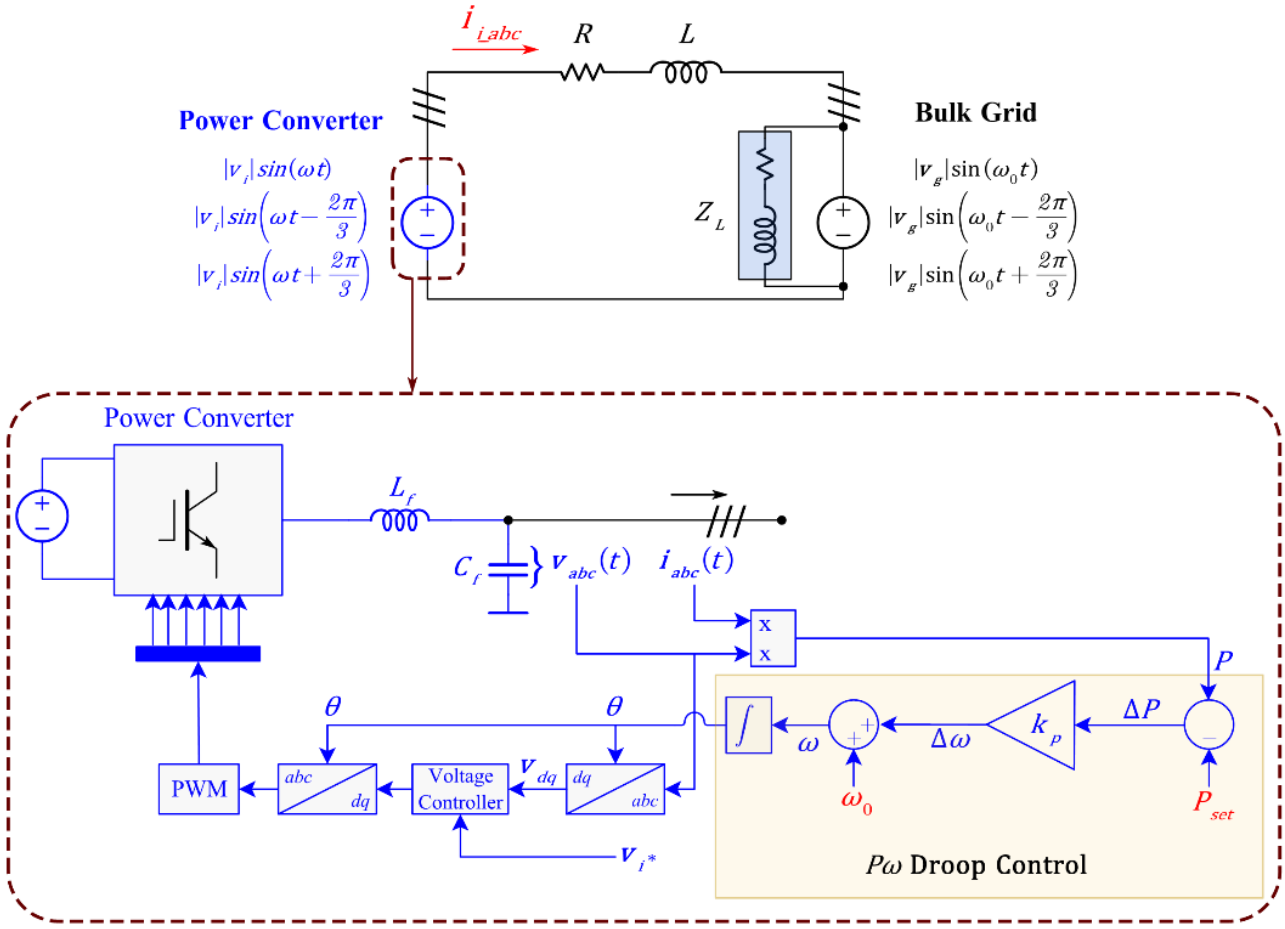

Figure 28: Design of Power-Frequency Droop Control Loop

Since this is a linear control system, the frequency domain equation for the angle θ can be written as follows:

$$\boldsymbol{\theta(s) = \frac{1}{s}\left[\omega_0 - k_p(P_{set} - P)\right]} \quad \textbf{(6)}$$

The value of the droop coefficient is selected based on the allowable frequency range. This frequency range is dictated by standards. One of the widely used standards for frequency ride through and trip in IBRs is IEEE 1547-2018 [32]. Figure 29 presents the frequency limits described

by this standard. All inverters are required to maintain continuous operation capability in the range of 58.8 Hz and 61.2 Hz, while the nominal frequency is 60 Hz.

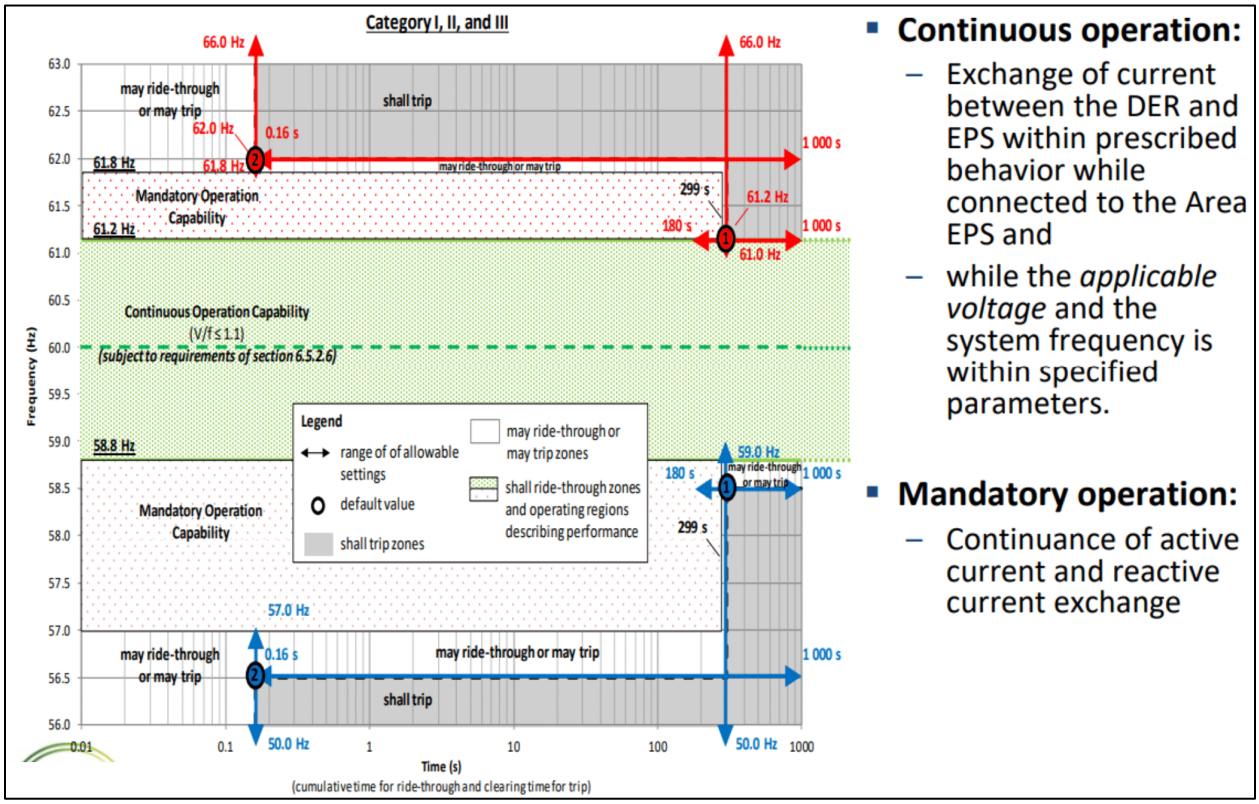

Figure 29: Droop control operation guidelines for inverters according to IEEE 1547-2018

In the continuous operation range, ω_{max} is 61.2 Hz, and ω_{min} is 58.8 Hz. This constitutes a total frequency difference of 2.4 Hz, or 4% frequency droop considering the nominal frequency of 60 Hz. The droop coefficient k_p therefore, can be calculated by the following equation:

$$k_p = \frac{\omega_{min} - \omega_{max}}{P_{rated}} \tag{7}$$

For the Lanai grid test system, the value of k_p is calculated as follows (considering $P_{rated} = 1.3\ MW$).

$$k_p = -1.16 * 10^{-5}$$

4.2.5 Working principle of power frequency droop control

In order to illustrate how exactly droop control loop regulates the power P and synchronizes with the grid voltage in the circuit presented in Figure 22, a case can be considered in which a disturbance event at the grid voltage causes a sudden phase jump.

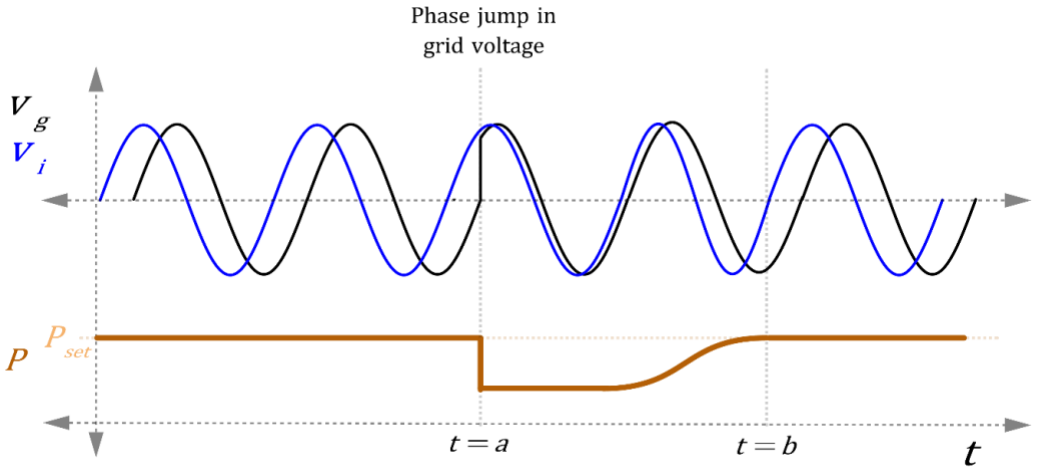

Figure 30: Response of Droop control loop to a sudden phase jump in the grid voltage

Figure 30 shows the voltage and power waveforms in which the system is initially at a steady state with v_g and v_i having an angle difference of δ at frequency ω, causing P to track the reference power P_{set}. A phase jump in v_g at time $t = a$ causes the power angle δ to decrease, resulting in a decrease in the value of P, as shown in the transition from point (a) to point (b) in Figure 32. The droop control loop uses the relationship between power and frequency, as shown in Figure 31, to bring the power back to the reference setpoint. The control loop commands the frequency to increase so that δ can be increased again, as shown in the transition from point (b) to (a) in Figure 32. At time $t = b$, the error difference between P_{set} and P reduces to zero, which

causes the frequency to return to its steady state value ω. This behavior is consistent with the GFM behavior according to the definitions mentioned in Chapter 3, as shown previously in Figure 16.

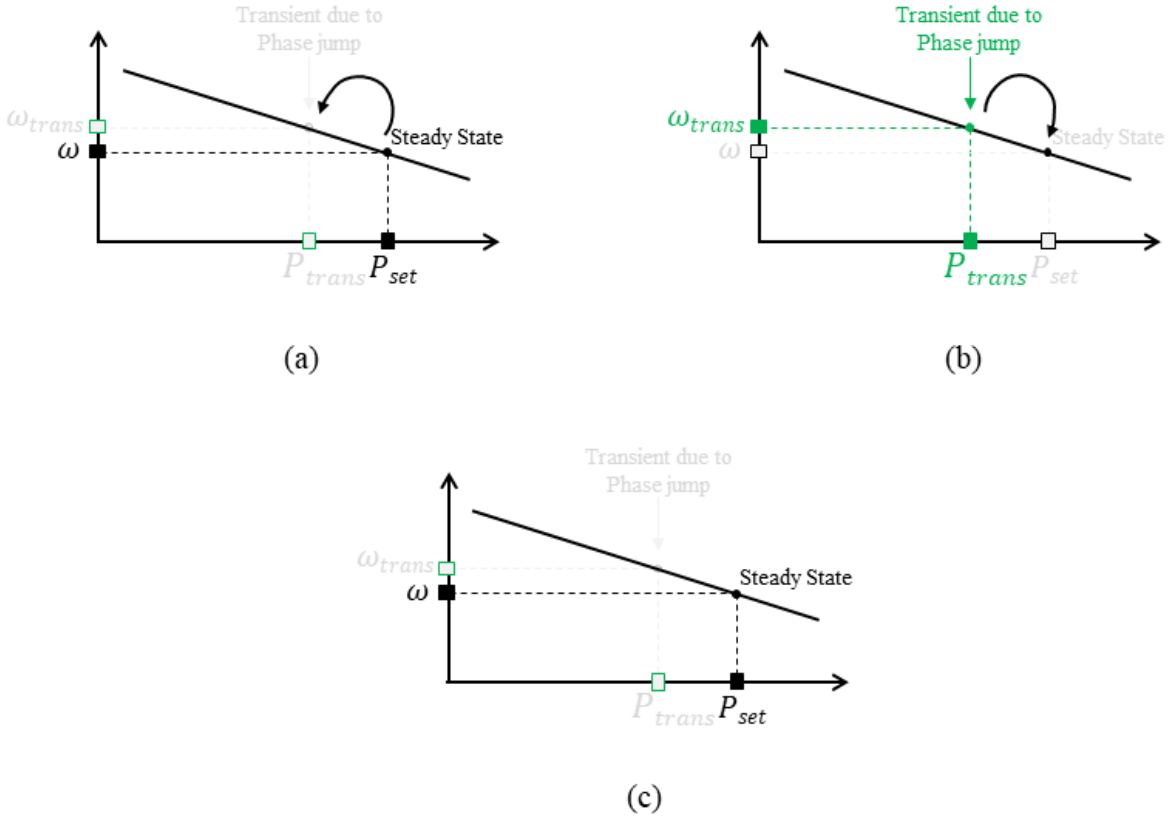

Figure 31: (a) Initial steady state point (b) Operating point shifts to a transient point on the curve due to disturbance (c) Steady state is attained due to corrective action of the loop

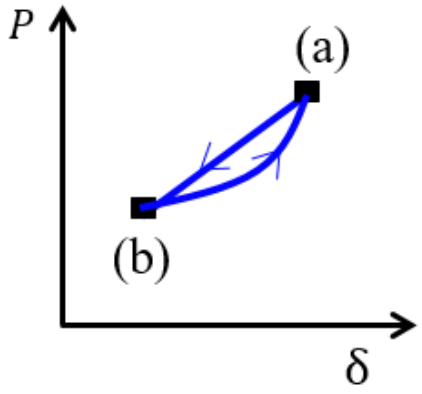

Figure 32: (a) Initial steady state (b) ***δ*** and ***P*** move to a new point due to the disturbance event

As shown in Figure 32, by regulating $\boldsymbol{P}$ to the setpoint P_{set}, δ is also being tracked to a constant value. Since the droop control loop causes the angle between the two voltage sources to be constant, this results in synchronization.

4.3 Virtual Synchronous Machine (VSM) Control

4.3.1 Origins and adoption in Power Electronics

Inspired by the 140+ years of success of the legacy power system consisting of synchronous machines, this concept of Virtual Synchronous Machines (VSM) is a control scheme that makes power converters mimic the dynamics of a synchronous generator. In VSM modes, the three most commonly used dynamic behaviors of synchronous machines are discussed in this chapter:

- Speed control through Governor droop control
- Voltage magnitude control through the exciter.
- Rotor shaft swing dynamics – inertia

A simplified representation of the structure of a synchronous machine is presented in Figure 33. The generator's shaft is mechanically coupled with the prime mover. A rotating magnetic field is produced due to the rotation of the rotor shaft, which induces voltage in the armature windings, according to Faraday's law of electromagnetic induction [33]. The induced voltage depends on the number of turns in armature winding N, the magnetic flux $\emptyset$, and rotor shaft speed ω:

$$v_a(t) = N\emptyset\omega \cos \omega t \tag{8}$$

The frequency of output voltage v_{abc} depends on the speed of rotation ω of the rotor shaft. The speed of the prime mover is controlled by the governor, which implements the power-frequency droop curve. The voltage magnitude depends on the magnetic flux, which is controlled by the field voltage v_f, represented by equation 9. v_f is controlled by the exciter, which implements the reactive power-voltage droop curve.

$$\emptyset \propto v_f \tag{9}$$

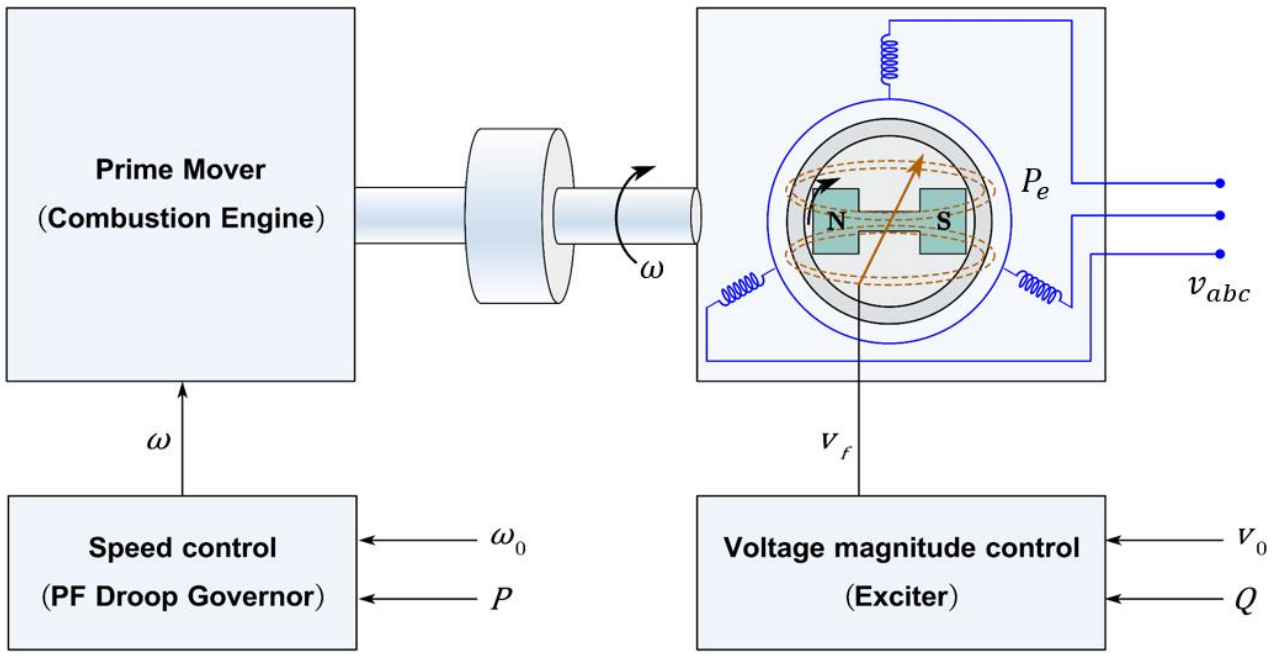

Figure 33: Generator structure and operation principle

The rotating mass of the machine exhibits the properties of inertia, because it stores kinetic energy during its motion. Due to this inertia, the rotor shaft changes its rotation speed slowly. The dynamics of this rotating mass can be described with an equation, known as the synchronous generator swing equation:

$$T_a = T_m - T_e \approx J\left(\frac{d}{dt}\Delta\omega\right) + D\Delta\omega \tag{10}$$

Any change in the rotor speed requires an accelerating torque T_a, which is the difference between the electrical torque T_e delivered to the load and the mechanical torque P_m utilized to rotate the rotor shaft. T_a depends on the total moment of inertia J of the rotating mass, the difference $\Delta\omega$ between the system's operating frequency ω and nominal frequency ω_0, and the damping coefficient D of the generator windings.

Since this is an emulation, there is no physical torque. It is helpful to write this equation in terms of electrical power P_e, which is analogous to the power delivered to the load P, and mechanical power P_m, which is analogous to the power setpoint P_{set}.

$$P_m - P_e \approx \omega_0.J\left(\frac{d}{dt}\Delta\omega\right) + \omega_0.D\Delta\omega \tag{11}$$

Inertia is considered as an essential feature of stable power systems, because the slow response in speed change is attributed as voltage magnitude and frequency stiffness of the voltage source [34]. In VSM, power converters mimic the inertial behavior of machines artificially by means of a control system based on the swing equation – this is called virtual inertia. The swing equation can be rearranged as follows to create a form that is useful in deriving a control loop:

$$\omega_0.J\left(\frac{d}{dt}\Delta\omega\right) = P_{set} - P - \omega_0.D\Delta\omega \tag{12}$$

4.3.2 VSM Control Loop Implementation in Power Electronics

Figure 34 shows the VSM implementation with power converters. The generator and prime mover blocks in Figure 33 are replaced by a voltage source inverter. The swing equation and

governor block provide the virtual inertia and Power-Frequency droop to generate the angle of the output voltage. The exciter block implements the Reactive Power-Voltage droop to provide the magnitude of the output voltage.

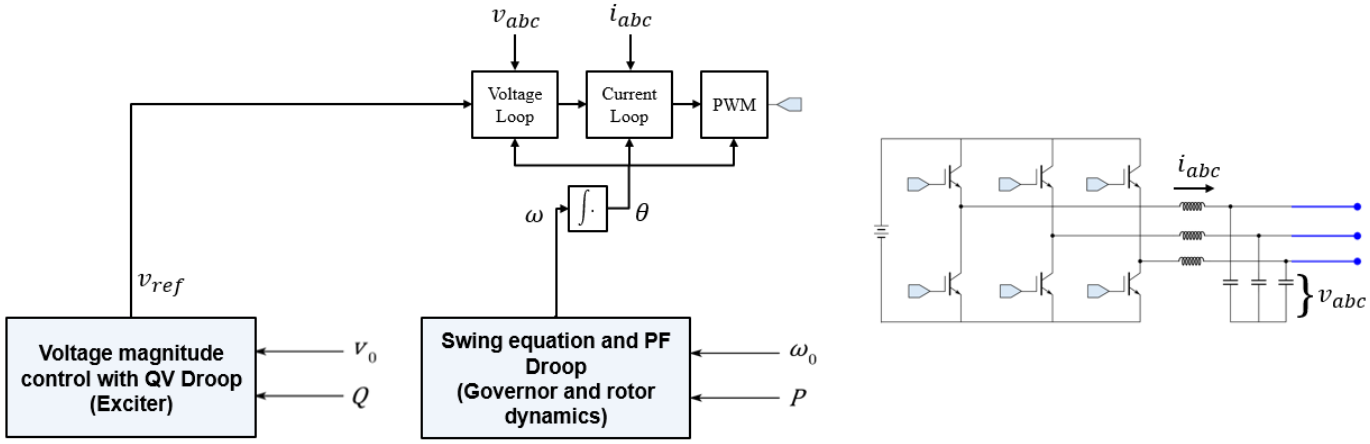

Figure 34: Implementation of Virtual Synchronous Machine with Power Electronics

Using equation 12, a linear control loop can be designed by solving for $\Delta\omega$:

$$\Delta\omega(s) = \frac{1}{\omega_0(Js + D)}(P_{set} - P)$$

$$\boldsymbol{\theta(s) = \frac{1}{s}\left[\omega_0 - \frac{1}{\omega_0(Js + D)}(P_{set} - P)\right]} \quad \textbf{(13)}$$

The exciter provides the voltage magnitude reference by implementing the QV droop curve, as shown in Figure 34. The QV droop curve relates the voltage magnitude to the reactive power Q using the QV coefficient k_q.

$$\Delta v = k_q(Q_{set} - Q) \quad (14)$$

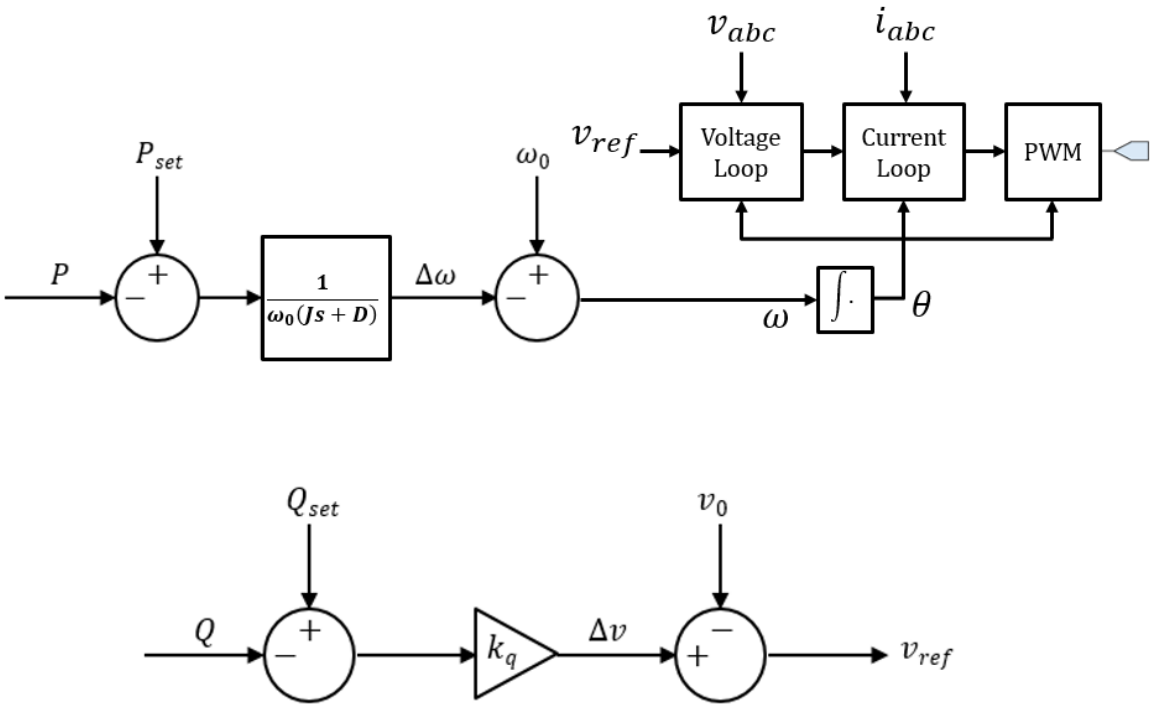

Figure 35: Control loops for VSM implementation

A simple way to describe the behavior of the control loop in Figure 35 is to consider that the error between P_{set} and P is multiplied by a gain and allowed to accumulate over time. This slows down the loop, instead of directly translating the error into a control command that corrects the error instantaneously. The smaller the gain, the slower the loop, and therefore, the larger the virtual inertia of the inverter output voltage.

4.3.3 Equivalence of VSM and Droop Control

The power-frequency relationship in droop control and VSM without inertia is identical [35]. This stems from the fact that droop control was inspired by the behavior of the speed governor of rotating machines, as explained earlier in this chapter. The primary difference between droop-based control and VSM is the property of VSM to exhibit virtual inertia. Essentially, VSM is

simply a 'stiffer' version of droop control. A closer look at Equation 13 reveals the equivalence of VSM and droop control when inertia is removed, i.e. $J = 0$:

$$\theta(s) = \frac{1}{s}\left[\omega_0 - \frac{1}{\omega_0 D}(P_{set} - P)\right] \tag{15}$$

Comparing the above equation with Equation 8, it can be observed that the form is identical. The relationship between damping coefficient D of the machine windings and $P\omega$ droop coefficient k_p can be equated as follows:

$$k_p = \frac{1}{\omega_0 D} \tag{16}$$

Droop control is often used with a low pass filter to suppress higher ordered harmonics. This is often required for real world systems with high frequency harmonics generated by power electronics converters. Figure 36 represents the $P\omega$ droop control with a first order low pass filter having cutoff frequency ω_c. The value of ω_c is designed to allow sufficient attenuation of the high frequency harmonics.

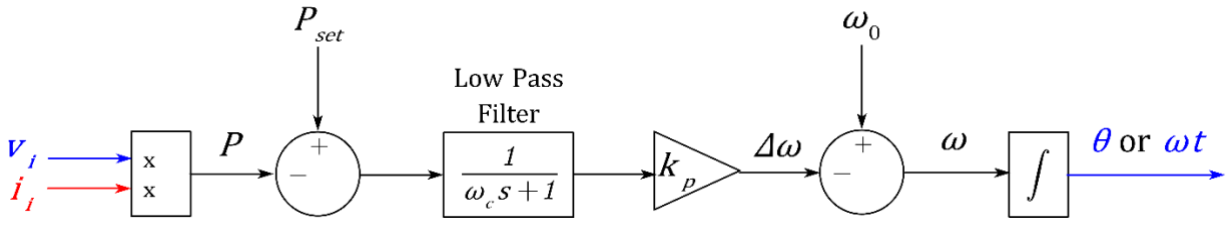

Figure 36: Power-Frequency Droop control loop with Low Pass Filter

The frequency domain equation for the angle θ can be written as follows:

$$\boldsymbol{\theta(s) = \frac{1}{s}\left[\omega_0 - \frac{k_p}{\omega_c s + 1}(P_{set} - P)\right]} \tag{17}$$

Taking a close look at equations 13 and 17, the similarity can be observed. In both control loops, the error between P_{set} and P is multiplied by an integral term. An equivalent design of VSM and droop control with low pass filter may be developed if this term is designed to be equal. This can be expressed as follows:

$$\frac{k_p}{\omega_c s + 1} = \frac{1}{\omega_0 (Js + D)}$$

$$\frac{k_p}{\omega_c s + 1} = \frac{1/\omega_0 D}{\frac{J}{D} s + 1} \tag{18}$$

Equation 17 shows the relationship between all parameters required for an equivalent design of VSM and droop control with low pass filter. The relationship between Damping coefficient D of the machine windings and $P\omega$ droop coefficient k_p is the same as previously derived in equation 16. Additionally, the relationship between the low pass filter cutoff frequency ω_c and moment of inertia J can be represented by the equation:

$$\omega_c = \frac{J}{D} \tag{19}$$

4.3.4 VSM Control Loop Design Example

There are two parameters to be selected in the design of this control loop – the damping coefficient D, and the virtual moment of inertia J. A design example is presented for these parameters, considering the Lanai grid:

1. <u>The Damping Coefficient D:</u>

Damping coefficient of the machine has the same effect as the $P\omega$ droop coefficient, as presented in equation 16. Therefore, the value of D is designed to achieve the same effect as the $P\omega$ droop curve. For the Lanai grid example, the value of D can be calculated using $k_p = -1.16 * 10^{-5}$ (as calculated in section 4.2.4), and $\omega_0 = 2\pi 60\ Hz$

$$\boldsymbol{D = 228.67}$$

2. Virtual Inertia J:

Virtual inertia is designed to mimic the slow response of synchronous generators. Each generator has a fixed moment of inertia J [36], which is dependent on the physical size of its rotating mass. The Kinetic energy E_k stored by the rotor shaft is dependent on the moment of inertia J, and the frequency of rotation ω. E_k can be calculated using the equation:

$$E_k = \frac{1}{2} J\omega^2$$

$$E_k = HS_g$$

The inertia constant H characterizes the ability of a synchronous generator to maintain its speed following a disturbance. It is defined as the unit Kinetic energy divided by the rated generator capacity S_g at nominal rotation speed ω_0 [37]. The unit of H is seconds if S_g is defined in MVA.

$$H = \frac{J\omega^2}{2S_g} \tag{20}$$

The common range of inertia constant is 2 – 7 seconds for synchronous generators with MW range power rating [36]. For the Lanai grid example, J can be calculated by using $H = 4\ sec$, $\omega = 2\pi 60\ Hz$, and $S_g = 1.3\ MVA$:

$$\boldsymbol{J = 7.3 * 10^{-5}}$$

For rotating machine and power converter to have equivalent inertia, the energy stored by the rotating mass must be equal to the energy stored in the DC link of the inverter. If the inverter

has capacitance C across the DC link voltage V_{DC}, the energy stored by the capacitor E_C is given by:

$$E_C = \frac{1}{2} C {V_{DC}}^2$$

The value of the capacitor can be calculated by using $E_C = 1.44\ kWhr$, and $V_{DC} = 5\ kV$:

$$\boldsymbol{C = 416\ mF}$$

4.4 Summary

- The origins of droop control can be traced back to the principle of power sharing and synchronization among rotating machines operating in parallel. The fundamental assumptions of droop control are:
    - The power angle δ between the sources is small enough to be approximated as $\sin \delta \approx \delta$
    - Increasing frequency ω indirectly increases the power angle δ while decreasing frequency ω indirectly reduces the power angle δ
- The VSM makes power converters emulate the dynamics of synchronous machines. These dynamics include the behavior of the governor, exciter, and inertia of the rotor shaft.
- The physical energy storage for inertia in the machine comes from the rotating mass. When virtual inertia is implemented in inverters, the energy stored across the DC link voltage is utilized.
- Droop control with a low pass filter is identical to the VSM. Therefore, they can be designed to be equivalent.

Chapter 5: Fundamental Challenges in Droop and VSM Control Schemes

5.1 Introduction

This chapter explains the fundamental challenges in droop and VSM control schemes. The assumptions of these control schemes are analyzed, and it is shown that the control behavior can exhibit unexpected results when these assumptions are invalid. The steady state power flow equation, that is the basis of droop control laws, has three assumptions: small power angle δ, constant frequency ω, and no harmonics. These three assumptions have been considered true for more than 140 years in the electrical machine-based power systems. However, they may be invalid for power-electronics based power systems.

Furthermore, a consequence of using VSM control in power converters is also explained in this chapter. Electrical machines have high over-current capability, which allows the machine to supply a large amount of current during transients, faults and disturbances. However, power converters do not have such large over-current capability, which causes the control loop of the converter to enforce a current limit. Due to this current limit, power converters cannot exactly mimic the behavior of electrical machines during transient and fault conditions.

In order to demonstrate the cases in which droop and VSM control schemes exhibit unexpected control behavior, two transient conditions have also been specified: Phase angle jump in the bulk grid voltage, and a step change in the power setpoint of the inverter.

5.2 Transients Used to Examine Control Behavior

For the defined system and equivalent test circuit, there are two transient cases that can be considered. The first transient case is a voltage sag in the power system that causes a phase angle jump [38] in the grid voltage v_g at time $t = a$, as represented in Figure 37. The phase jump causes a disturbance in the power delivered by the inverter.

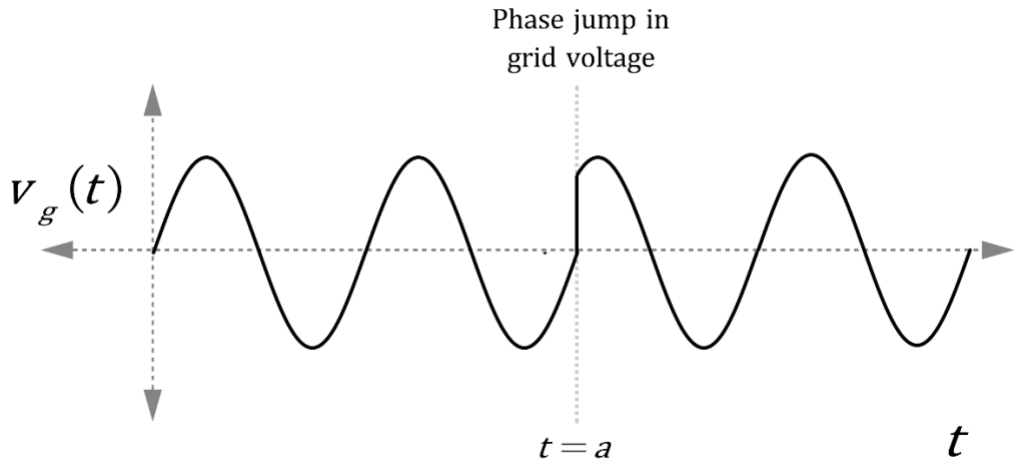

Figure 37: Representation of phase jump in grid voltage

The second transient case is simply a step change in the active power *P* setpoint. This test case will also be used in the rest of this thesis to highlight how the power reference setpoint is followed by the different control schemes.

5.3 Issues with Droop Control

The assumptions in the power flow equation, which form the basis for droop control laws, pose three distinct challenges., as represented in Figure 38.

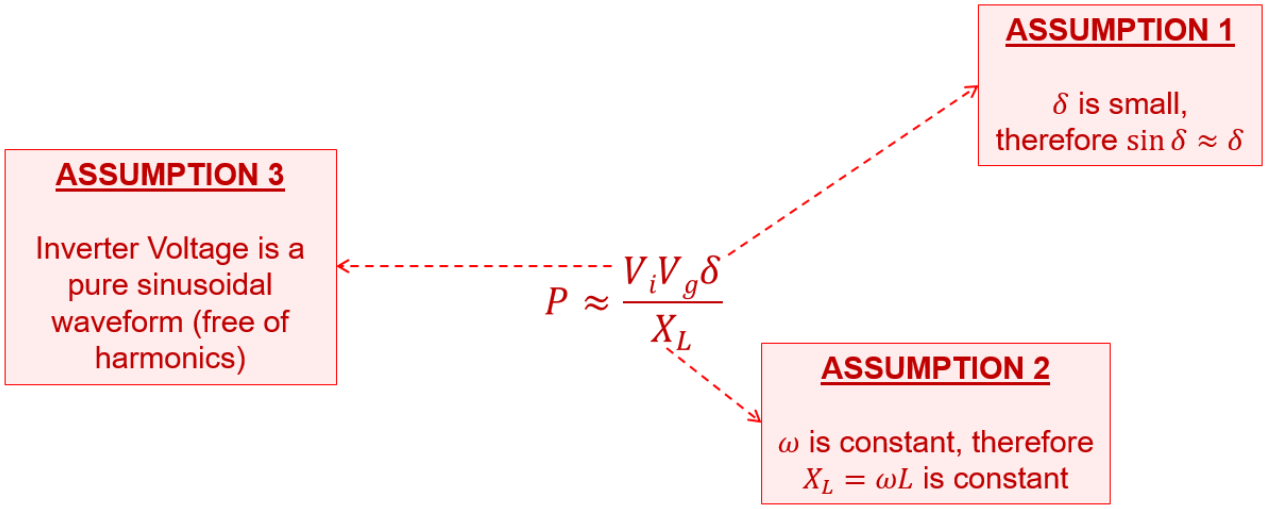

Figure 38: Assumptions in steady state power flow equation

- **ASSUMPTION 1: APPROXIMATION OF $\sin\delta \approx \delta$**

The first assumption stems from the approximation that δ is a small value. In synchronous generators-based power systems, this assumption holds true, as δ changes only slightly when the machines are synchronized together, due to the machine's rotating mass [39]. Any sudden or large change in δ may lead to the risk of a rotating shaft being damaged due to significant torque. However, in power electronics-based power systems, this assumption may not always apply, as the output sine wave is generated by a control system, allowing δ to have any value between 0 and 360° at any given moment depending on the control commands. As represented in Figure 39, there are three separate regions of operation in the $P - \delta$ relationship. Region 1 is the well-recognized region when δ is between 0 and 90°, in which the active power P increases with the increase in δ. Region 2 is the commonly neglected region when δ is between 90° and 270°, in which the active power P decreases with the increase in δ. Region 3 is also similar to Region 1 with respect to the relationship between P and δ.

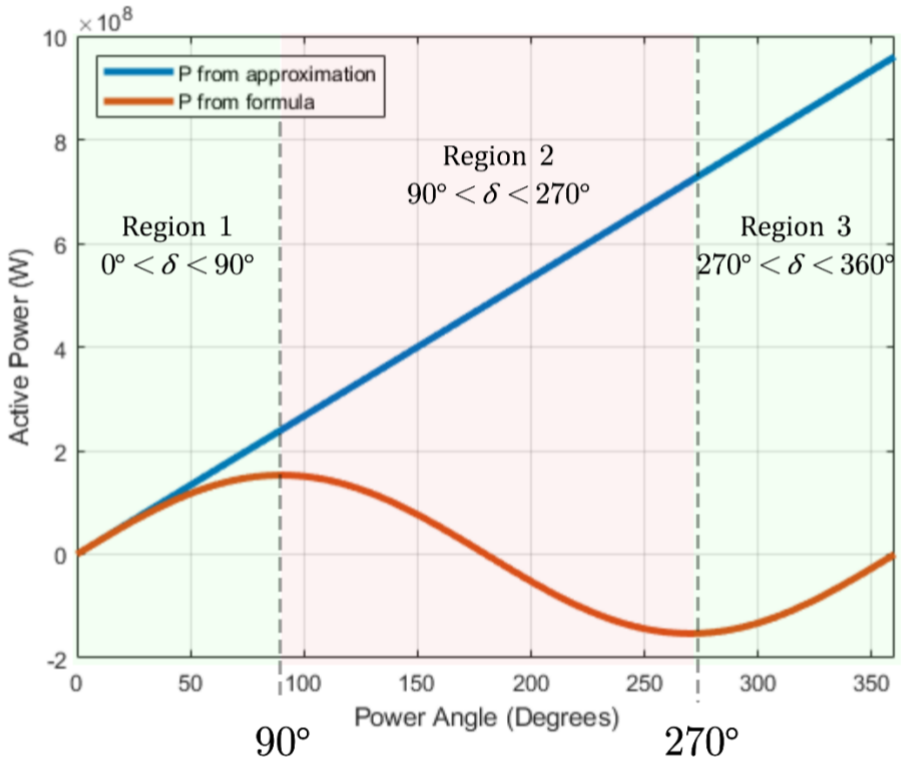

Figure 39: Regions of operation in Power-Frequency Droop Curve

Droop control law is based on region 1 and 3. However, droop control will produce unexpected behavior when it encounters the situation of δ being between 90° and 270°. This behavior can be attributed as positive feedback in the control loop. In order to demonstrate the control law breakdown in this region, a simulation is setup with the same balanced three phase circuit presented in Figure 28.

Figure 40 presents the simulation result in which the objective of the droop control loop is to regulate the active power P to a P_{set} value of 0. Hence, the steady state value of δ is 0°. At time $t = a$, a phase jump in v_g makes δ jump to a new value of 15°. An oscillation can be seen in P after the disturbance event, because of the inverter currents. As seen in Figure 40, the transient inverter currents have a DC offset initially due to the inductive transmission line. As seen in the

simulation result, the phase jump causes P to increase, due to increase in δ. The control loop responds by decreasing the frequency ω, which causes v_i to realign with v_g and a decrease in δ. Subsequently, P goes back to the P_{set} value of 0 within the duration of a few cycles, depending on the value of the droop coefficient k_p. This case represents the expected and well-recognized behavior of the droop control loop.

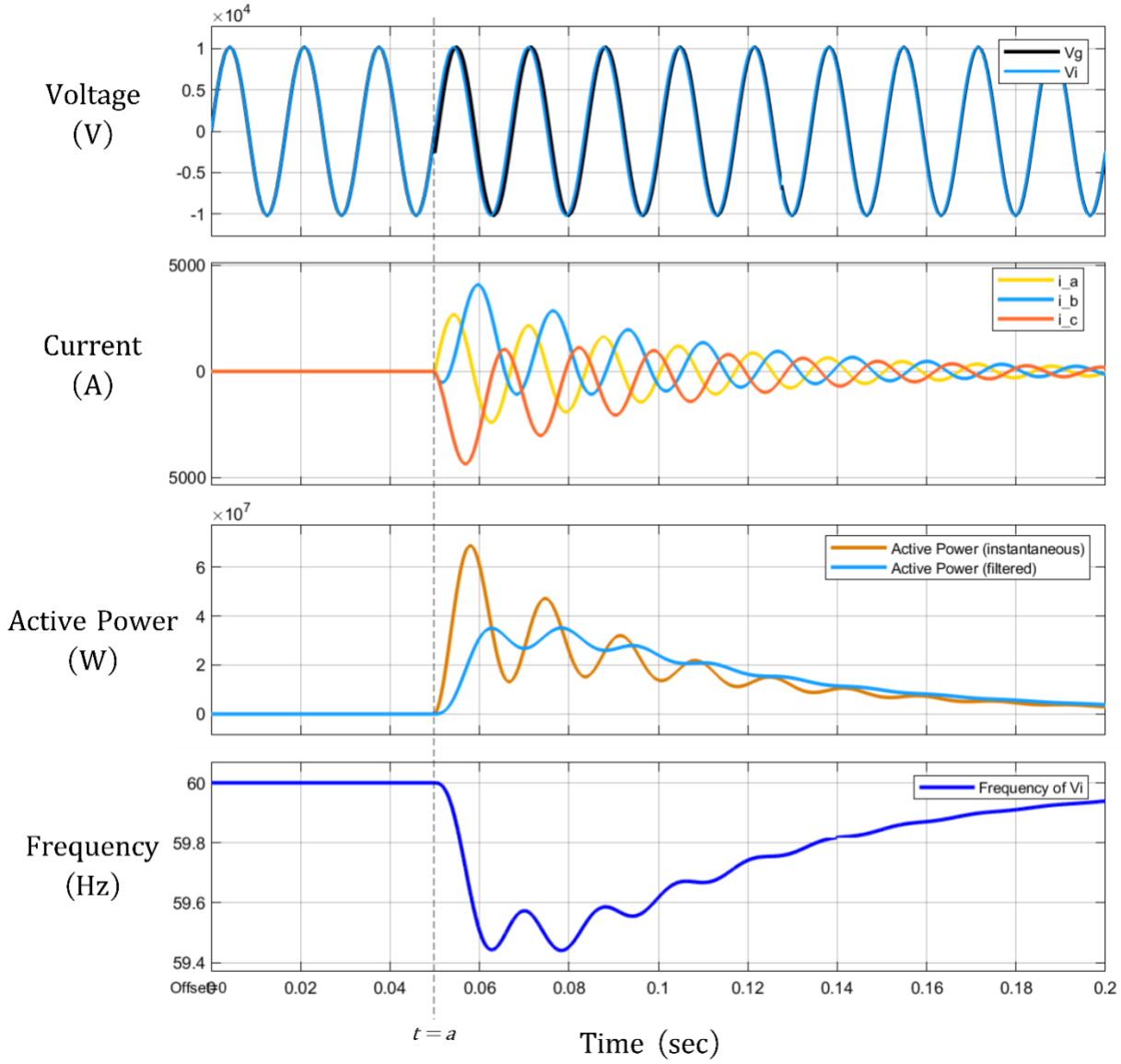

Figure 40: Simulation results representing normal behavior of droop control (response to 15° phase jump in grid voltage)

Figure 41 presents the simulation result in which there is a phase jump in v_g time $t = a$, that makes δ jump to a new value of 180°. As seen in the simulation result, the phase jump causes P to increase. The control loop responds by decreasing the frequency ω. The expected result is that P should decrease and go back to the P_{set} value of 0. However, since δ is in between 90° and 270°, the relationship between P and δ is inverted as described in the region 2 mode of operation. As a result, P keeps on increasing because the control loop responds by decreasing the frequency ω. This case represents the unexpected scenario in which the well-recognized behavior of the droop control loop falls apart, and the controller is unable to regulate P to the value of P_{set}.

Due to the unexpected behavior when δ is not small, the active power P may exceed the maximum power capability of the inverter, causing the inverter to trip. This may lead to a power system blackout if the inverter supplies a significant portion of the total power of the system.

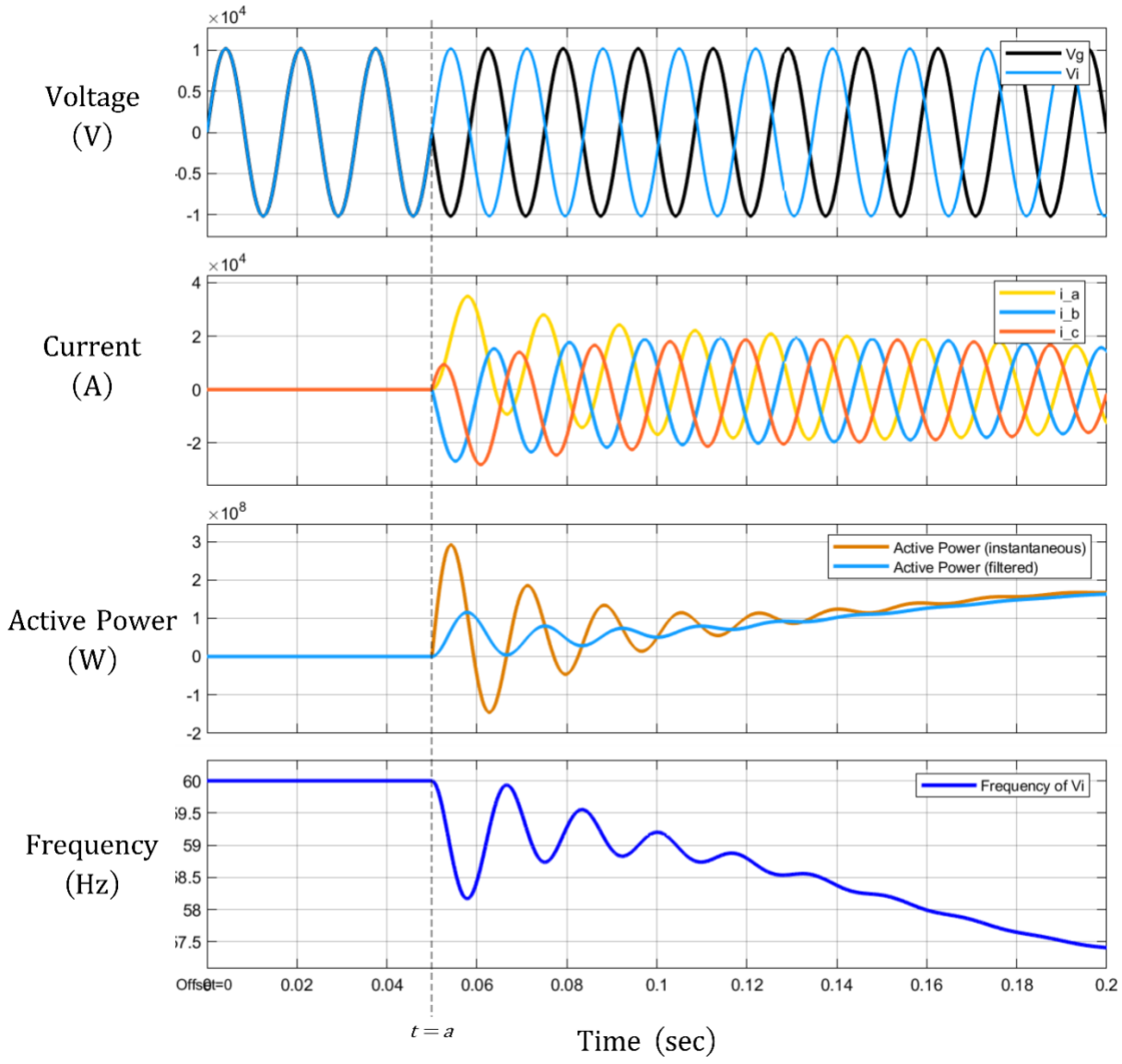

Figure 41: Simulation results representing normal behavior of droop control (response to 180° phase jump in grid voltage)

- **ASSUMPTION 2: CONSIDERATION OF ω AS A CONSTANT**

The second challenge stems from the assumption that the frequency ω is a constant value in the power flow equation.

This is true only if the frequency of both sources in the equivalent test circuit (shown in Figure 28) ω and ω_0 are constant. However, in reality, droop control changes ω as the control command. The power flow calculated in Equation 3 is actually a steady state value. A dynamic equation for active power can also be derived. From the circuit in Figure 28, if the line resistance R is considered negligible, the voltage across the inductor v_L in each phase can be calculated using the inverter and grid voltage sinusoidal functions with frequencies ω and ω_0 respectively.

$$v_L(t) = v_i(t) - v_g(t)$$

$$v_L(t) = V_i \sin \omega t - V_g \sin \omega_0 t$$

The equation for the voltage across inductor can then be used to calculate the inverter current i_i.

$$v_L(t) = L\frac{d}{dt} i_i$$

$$i_i(t) = \frac{1}{L}\left[\int V_i \sin \omega t \,.\, dt - \int V_g \sin \omega_0 t \,.\, dt\right]$$

$$i_i(t) = \frac{\omega V_g \cos \omega_0 t - \omega_0 V_i \cos \omega t}{\omega \omega_0 L}$$

The instantaneous power P_a delivered to the grid in phase A is:

$$P_a(t) = v_{ga}(t).\, i_{ia}(t)$$

$$P_a(t) = \frac{\omega {V_g}^2 \cos \omega_0 t - \omega_0 V_i V_g \cos \omega t}{\omega \omega_0 L} \sin \omega_0 t = |P_a|_{(t)} \sin \omega_0 t \qquad (21)$$

Similarly, it is possible to calculate the instantaneous power $P_b(t)$, and $P_c(t)$ delivered to the grid in phases B and C respectively. The three power $P(t)$ is shown below.

$$P(t) = P_a(t) + P_b(t) + P_c(t)$$

It is evident from Equation 21 that $P_a(t)$ has a time-varying magnitude $|P_a|_{(t)}$ that depends on both the inverter and grid voltages frequencies ω and ω_0. Figure 42 shows a visualization of the instantaneous three phase power $P(t)$ for $\omega_0 = \omega$ and also $\omega_0 > \omega$. The condition for maximum steady state power delivered to the grid will be when $\omega = \omega_0$ and the angle between v_i and v_g is 90°. The maximum steady state three phase power can be calculated by:

$$P_{max} = \frac{3V_iV_g \sin 90°}{X_L} = \frac{3V_iV_g}{X_L}$$

As seen in Figure 42, there is a decrease in the peak power that can be delivered to the grid as the frequency ω of inverter voltage increases. As a consequence, any power setpoint within the red region as highlighted in the figure cannot be achieved by the inverter.

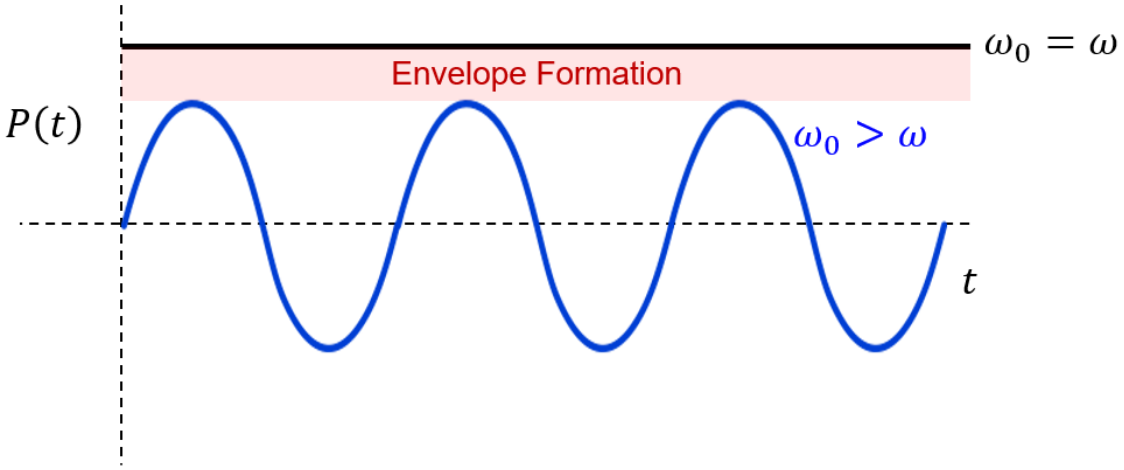

Figure 42: Plots of instantaneous three-phase power $\boldsymbol{P(t)}$ for different values of source frequencies $\boldsymbol{\omega}$ and $\boldsymbol{\omega_0}$

Similar to the previously highlighted issue, this problem may not be significant for the legacy power systems with synchronous generators because the frequency is tightly regulated within a specific range according to the standards [32], and the power angle δ is rarely above 15° [39]. However, for a power electronics-based system, this problem could be encountered if a faster droop control loop is used with a bigger droop coefficient k_p. In such a scenario if a power setpoint P_{set} and it's corresponding commanded frequency lies within one of the red regions highlighted in the figure, the control loop will be unable to track the P_{set} command.

- **ASSUMPTION 3: NO HARMONICS IN INVERTER VOLTAGE**

The third assumption is that the grid voltage v_g is an ideal sinusoidal voltage source with no harmonics. However, in reality, v_g could contain multiple harmonics due to switching of the inverter. In such a case, the calculated instantaneous three phase power $P(t)$ may contain oscillations. Therefore, a low pass filter must be used to filter out the oscillations from the calculated power $P(t)$.

5.4 Issues with Virtual Synchronous Machine (VSM) Control

The fundamental challenge with VSM is the assumption that power electronics converters can completely emulate synchronous machines in all operating conditions. The strength of power electronics is fast control bandwidth, and its weakness is limited overcurrent capability. By forcing power converters to mimic the slow dynamics of machines, the strength of power electronics is not fully utilized and the weakness of limited over-current capacity is exposed.

Inertia in electrical machines is an inherent property that exists because of the machine's rotating mass. Kinetic energy is stored in the rotor, which is utilized and then stored up again during transients, disturbances, and faults. On the other hand, with power electronics, there is usually a capacitor at the DC link that provides physical energy storage, along with optional battery energy storage, as shown in Figure 43. The energy stored by the capacitors is usually much lesser than the energy stored by the machine's shaft.

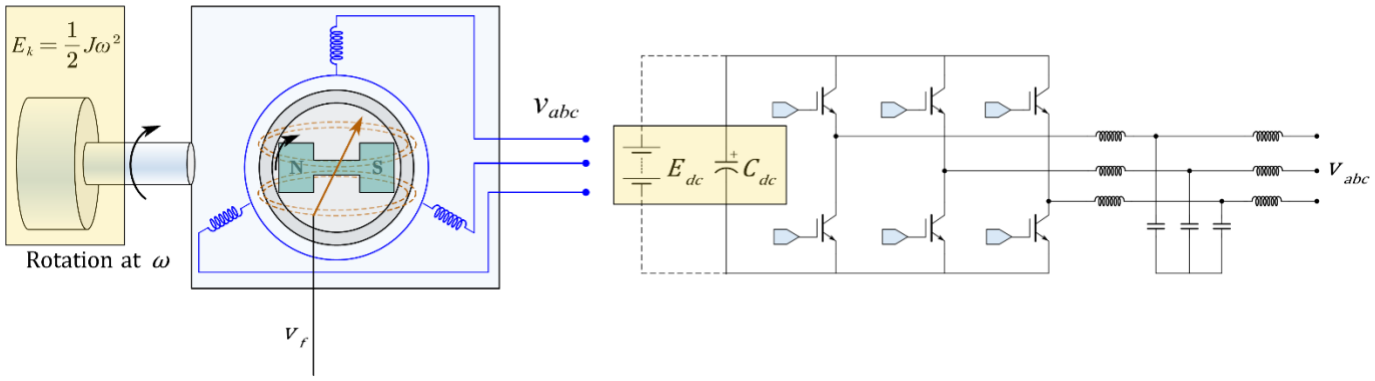

Figure 43: Energy storage components for providing inertia through rotating machines vs. power converters

Electrical machines can provide output current up to 8 – 10 times of their nominal rating [40] in the event of transients and faults. However, in power electronics, it is possible to only provide a maximum output current of 1.5 – 2 times of their nominal rating [41]. Figure 44 shows the range of voltages and currents for power converters. The maximum possible current magnitude effectively creates a region of operation as shown in the figure. This region represents the rated approximate power (MVA rating) of the inverter. The maximum output voltage magnitude of the inverter is also limited by the DC link voltage V_{DC},

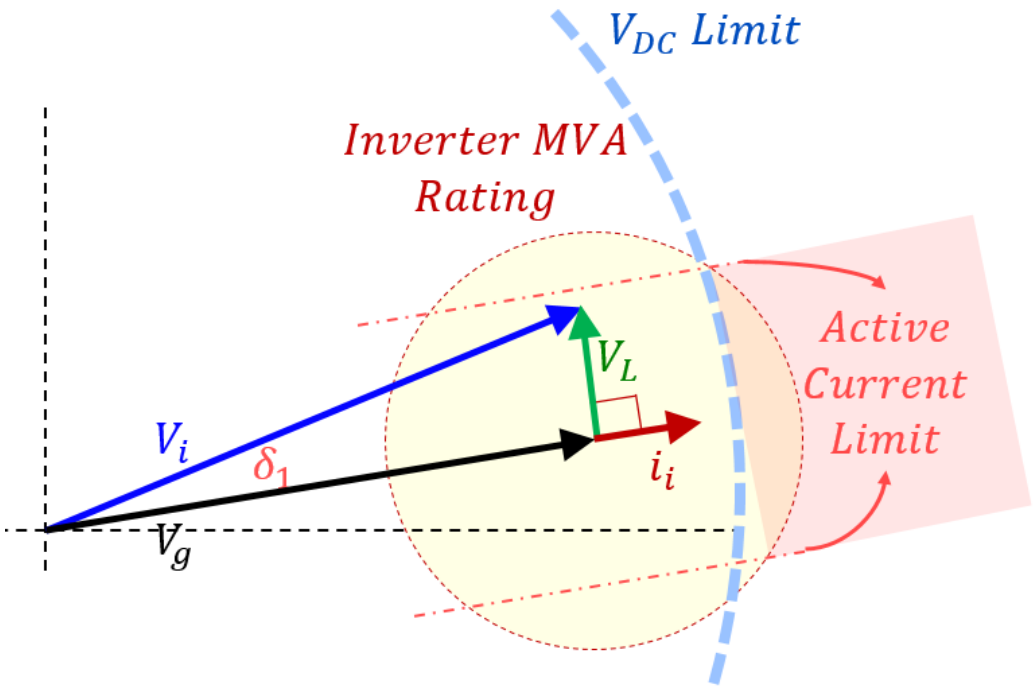

Figure 44: Steady State Range of Operation in Power Converters

The region of operation represented in Figure 44 specifies the current limit of power converters. If the current exceeds this threshold, the converter will either trip, or enforce a current limit i_{max} (as shown in Figure 45) to protect the semiconductor switches.

When virtual inertia is emulated by power converters, as shown in the VSM control loop in Figure 35, the inertial term slows down the corrective action of the droop control loop, just like an electrical machine would react to a disturbance. Due to the delay in corrective action in case of a disturbance, the inverter may be required to produce output current much greater than the over-current threshold.

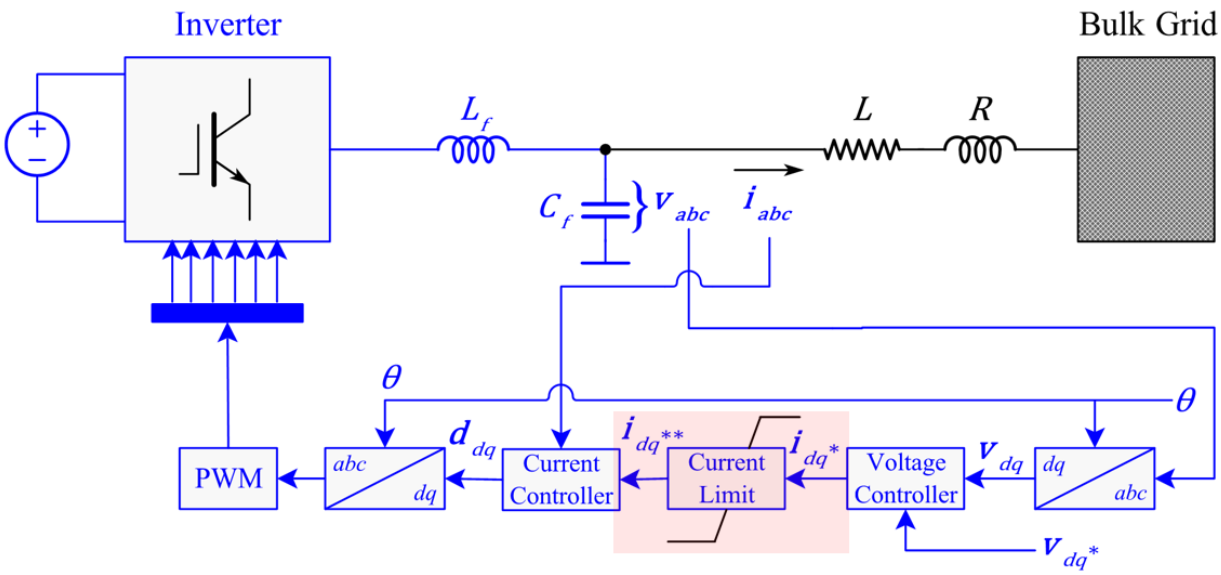

Figure 45: A typical inverter control loop with inner current and outer voltage loop, highlighting the current limit block

Figure 46 presents the simulation result that shows the inverter current exceeding the over-current threshold, due to the VSM control loop. In this simulation, P_{set} is 0, therefore the steady state value of δ is 0°. At time $t = a$, a phase jump in v_g makes δ jump to 5°. P increases due to increase in δ. The control loop responds by slowly decreasing the frequency ω, which causes v_i to realign with v_g, which decreases δ. Subsequently, P goes back to the P_{set} value of 0 within a duration that is clearly larger than the duration taken by the droop control loop. The slow corrective action of the control loop causes a significant flow of output current. The inverter's over-current threshold is highlighted in the figure.

The inverter has two options to deal with over-current. The first option is to trip, and the second is to enforce a current limit, which would cause the voltage to become uncontrolled. In this case, the inverter ceases to remain 'Grid Forming' and does not establish the voltage and

frequency. If the inverter supplies a significant portion of the total power of the system, this could also lead to a power system blackout.

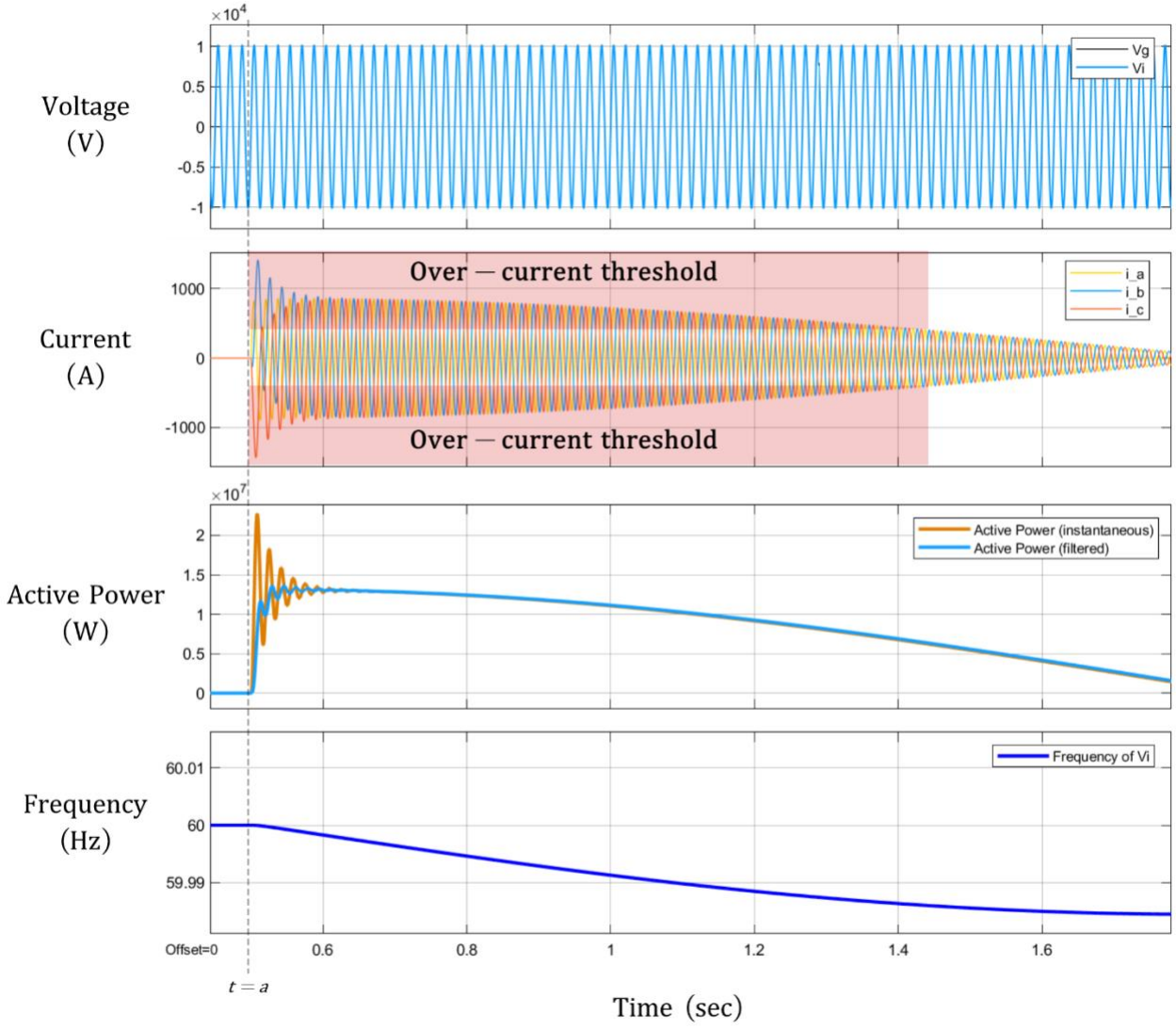

Figure 46: Simulation results representing behavior of VSM (response to 5° phase jump in grid voltage)

5.5 Summary

- The three fundamental underlying assumptions of droop control (small δ, Constant ω, and no harmonics) may have been true for the legacy power systems comprising of electrical machines connected to load. However, these assumptions may not be valid for power electronics-based power systems.
- By emulating rotating machines, the strength of power converters (fast control dynamics) is not fully utilized, and its weakness (limited overcurrent capability) is exposed.
- Power converters cannot completely emulate inertia like rotating machines, even if the physical energy storage at DC link is provided, because of limited overcurrent capability. Therefore, even though virtual inertia may be programmed within the software controls of the inverter, the limited over-current capability of the semiconductor switches causes a bottleneck in virtual inertia implementation.
- When the current limit of inverters is exceeded, the inverter either trips, or enforces a current limit that causes the inverter to supply a constant current – hence, it ceases to be grid forming.

Chapter 6: Challenges of Phasor Representation for Power Electronics Control

6.1 Introduction

This chapter introduces the fundamental issue with phasor-based representation. Phasors were introduced to simplify calculations in AC power systems by reducing the time-varying sinusoidal functions to two steady state values: magnitude and phase. By eliminating time from the sinusoidal functions of electrical quantities, it is assumed that the frequency is a steady state value which remains constant throughout the AC cycle. In electrical machines, the sinusoidal voltage is generated by rotation of the machine's shaft. Therefore, the frequency within the cycle can be determined at every point in time by measuring the rate of change of the angular velocity of the shaft. However, in power electronics-based systems, frequency within the cycle may not be constant at every point due to the fast control dynamics. Phasor-based representation cannot represent these instantaneous changes within the AC cycle. This chapter also explains how the dynamic phasor attempts to create a more dynamic representation, but it is not truly instantaneous due to the presence of a sliding time window in the calculation.

Due to inaccurate representation of electrical quantities when the frequency within the AC cycle is not constant, it is not suitable to use phasor-based calculations to develop control methods for power electronics.

6.2 Fundamental assumption of phasor-based representation

Phasor representation is only valid for steady state quantities in which the frequency does not change within the AC cycle. Therefore, phasors cannot represent the dynamics within the cycle. Power systems with electrical machines have slow dynamics in the timescale of multiple cycles. However, in power electronics-based systems, the dynamics within the cycle cannot be neglected because of the fast control bandwidth.

In AC power systems, electrical quantities are time varying but periodic, sinusoidal functions. As an example, a sinusoidal voltage $v(t)$ can be expressed using the voltage magnitude $|V_m|$, the angle which is calculated using a constant frequency ω, and any phase shift in the angle given by $\emptyset$. $v(t)$ can be represented by the following equation:

$$v(t) = |V_m| \sin(\omega t + \emptyset) \tag{22}$$

Phasor representation is a very useful method of expressing electrical quantities in power engineering because it can reduce periodic functions of an independent variable, time, to a constant numerical quantity. Time is eliminated from this function by assuming it as a constant. This assumption significantly reduces the calculations in AC systems to elementary algebra of constant quantities [42]. Phasors can be graphically represented using complex exponential functions:

$$V_m \cos(\omega t + \emptyset) + iV_m \sin(\omega t + \emptyset) = V_m e^{i(\omega t + \emptyset)} \tag{23}$$

If ωt is assumed to be constant, $v(t)$ can simply be represented by defining the voltage magnitude V_m and the phase shift $\emptyset$. This fundamental assumption gives rise to the phasor notation $V_m \angle \emptyset$, and the phasor diagram as shown in Figure 47.

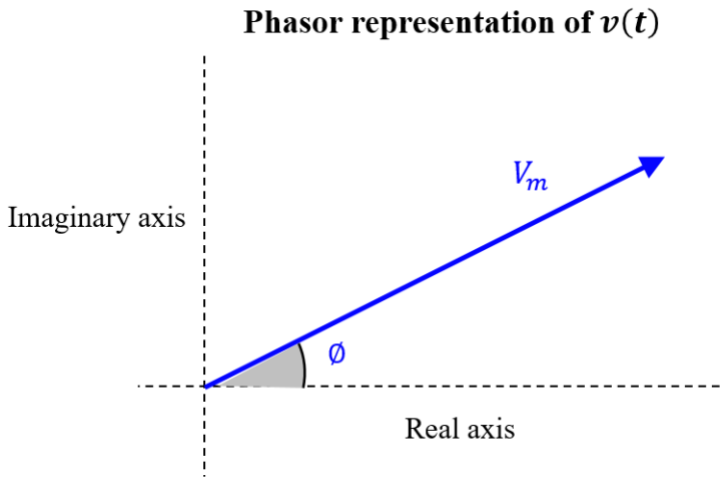

Figure 47: An example of a phasor representation for a time varying voltage $\boldsymbol{v(t)}$

Using phasors in calculations and analyses of electrical machines-based power system has been very useful. However, caution must be exercised while using phasor representation for systems with fast dynamics within the timescale of a cycle or less. It is essential to always remember the fundamental assumption of phasors that frequency is treated as a constant.

6.3 Frequency Measurement in Mechanical vs. Electrical Systems

The fundamental assumption of phasors leads to a fundamental question – What does frequency even mean? (in the context of electrical machines and power electronics in a power system). Figure 48 shows the measurement of frequency in rotating machines and power electronics. Frequency ω is defined as the rate of change of angular displacement. The change in angular displacement is represented by θ. If the frequency is measured within the cycle in between two points in time t_1 and t_2, it can be referred to as instantaneous frequency $\omega_{(t)}$.

$$\omega_{(t)} = \frac{d\theta}{dt} = \frac{\theta}{t_2 - t_1} \tag{24}$$

In mechanical systems, θ is a physical displacement that can be measured at every instant. Therefore, the frequency of a machine can be defined instantaneously at any point in time within the cycle of rotation.

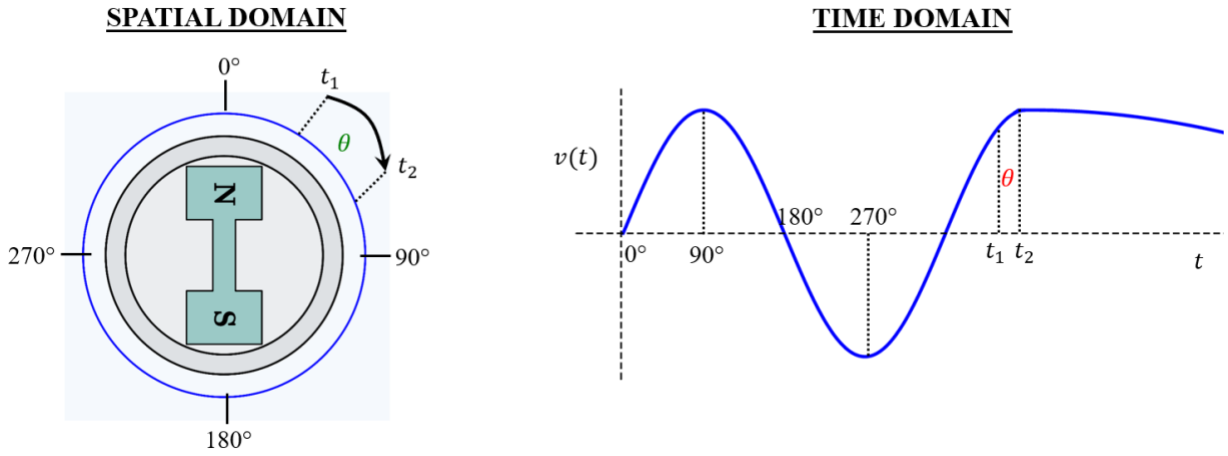

Figure 48: Measurement of frequency in electrical machines (spatial domain) vs. power converters (time domain)

As for the time domain-based representation, the frequency ω is defined as the rate of change of the electrical angle. There is a major drawback in the measurement of frequency for time domain signals. The change in electrical angle cannot be measured instantaneously, because the angle cannot be specified with certainty at time t_1 and t_2, without knowledge of the future. As shown in Figure 48, the waveform of $v(t)$ could have any value after time t_2. Therefore, it is not possible to accurately specify instantaneous frequency in the time domain at any arbitrary point within the cycle.

In power systems dominated by power electronics, the instantaneous frequency $\omega_{(t)}$ may vary within the cycle due to fast control dynamics. This variation in $\omega_{(t)}$ goes against the fundamental assumption of phasors i.e. constant frequency.

6.4 Dynamic Phasor as a Possible Solution for Power Electronics Control

A dynamic phasor is a method of expressing time varying quantities that do not have a fixed frequency or contain multiple frequency components [43]. In recent literature, this technique is stimulating a lot of research for modeling of large power electronics-based systems [44].

Dynamic phasors are time varying phasors that are updated dynamically using a moving average with a sliding window of time period T, as shown in Figure 49. If V_{mk} and ω_k are the magnitude and frequency of the k^{th} phasor, a dynamic phasor is represented as follows:

$$v(t) = \sum_{k=-\infty}^{\infty} V_{mk} e^{ik\omega_k t} \tag{25}$$

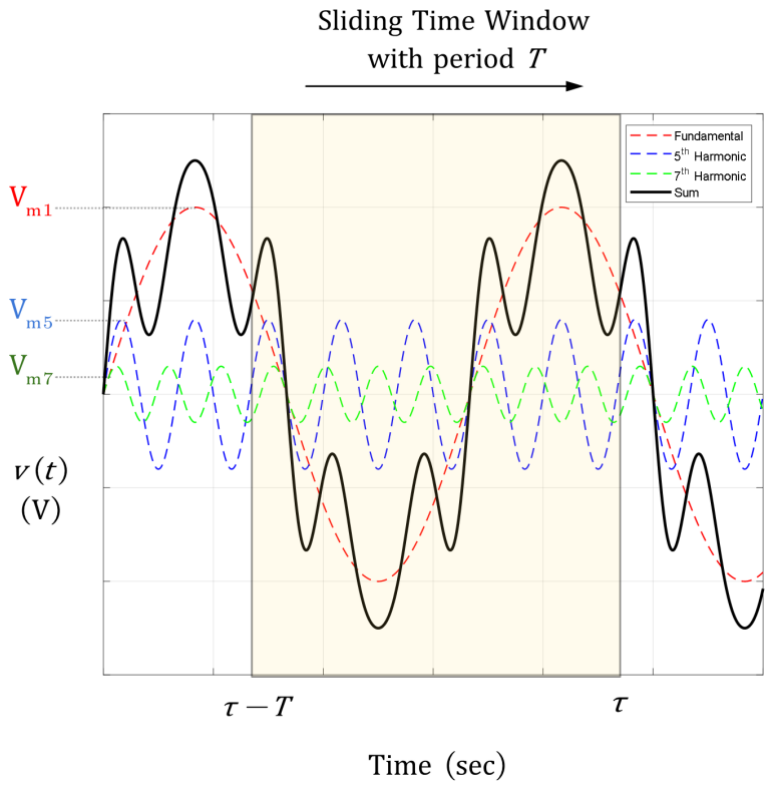

Figure 49: Example voltage waveform v(t) consisting of multiple frequency components

To illustrate how dynamic phasor represents a time domain waveform, a voltage waveform $v(t)$ consisting of multiple frequency components – a fundamental frequency ω_1, and its fifth and seventh harmonics ω_5, and ω_7, having magnitudes V_{m1}, V_{m5}, and V_{m7} respectively, is shown in Figure 49. $v(t)$ can be described as the sum of phasors using the expression:

$$v(t) = V_{m1}e^{i(\omega_1 t)} + V_{m3}e^{i(\omega_3 t)} + V_{m5}e^{i(\omega_5 t)}$$

Given the time domain voltage waveform $v(t)$, it is possible to extract the magnitudes V_{mx} (V_{m1}, V_{m3}, V_{m5}, …… V_{mn}) at any point in time τ of the frequency components ω_x (ω_1, ω_3, ω_5, …… ω_n) for a specified time duration T using Fourier transform:

$$V_{mx} = \frac{1}{T}\int_{t-T}^{t} v(\tau)\, e^{-i(\omega_x \tau)}.\, d\tau \qquad (26)$$

In this way, the dynamic phasor represents a time domain signal using a set of magnitudes and frequencies that are updated instantaneously. Since the magnitudes and frequencies are calculated over a time window with period T, the dynamic phasor is dependent on the time period T. If there is a sudden change in the instantaneous value of $v(t)$, it will be represented in dynamic phasor with a delay, because of the moving average with sliding time window.

6.5 Summary

- Phasors can accurately represent the steady state sinusoidal functions that have constant frequency within the AC cycle. However, phasors cannot represent signals when the instantaneous frequency varies within the AC cycle.

- This assumption of the frequency being constant is also inherent in GFM control laws derived in the phasor domain. Therefore, this leads to the problem of steady state control laws being used to control dynamic power electronics-based systems.
- Dynamic Phasors are time varying phasors that can represent the dynamics within the AC cycle. However, dynamic phasors cannot accurately represent sudden changes in the time-domain waveform, as it is dependent on past values due to the use of sliding time window in the calculation.

Chapter 7: Vector Representation of Electrical Quantities

7.1 Introduction

This chapter introduces vector representation of electrical quantities. Since phasors cannot accurately represent dynamics within the AC cycle, vectors are introduced as an alternative to the phasor-based representation. Vectors provide instantaneous representation of electrical quantities at every point in time. Vectors use spherical coordinates to define electrical signals in the $\alpha\beta 0$ frame. In this way, all voltages and currents can be defined by three time varying values: one magnitude and two angles. The main advantage of converting electrical quantities in abc frame to vectors, is that the calculations involving these quantities becomes a matter of elementary algebra of vectors [45].

Vector representation is not a new mathematical concept. The transformation of voltages and currents from abc frame to $\alpha\beta 0$ frame, known as the Clark transform, has previously been widely used in the control of power electronics. In this thesis, vector representation is introduced with the intent of developing new control methods for power converters in grid applications.

7.2 Vector Representation and Definition

A vector is a representation of a time varying electrical signal, defined by three time varying values. Vector $\vec{v}$ in a three-dimensional space can be defined by magnitude $|V_m|_{(t)}$, polar angle $\theta_{(t)}$, and azimuthal angle $\emptyset_{(t)}$, using the spherical coordinate system, as shown in Figure 50, and expressed as follows:

$$\vec{v} = \langle |V_m|_{(t)}, \theta_{(t)}, \emptyset_{(t)} \rangle \tag{27}$$

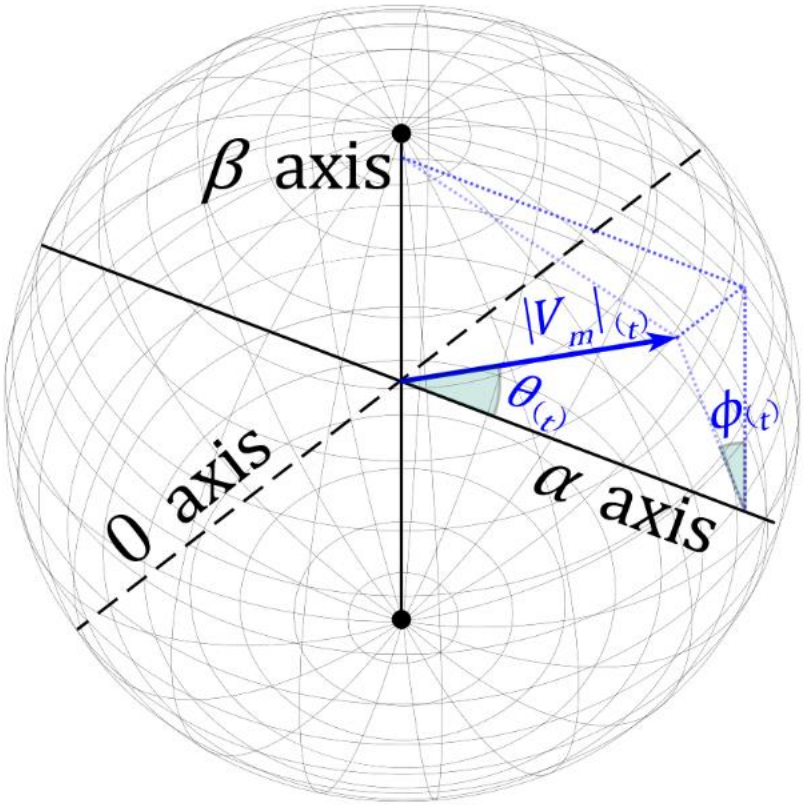

Figure 50: Vector representation through spherical coordinates in a 3-dimensional space

Electrical signals can be converted to a vector in two sequential mathematical transformations, as shown in Figure 51. The first step is the Clark transform, which transforms electrical signals from *abc* frame to $\alpha\beta 0$ frame, shown by the following equation [46]:

$$\begin{bmatrix} v_\alpha(t) \\ v_\beta(t) \\ v_0(t) \end{bmatrix} = \frac{2}{3} \begin{bmatrix} 1 & -\frac{1}{2} & -\frac{1}{2} \\ 0 & \frac{\sqrt{3}}{2} & -\frac{\sqrt{3}}{2} \\ \frac{1}{2} & \frac{1}{2} & \frac{1}{2} \end{bmatrix} \begin{bmatrix} v_a(t) \\ v_b(t) \\ v_c(t) \end{bmatrix} \tag{28}$$

When the three-phase waveform is balanced, the signal can be represented sufficiently by $\alpha\beta$ axes. However, if there is a zero sequence, it can be observed in the *0* axis. For the example shown in Figure 51, the three-phase signal is balanced and therefore, there is no zero sequence.

The instantaneous value of the signal can be represented in the 3-dimensional space of $\alpha\beta 0$ axes, using spherical coordinates. This is done by using the transformation from rectangular coordinates to spherical coordinates as follows:

$$|V_m|_{(t)} = \sqrt{{v_{\alpha}}_{(t)}^{\,2} + {v_{\beta}}_{(t)}^{\,2} + {v_0}_{(t)}^{\,2}} \tag{29}$$

$$\theta_{(t)} = \tan^{-1}\left(\frac{v_{\beta(t)}}{v_{\alpha(t)}}\right) \tag{30}$$

$$\emptyset_{(t)} = \cos^{-1}\left(\frac{v_{0(t)}}{\sqrt{{v_{\alpha}}_{(t)}^{\,2} + {v_{\beta}}_{(t)}^{\,2} + {v_0}_{(t)}^{\,2}}}\right) \tag{31}$$

As the value of the electrical signal changes sinusoidally with respect to time, vector $\vec{v}$ rotates in the three-dimensional $\alpha\beta 0$ axes with instantaneous frequency $\omega_{(t)}$, as shown in Figure 51.

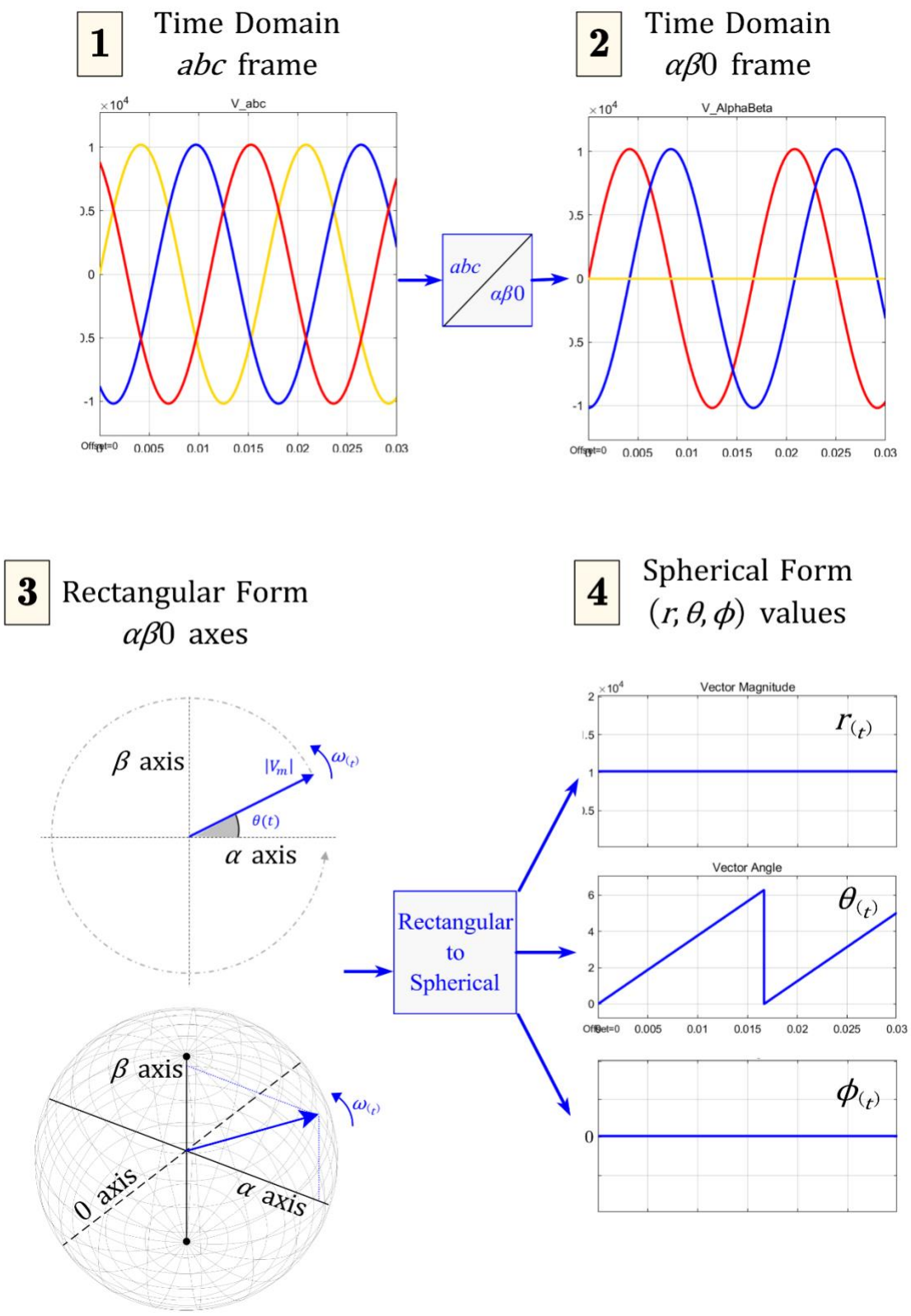

Figure 51: Stepwise conversion of electrical signal to vector

7.3 Advantages of Using Vector Representation

By representing electrical signals as vectors, all voltages and currents in the system can be represented in the three-dimensional space with $\alpha\beta 0$ axes. Simple vector algebra rules can be used for performing calculations on these vectors and their projections. Considering the example of a balanced three phase system with no zero sequence, the voltage and current vectors $\vec{v}$ and $\vec{\imath}$ rotating at a speed of $\omega_{(t)}$ with the angles of $\theta_{1(t)}$ and $\theta_{2(t)}$ respectively can be seen in Figure 52. The current vector $\vec{\imath}$ can be split into its projections in parallel with and perpendicular to $\vec{v}$. The horizontal and vertical projections $\overrightarrow{\imath_x}$ and $\overrightarrow{\imath_y}$ can be calculated as follows:

$$|\overrightarrow{\imath_x}|_{(t)} = |I|_{(t)} \cos(\sigma_{(t)})$$

$$|\overrightarrow{\imath_y}|_{(t)} = |I|_{(t)} \sin(\sigma_{(t)})$$

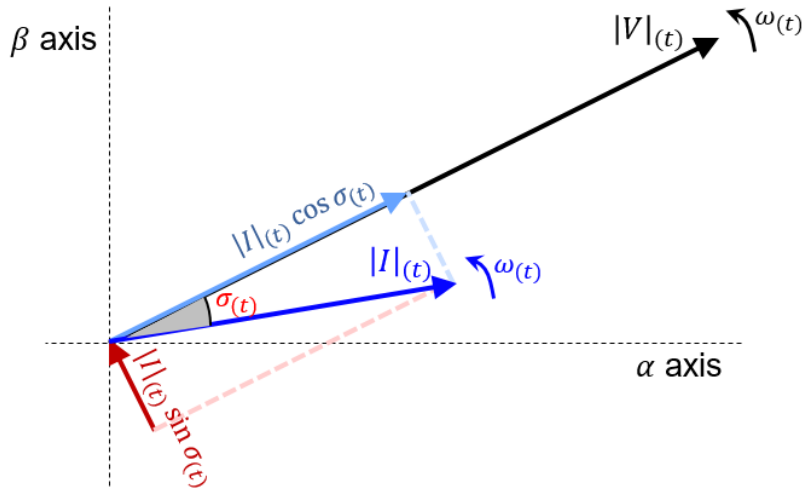

Figure 52: Vector representation of voltages and currents showing projection of vectors and vector algebra

Vector projections can be used to represent the components of a signal along each axis. In the future, these vector components could be controlled dynamically using relationships derived using vector algebra.

The other advantage is that one vector can represent a single or polyphase system, if it is projected onto an axis or multiple axes. Vector $\vec{v}$ can represent either a single phase or three phase system as shown in Figure 53.

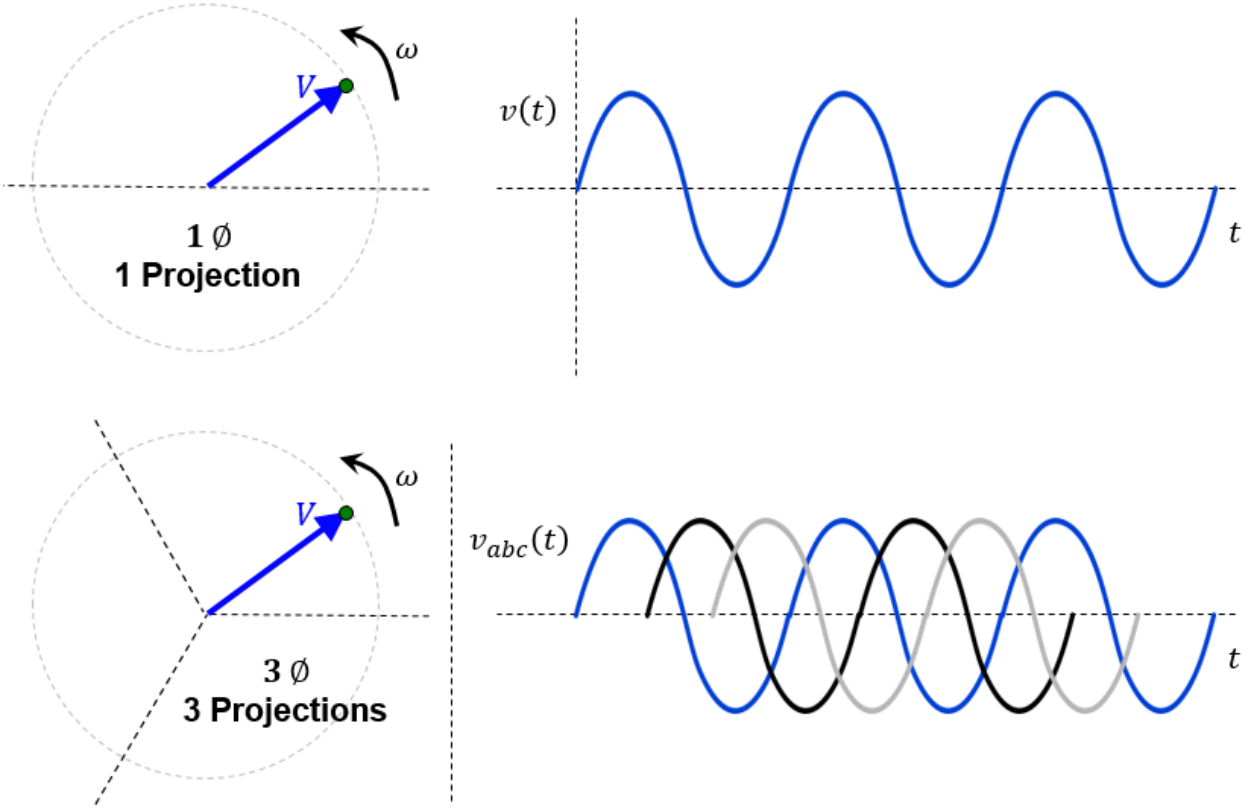

Figure 53: One vector representing single phase and three phase values, depending on the number of projections

7.4 Vector Representation as a Bridge between Mechanical and Electrical Systems

The rotating vectors can also be linked to the operation of rotating machines. The rotor rotates in a circular motion at a speed ω that can be accurately defined at every point within the cycle. A rotating vector representation provides a similar view of looking at electrical quantities as if they are rotating within a spatial domain. Vectors bridge the gap between time domain and spatial domain, as shown in Figure 54.

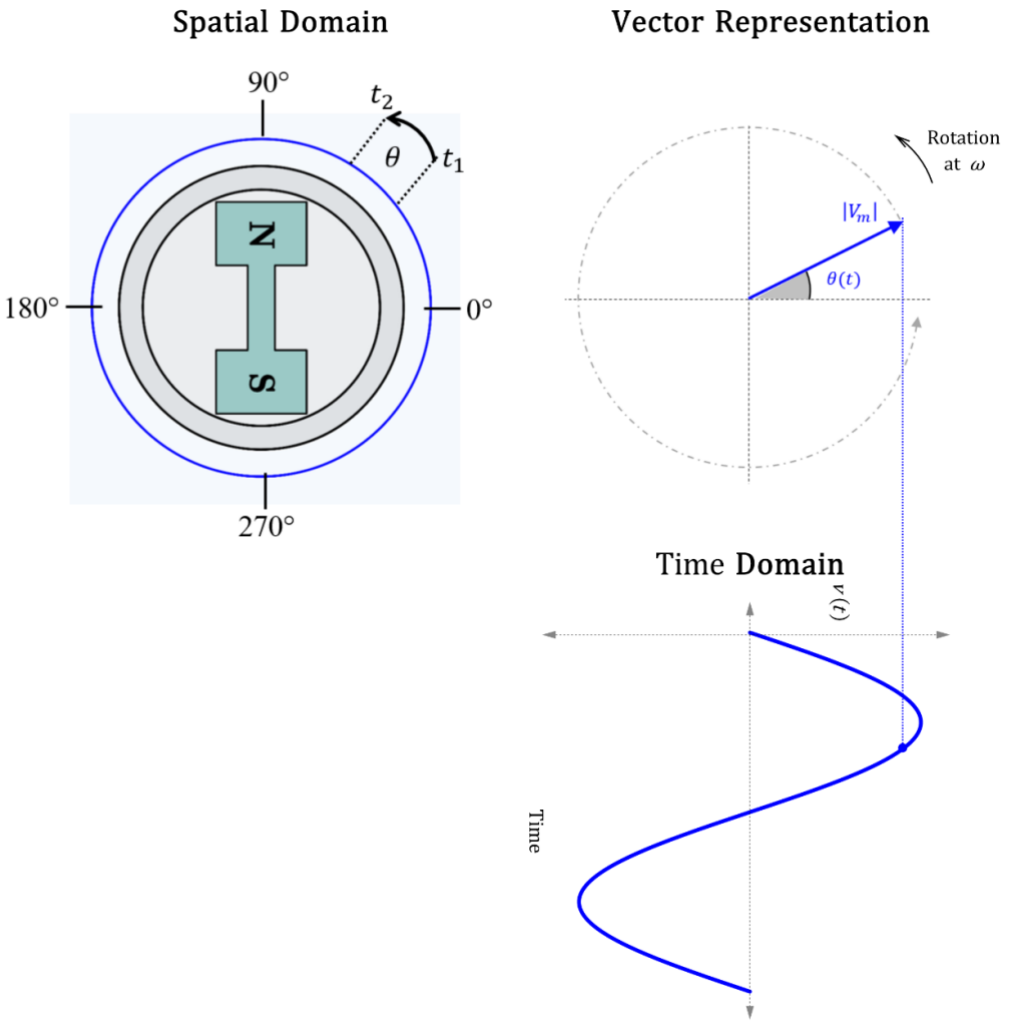

Figure 54: Vector representation as a bridge between spatial domain and time domain

7.5 Summary

- The vector representation of electrical quantities provides an instantaneous representation of voltages and currents in a three-dimensional space, as opposed to phasors, whose values are static and only specified for one constant frequency.
- Measured electrical signals can be instantaneously converted into a vector using two sequential steps – Clark transform and rectangular to spherical coordinate conversion. As the electrical signals vary sinusoidally with respect to time, the vector rotates along three-dimensional space.
- Vectors may be projected onto axes or other vectors. Similar to phasors, simple vector algebra can be used to perform calculations on these vectors and their projections.
- Rotating vectors that have no zero sequence provide a representation that that can be viewed as the rotor of a synchronous machine. Vectors rotate with frequency $\omega_{(t)}$ following a circular path, similar to machine rotors.
- Dynamic controls may be developed to control the voltage and current vectors in a system, to make the vectors track a certain reference setpoint magnitude $|V_m|_{(t)}$, polar angle $\theta_{(t)}$, or azimuthal angle $\emptyset_{(t)}$.

Chapter 8: Vector Based Control Implementation

8.1 Introduction

This chapter presents an initial attempt of using vectors to develop a new control method for power converters in grid applications, by controlling the output voltage vector of each inverter in the grid. In this initial attempt, the inverter voltage vector is generated to track active and reactive power setpoints. At every timestep, the power setpoints and grid voltage measurement is used to calculate the required steady state inverter current vector, and the inverter voltage vector is generated to supply the calculated current vector. By implementing vector-based control, it is shown that the required steady state is achieved within a fraction of the AC cycle, as compared to multiple cycles required by GFM control methods, such as droop control.

Similar to the proposed control method, vector-based control can be used to generate individual inverter voltage vectors to fulfill any control objectives. For creating a 100% power electronics-based grid, the collective control objective of all inverters would be the regulation of the grid bus voltage vector.

8.2 Vector Based Control for Realization of 100% Power Electronics Based Grid

To create a 100% power electronics-based grid, all power converters connected to the grid must operate together to collectively form the grid. Figure 55 (a) represents an example of a power electronics-based grid, in which the grid bus voltage vector $\overrightarrow{v_{bus}}$ is collectively created by several power converters that are supplied by PV and energy storage. To have a reliable and resilient electrical grid, $\overrightarrow{v_{bus}}$ must always be within a certain range of voltage, frequency, harmonic content,

etc. so that all the loads connected to the grid have uninterrupted power supply. The collective operation of all the power converters to ensure the integrity of $\overrightarrow{v_{bus}}$ can be achieved using vector-based control. If the control objective of all power converters is specified to be the establishment of the grid bus voltage vector $\overrightarrow{v_{bus}}$, each individual inverter output voltage vector $\overrightarrow{v_{i1}}$, $\overrightarrow{v_{i2}}$,….. $\overrightarrow{v_{in}}$ can be controlled to create $\overrightarrow{v_{bus}}$ collectively, as shown in Figure 55 (b).

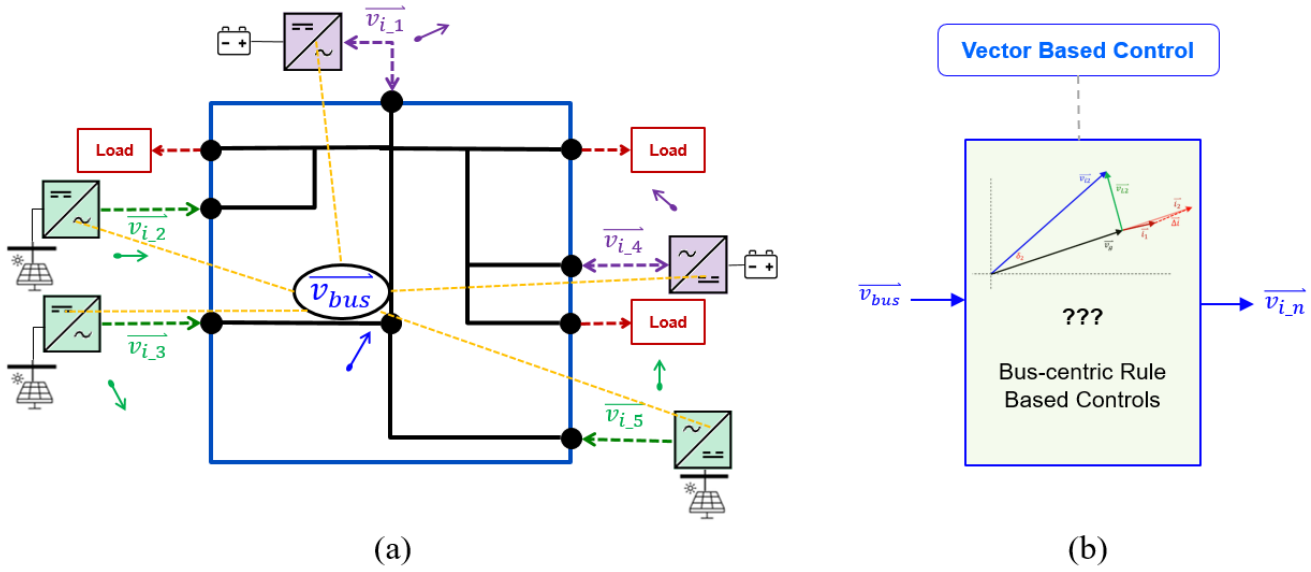

Figure 55: (a) Creating a 100% Power Electronics based grid having a grid voltage vector collaboratively created by several inverter voltage vectors (b) Vector-based control in every inverter connected to the grid

8.3 Initial Attempt of Using Vector Based Control for Power Electronics in Power Systems

An initial attempt to demonstrate the capability of vector-based control is shown by regulating the active and reactive power in inverters connected to the grid. Inverter output voltage vector $\overrightarrow{v_i}$ is generated to achieve P and Q setpoints within a few timesteps of the control loop, while considering the inverter's maximum DC link voltage limit constraint.

8.3.1 Example System and Equivalent Circuit

The test system is the same as previously introduced in Chapter 5 – The power converter with voltage v_{i_abc} is connected to the three-phase bulk power system v_{g_abc} through a transmission line with symmetrical impedance comprising of an equivalent resistance R and inductance L, as shown in Figure 56. The voltage drop across the transmission line v_{L_abc} is given by the difference between v_{i_abc} and v_{g_abc}. Current i_{i_abc} flows from the power converter to the bulk grid, causing the inverter to deliver active and reactive power P and Q to the grid.

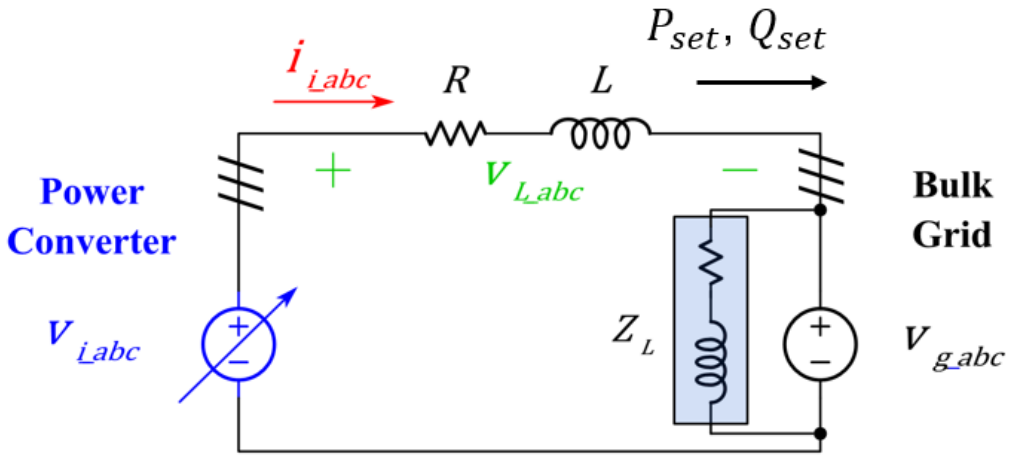

Figure 56: Test three-phase circuit with power converter connected to the bulk grid through resistance and inductance

8.3.2 Control Objective

The control objective of the inverter is to regulate active and reactive power P and Q to a reference value P_{set} and Q_{set}. The system initially operates in steady state at time $t = k - 1$ with $P = P_{set1}$ and $Q = 0$. A step change in P is required at time $t = k$ which changes the value of active power to $P = P_{set2}$. As a result of this transition, the system reaches a new steady state at time $t = k + 1$ with $P = P_{set2}$ and $Q = 0$, as shown in Figure 57.

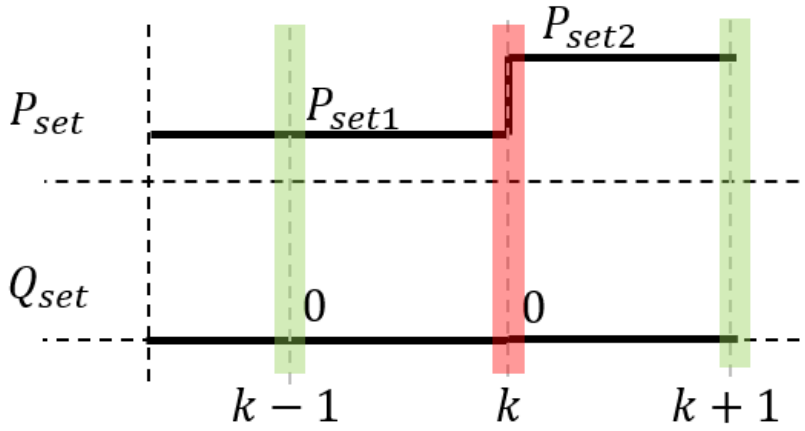

Figure 57: Control objective for regulating Active and Reactive Power using Vector based Control

8.3.3 Inverter Voltage Vector Generation Methodology

The methodology of generating the inverter output voltage vector $\overrightarrow{v_i}$ consists of the calculation of the following vectors:

1. Required steady state current vector $\overrightarrow{i_2}$, corresponding to P_{set} and Q_{set}
2. Difference between present and required current vector $\overrightarrow{\Delta i} = \overrightarrow{i_2} - \overrightarrow{i_1}$
3. Required voltage across impedance vector $\overrightarrow{v_L}$ to inject current $\overrightarrow{\Delta i}$
4. Inverter voltage vector $\overrightarrow{v_i} = \overrightarrow{v_L} + \overrightarrow{v_g}$ required to create $\overrightarrow{v_L}$
5. If $\overrightarrow{v_i}$ has a magnitude greater than DC link voltage V_{DC}, $\overrightarrow{v_i}$ is recalculated so that:
    a. Magnitude of $\overrightarrow{v_i}$ is clamped at maximum DC link voltage V_{DC}
    b. Angle of $\overrightarrow{v_i}$ is calculated to produce current vector $\overrightarrow{i_{k+1}}$ to have the same angle as steady state current vector $\overrightarrow{i_2}$

The control algorithm flowchart based on this methodology is shown in Figure 58.

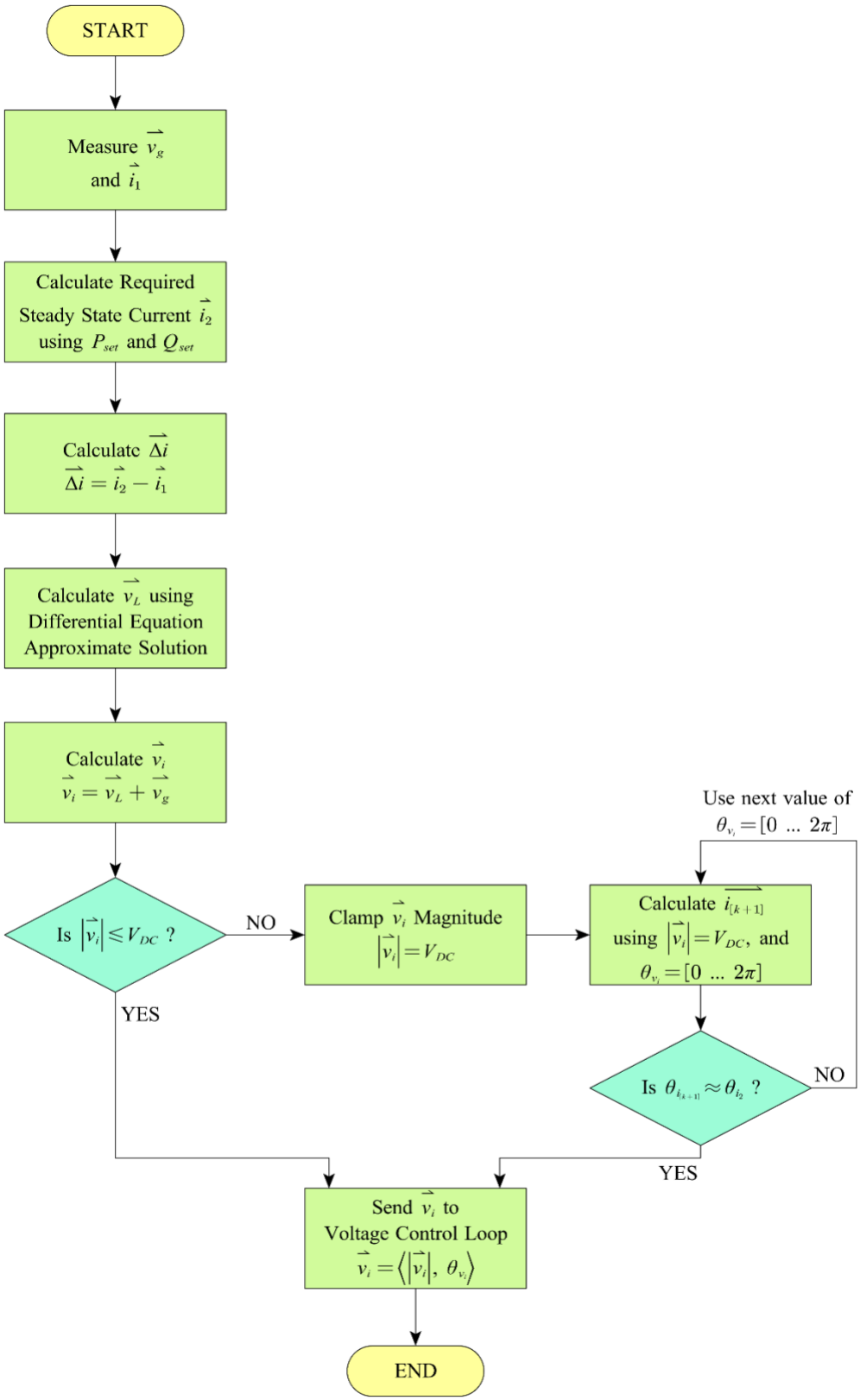

Figure 58: Vector-based control algorithm flowchart diagram

The steps in this control methodology are explained in detail as follows:

1. <u>Calculation of Steady state current vector $\overrightarrow{\iota_2}$</u>

$\overrightarrow{\iota_2}$ is calculated using P_{set} and Q_{set}. First, the power angle δ between $\overrightarrow{v_\iota}$ and $\overrightarrow{v_g}$ is calculated. This is followed by the calculation of voltage drop across the impedance. Finally, the current is calculated using the impedance and voltage drop.

$\overrightarrow{v_g}$ and $\overrightarrow{v_\iota}$ respectively are defined by their time varying magnitudes and angles as follows:

$$\overrightarrow{v_g} = \langle \left|\overrightarrow{v_g}\right|_{(t)}, \theta_{g(t)} \rangle \tag{32}$$

$$\overrightarrow{v_\iota} = \langle |\overrightarrow{v_\iota}|_{(t)}, \theta_{g(t)} + \delta_1 \rangle \tag{33}$$

P_{set} and Q_{set} are used to obtain the power angle δ_1 between $\overrightarrow{v_g}$ and $\overrightarrow{v_\iota}$ at time $t = k - 1$

$$P_{set1} = \frac{3}{2}.\frac{\left|\overrightarrow{v_g}\right|_{(t)} |\overrightarrow{v_\iota}|_{(t)} \sin\delta_1}{\omega L} \tag{34}$$

$$Q_{set} = 0 = \frac{3}{2}.\frac{|\overrightarrow{v_\iota}|_{(t)} \left(|\overrightarrow{v_\iota}|_{(t)} - \left|\overrightarrow{v_g}\right|_{(t)} \cos\delta_1\right)}{\omega L} \tag{35}$$

The voltage drop vector $\overrightarrow{v_L}$ across the impedance is calculated using the vector sum of $\overrightarrow{v_\iota}$ and $-\overrightarrow{v_g}$.

$$\overrightarrow{v_L} = \overrightarrow{v_\iota} + \left(-\overrightarrow{v_g}\right) \tag{36}$$

Vector $\overrightarrow{v_L}$ is defined as follows:

$$\overrightarrow{v_L} = \langle |\overrightarrow{v_L}|_{(t)}, \theta_{v_L(t)} \rangle \tag{37}$$

Finally, the steady state current vector can be obtained by the relationship between voltage drop and impedance:

$$\vec{\imath} = \langle \frac{|\overrightarrow{v_L}|_{(t)}}{|Z|}, \theta_{v_{L(t)}} - \theta_Z \rangle \tag{38}$$

For the initial steady state at time $t = k - 1$, P_{set1} causes the power angle to be δ_1, which leads to the steady state current $\overrightarrow{\imath_1}$. The vectors at this timestep are represented in Figure 59.

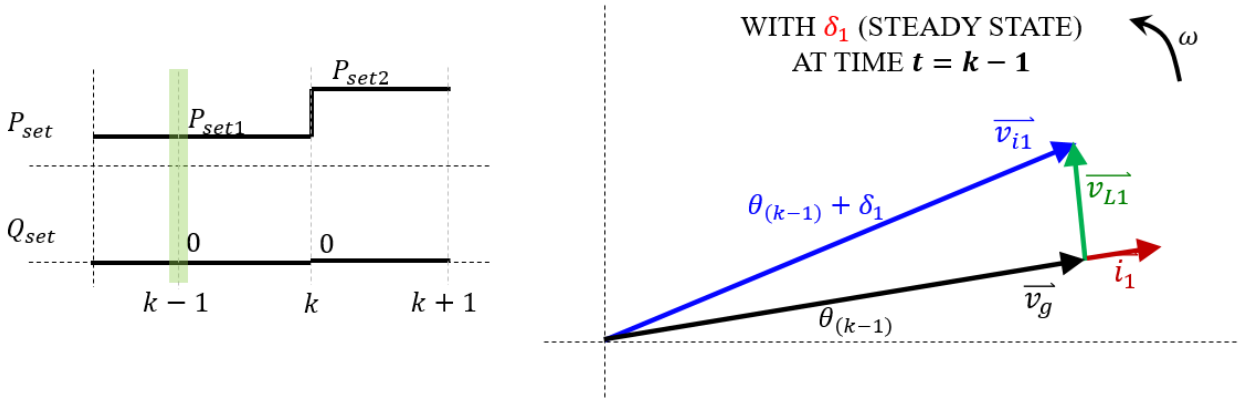

Figure 59: Initial Steady State Voltage and Current vectors at time $\boldsymbol{t = k - 1}$

Similarly, the required steady state at time $t = k + 1$, P_{set2} must have the power angle δ_2, which should lead to the steady state current $\overrightarrow{\imath_2}$. The vectors at this timestep are represented in Figure 60.

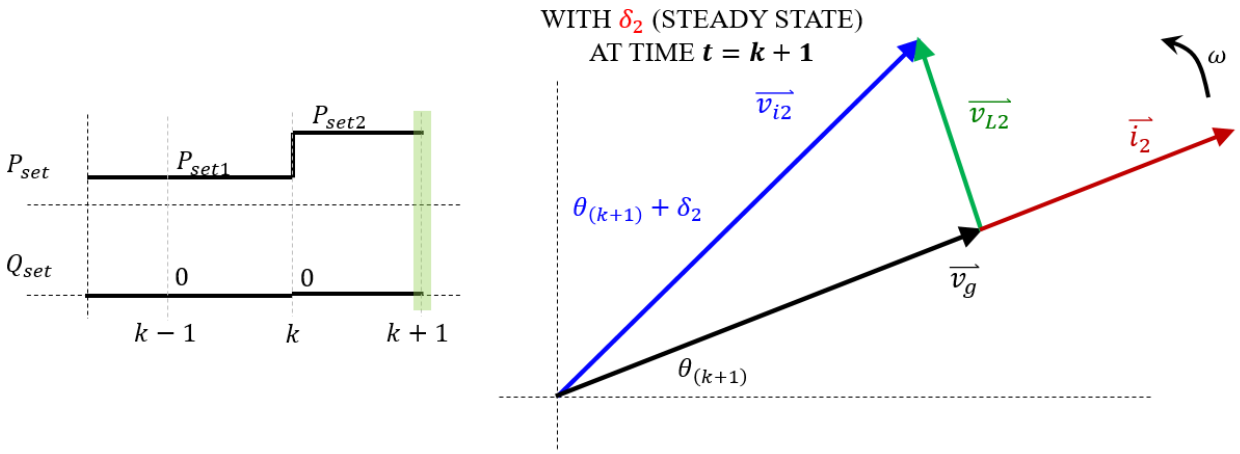

Figure 60: Required Steady State Voltage and Current vectors at time $\boldsymbol{t = k + 1}$

In order to achieve the required steady state at time $t = k + 1$, $\overrightarrow{v_i}$ must be generated at time $t = k$, which causes the current vector to change from $\overrightarrow{i_1}$ to $\overrightarrow{i_2}$ within the next timestep. The vectors immediately before timestep $t = k$ are represented in Figure 61.

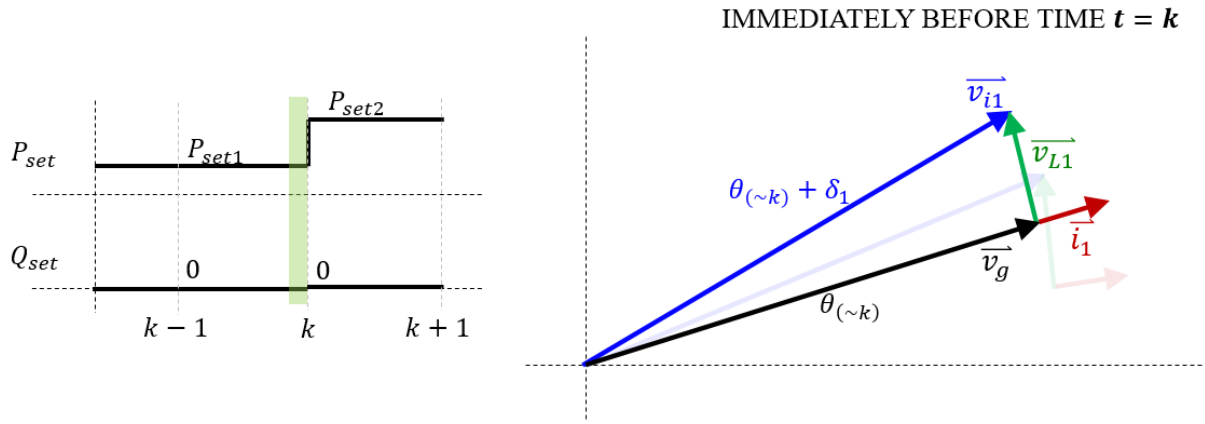

Figure 61: Steady State Voltage and Current vectors immediately before time $\boldsymbol{t = k}$

2. Calculation of current differential vector $\overrightarrow{\Delta \imath}$

The difference between $\overrightarrow{\imath_1}$ and $\overrightarrow{\imath_2}$ can also be calculated as a vector $\overrightarrow{\Delta \imath}$. The purpose of vector $\overrightarrow{\Delta \imath}$ is to find the required difference in current, and use a differential equation relationship to generate the inverter voltage $\overrightarrow{v_\imath}$ that achieves the current differential $\overrightarrow{\Delta \imath}$. The vector diagram for $\overrightarrow{\Delta \imath}$ is shown in Figure 62.

$$\overrightarrow{\Delta \imath} = \overrightarrow{\imath_2} + (-\overrightarrow{\imath_1}) \tag{39}$$

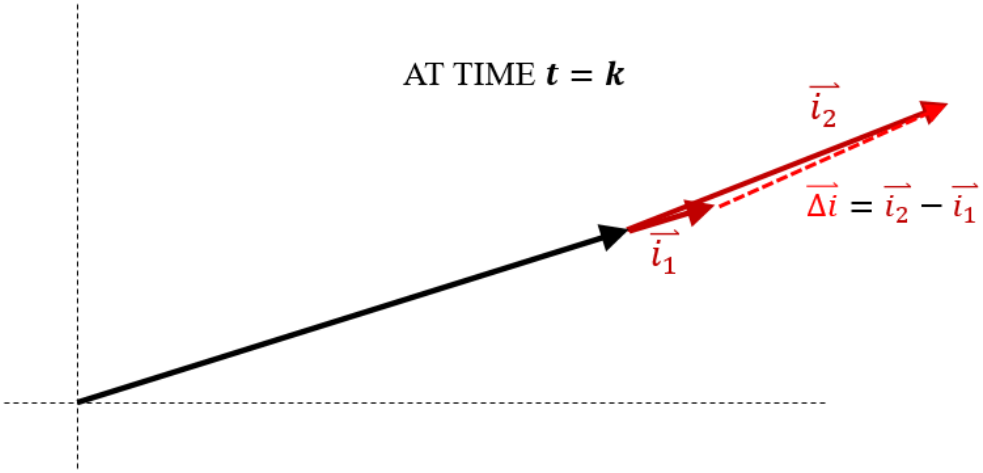

Figure 62: Vector difference between steady state currents $\overrightarrow{\boldsymbol{\imath_1}}$ and $\overrightarrow{\boldsymbol{\imath_2}}$

3. Calculation of required voltage across impedance vector $\overrightarrow{v_\imath}$

The loop equation for the circuit can be derived using KVL:

$$\frac{d}{dt}\vec{\imath} = -\frac{R}{L}\vec{\imath} + \frac{1}{L}\overrightarrow{v_L} \tag{40}$$

Differential equations can be used to calculate the approximate value of a variable at the next timestep ($t = k + 1$), if the value at the current timestep ($t = k$) is known. There are several types of approximations for differential equations – the simplest of these approximations is the Euler's method [47]. This method assumes that the differential function linearly increases or decreases (depending on whether the differential function is positive or negative) for the duration of the timestep h. Therefore, the value of the current vector $\vec{\imath}$ at time $t = k + 1$ is the sum of $\vec{\imath}$ at time $t = k$ and the differential of $\vec{\imath}$ for the timestep h, as represented in the following equation:

$$\overrightarrow{\imath_{k+1}} = \overrightarrow{\imath_k} + h\left\{\frac{d}{dt}\overrightarrow{\imath_k}\right\}$$

$$\overrightarrow{\imath_{k+1}} = \overrightarrow{\imath_k} + h\left\{-\frac{R}{L}\overrightarrow{\imath_k} + \frac{1}{L}\overrightarrow{v_{L_k}}\right\} \tag{41}$$

It is possible to derive the required $\overrightarrow{\Delta\imath}$ to move the current vector from $\overrightarrow{\imath_1}$ to $\overrightarrow{\imath_2}$ in a single time step h using the differential equation approximation as follows:

$$\overrightarrow{\Delta\imath} = h\left\{-\frac{R}{L}\overrightarrow{\imath_1} + \frac{1}{L}\overrightarrow{v_L}\right\}$$

The equation can be rearranged to solve for the required voltage drop across the impedance $\overrightarrow{v_L}$. A diagram depicting $\overrightarrow{v_L}$ and scaled vectors $\overrightarrow{\Delta\imath}$ and $\overrightarrow{\imath_1}$ are presented in Figure 63.

$$\overrightarrow{v_L} = \frac{L}{h}\overrightarrow{\Delta\imath} + R\overrightarrow{\imath_1} \tag{42}$$

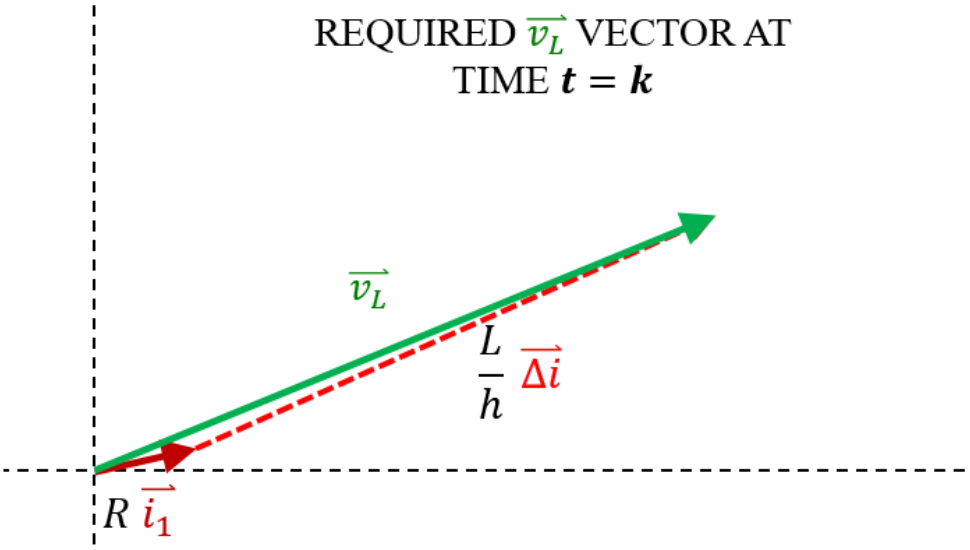

Figure 63: Obtaining vector $\overrightarrow{v_L}$ by adding scaled vectors $\overrightarrow{i_1}$ and $\overrightarrow{\Delta i}$

4. Calculation of required inverter voltage vector $\overrightarrow{v_i}$

Finally, $\overrightarrow{v_i}$ can be calculated by taking the vector sum of voltage drop $\overrightarrow{v_L}$ across the impedance and grid voltage vector $\overrightarrow{v_g}$. A diagram representation for the calculation of $\overrightarrow{v_i}$ is presented in Figure 64.

$$\overrightarrow{v_i} = \overrightarrow{v_L} + \overrightarrow{v_g}$$

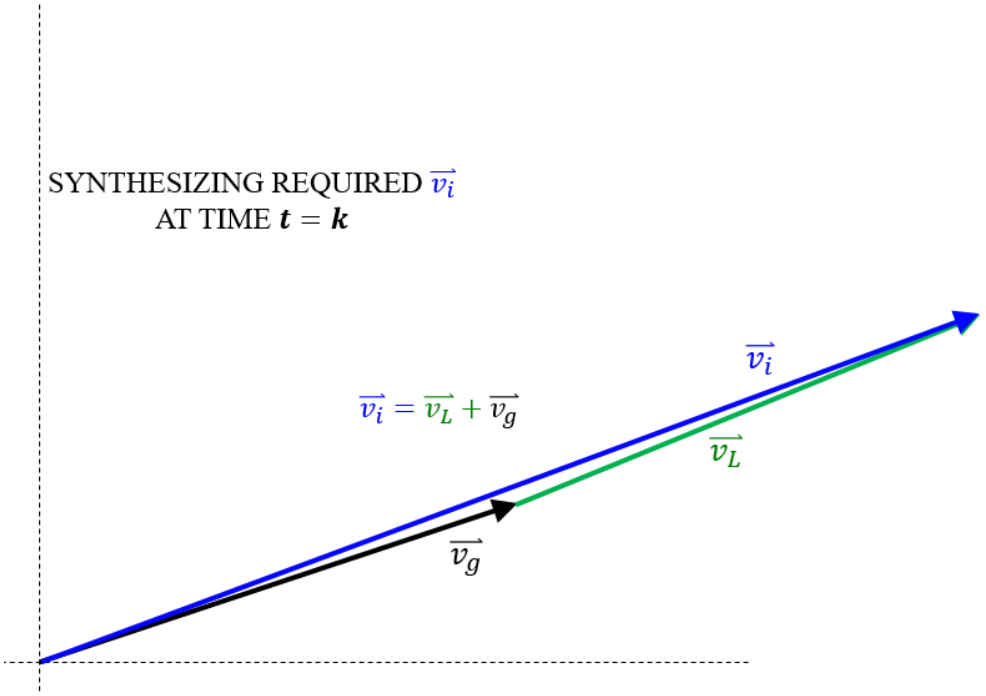

Figure 64: Synthesizing inverter output voltage vector $\overrightarrow{v_i}$ by adding vectors $\overrightarrow{v_L}$ and $\overrightarrow{v_g}$ (without considering DC link voltage constraints)

5. Recalculation of required inverter voltage vector $\overrightarrow{v_i}$ considering DC link voltage constraints

If $\overrightarrow{v_i}$ has a magnitude lesser than the inverter's DC link voltage V_{DC}, then the synthesized $\overrightarrow{v_i}$ is the final command propagated to the inverter's inner control loops. However, in case $\overrightarrow{v_i}$ has a magnitude greater than V_{DC}, $\overrightarrow{v_i}$ must be recalculated due to the physical limitations of the inverter. In such a case, the magnitude of $\overrightarrow{v_i}$ is limited to V_{DC}, as shown in Figure 65.

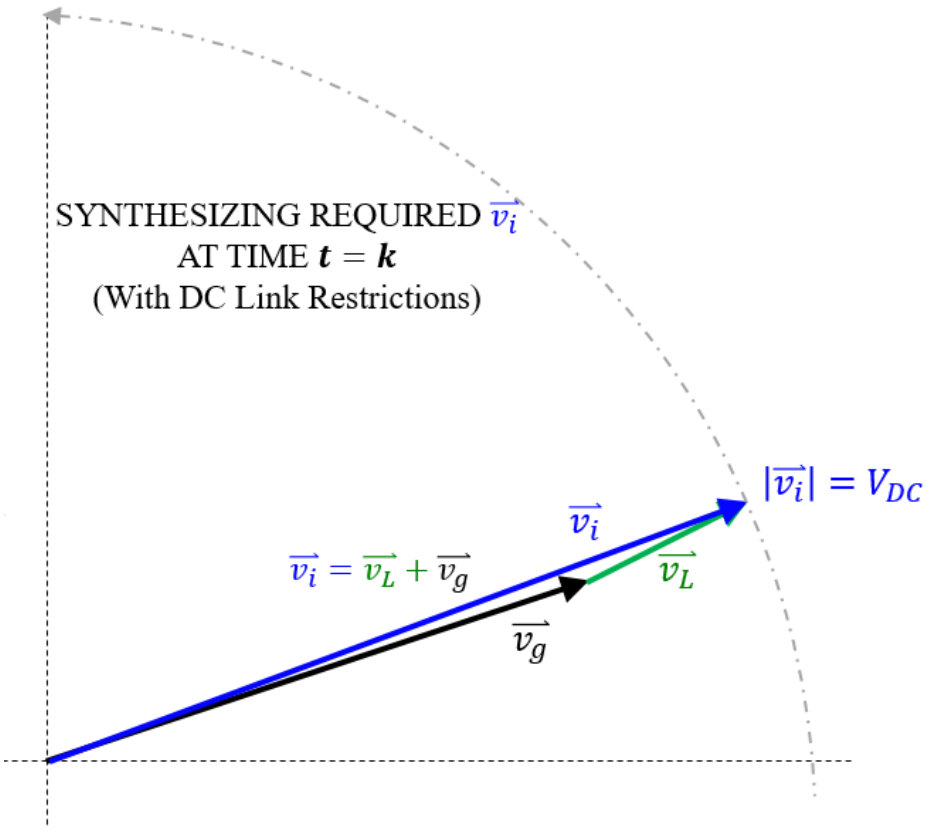

Figure 65: Clamping inverter output voltage vector $\vec{v_\iota}$ considering DC link voltage constraints

The angle of $\vec{v_\iota}$ must be recalculated, so that the current vector produced at the next timestep $\vec{\iota_{k+1}}$ has an angle that matches with the required steady state current vector $\vec{\iota_2}$. Therefore, the magnitude of $\vec{v_\iota}$ is locked at maximum DC link voltage V_{DC}, and the angle is varied from 0 to 2π to observe which angle of $\vec{v_\iota}$ produces a current vector $\vec{\iota_{k+1}}$ at the next timestep to have the same angle as steady state current vector $\vec{\iota_2}$. The final synthesized inverter voltage $\vec{v_\iota}$ in this case becomes:

$$\vec{v_\iota} = \langle |\vec{v_\iota}|_{(t)}, \theta_{v_i(t)} \rangle$$

$$|\vec{v_\iota}|_{(t)} = V_{DC}$$

$$\theta_{v_i(t)} = \theta_{v_i} \quad |_{\theta_{i(k+1)} \approx \theta_{i2}} \tag{41}$$

A graphical representation of the recalculated $\overrightarrow{v_i}$ is presented in Figure 66.

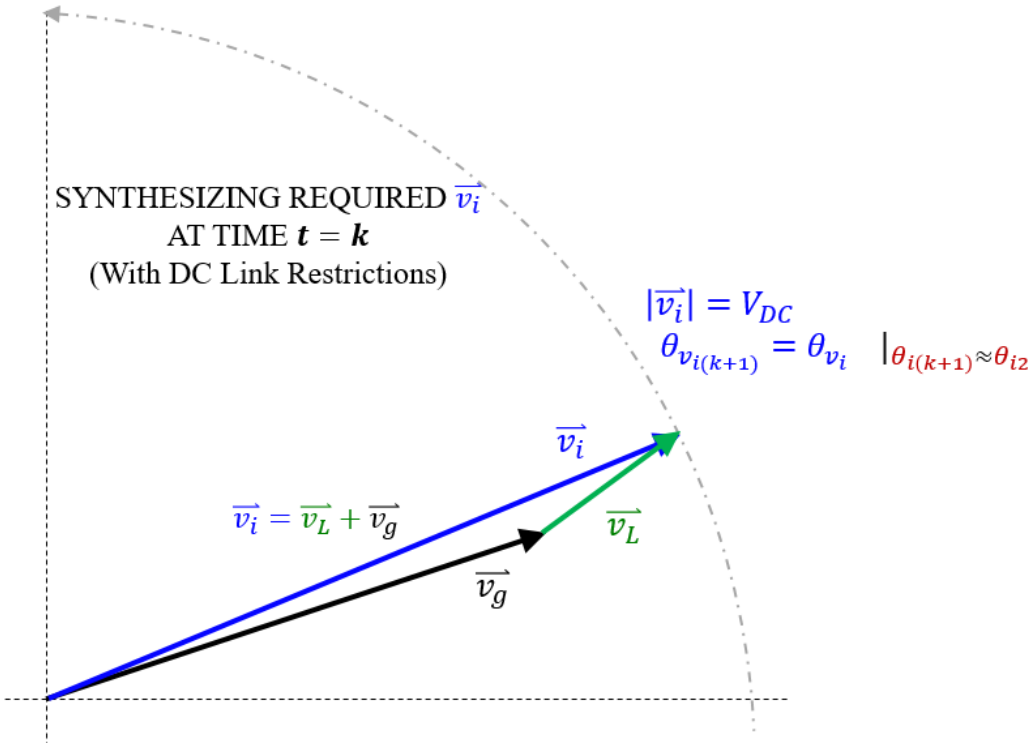

Figure 66: Synthesizing inverter output voltage vector $\overrightarrow{\boldsymbol{v_i}}$ that causes $\overrightarrow{\boldsymbol{\iota_{k+1}}}$ to have same direction as $\overrightarrow{\boldsymbol{\iota_2}}$ (considering DC link voltage constraints)

After the final $\overrightarrow{v_i}$ is synthesized at time $t = k$, the control loop is executed iteratively at the next timesteps. After every timestep, the current vector $\overrightarrow{\iota_{k+n}}$ moves closer to $\overrightarrow{\iota_2}$. After a few iterations of the control loop, the current vector reaches the desired magnitude and angle of $\overrightarrow{\iota_2}$, as shown in Figure 67. This causes the active power P to ramp up in the duration of a few timesteps, without any oscillation or overshoots.

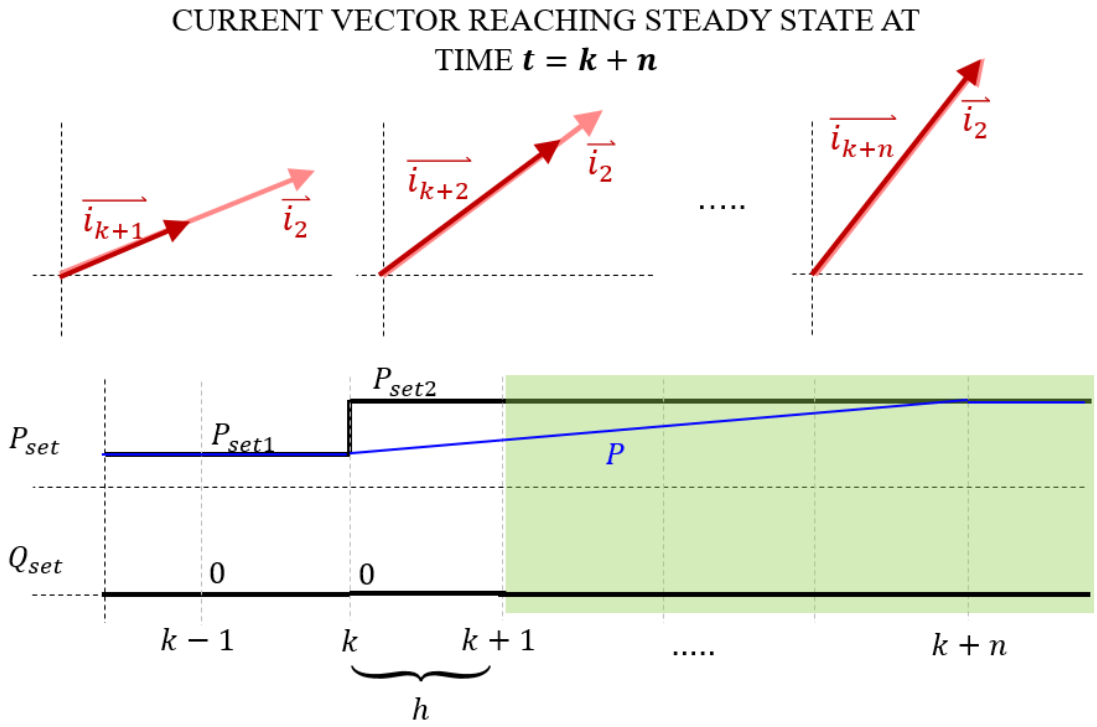

Figure 67: Current vector $\overrightarrow{\boldsymbol{i_{k+n}}}$ gradually reaches the required steady state $\overrightarrow{\boldsymbol{i_2}}$ in a few timesteps, causing the power $\boldsymbol{P}$ to ramp up to the desired setpoint

8.3.4 Control Loop Implementation for a Three Phase Inverter

The vector-based control methodology described above can be implemented in real time in a three-phase inverter, as represented in Figure 68. It is assumed that the inverter output voltage v_{abc} control loop has a high enough bandwidth to follow the reference setpoint voltage vector $\overrightarrow{v_i}$ instantaneously. The vector-based control law comprises of four blocks that are explained in this section:

1. Waveform to Vector Conversion
2. Current Vector Reference Generation
3. $\overrightarrow{v_i}$ Vector Generation Algorithm
4. $\overrightarrow{v_i}$ Magnitude Clamp Algorithm

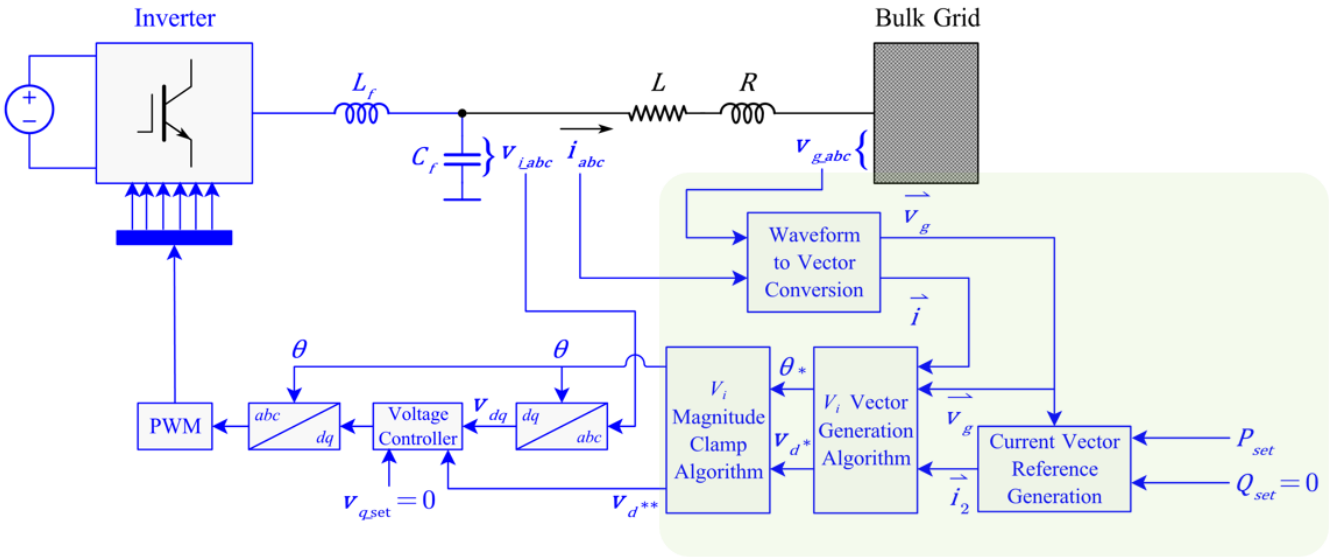

Figure 68: Vector-based control loop design for optimal tracking of power setpoint

1. **<u>Waveform to Vector Conversion</u>:**

Table 2: Block description of waveform to vector conversion

Input	Block Description	Output
v_{g_abc}, i_{abc}	Use of Clark's Transformation and Rectangular to Polar coordinate conversion in Alpha-Beta frame to get vector magnitude and angle	$\overrightarrow{v_g}$, $\overrightarrow{i_1}$

The conversion of time domain three phase waveforms to a vector representation is comprised of the following steps:

- Clark's Transformation is applied to the three-phase waveforms to go from *abc*-frame to αβ-frame. The voltage in αβ-frame is given by the equation:

$$v_{g\_\alpha\beta}(t) = \frac{2}{3}\begin{bmatrix} 1 & -\frac{1}{2} & -\frac{1}{2} \\ 0 & \frac{\sqrt{3}}{2} & -\frac{\sqrt{3}}{2} \end{bmatrix} . v_{g\_abc}(t)$$

- The orthogonal signals obtained from Clarke's transformation are plotted against each other on α and β axes. This produces a vector that rotates in time with a rotating speed corresponding to the electrical frequency ω_0.
- The instantaneous magnitude $\left|\overrightarrow{v_g}\right|_{(t)}$ and angle $\theta_{vg_{(t)}}$ of this rotating vector can be calculated by converting the rectangular components on the αβ plot to its polar form:

$$\left|\overrightarrow{v_g}\right|_{(t)} = \sqrt{\left(\overrightarrow{v_g}_{x\,(t)}\right)^2 + \left(\overrightarrow{v_g}_{y\,(t)}\right)^2}$$

$$\theta_{vg_{(t)}} = \tan^{-1}\left(\frac{\overrightarrow{v_g}_{y\,(t)}}{\overrightarrow{v_g}_{x\,(t)}}\right)$$

2. Current Reference Generation:

Table 3: Block description of required steady state current vector calculation

Input	Block Description	Output
P_{set}, Q_{set}, $\overrightarrow{v_g}$	Use of Steady state power flow equations to obtain the required steady state current vector $\overrightarrow{i_2}$ magnitude and angle	$\overrightarrow{i_2}$

This block uses steady state power flow equations to first calculate the required power angle δ_2 and inverter voltage magnitude $|\overrightarrow{v_i}|$. Once δ_2 and $|\overrightarrow{v_i}|$ are calculated, the magnitude and angle of the voltage vector $\overrightarrow{v_L}$ can be calculated. Finally, the voltage drop and impedance values can be used to calculate the required steady state current vector $\overrightarrow{i_2}$.

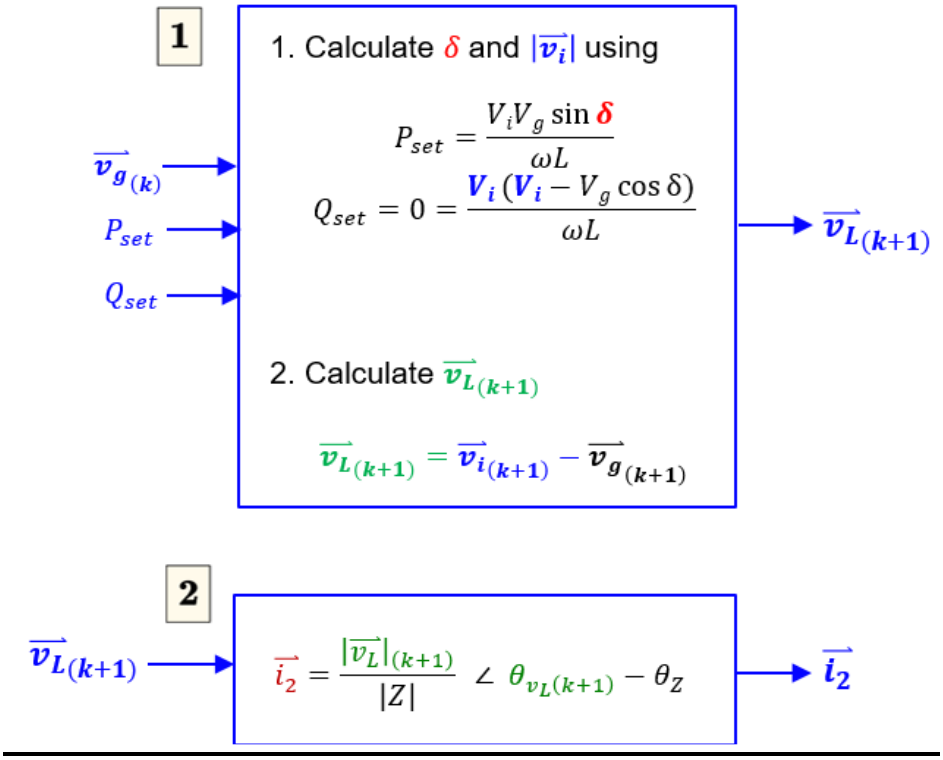

Figure 69: Generation of required steady state current vector $\overrightarrow{i_2}$

3. $\overrightarrow{v_i}$ Vector Generation Algorithm:

Table 4: Block description of inverter output voltage vector generation

Input	Block Description	Output
$\overrightarrow{v_g}$, $\overrightarrow{i_1}$, $\overrightarrow{i_2}$	Use of Euler's approximation for the vector-based differential equation to determine the required $\overrightarrow{v_i}$ vector	$\|\overrightarrow{v_i}\|_{(t)}^{*}$, $\theta_{vi\,(t)}^{*}$

This block uses the approximate solution of the inductor current differential equation to calculate the magnitude and angle of the final required inverter voltage vector $\overrightarrow{v_i}$.

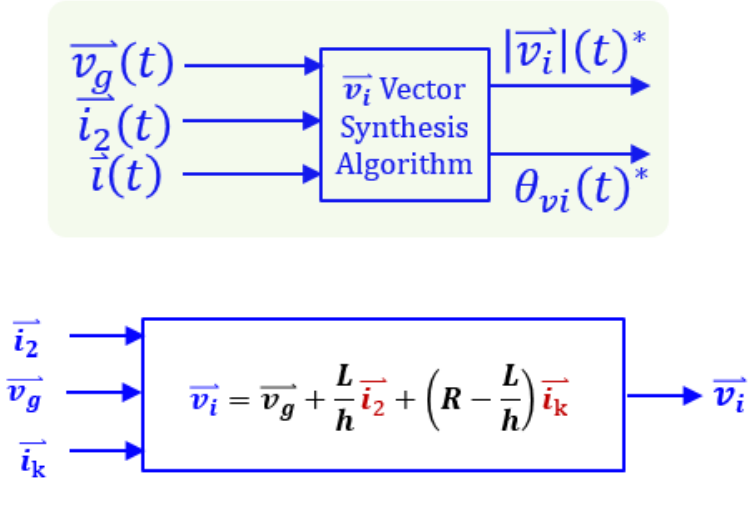

Figure 70: Generation of inverter output voltage vector $\overrightarrow{v_i}$

4. $\overrightarrow{v_i}$ Magnitude Clamp Algorithm:

Table 5: Block description of inverter voltage magnitude clamp algorithm

Input	Block Description	Output
$\lvert\overrightarrow{v_i}\rvert_{(t)}{}^{*}$, $\theta_{vi_{(t)}}{}^{*}$	This block recalculates $\overrightarrow{v_i}$ if the magnitude is greater than V_{DC}	$\lvert\overrightarrow{v_i}\rvert_{(t)}{}^{**}$, $\theta_{vi_{(t)}}{}^{**}$

If the magnitude is required to be clamped, this block ensures that the vector $\overrightarrow{v_i}$ angle is selected such that the error between $\overrightarrow{i_{k+1}}$ and $\overrightarrow{i_2}$ is minimal.

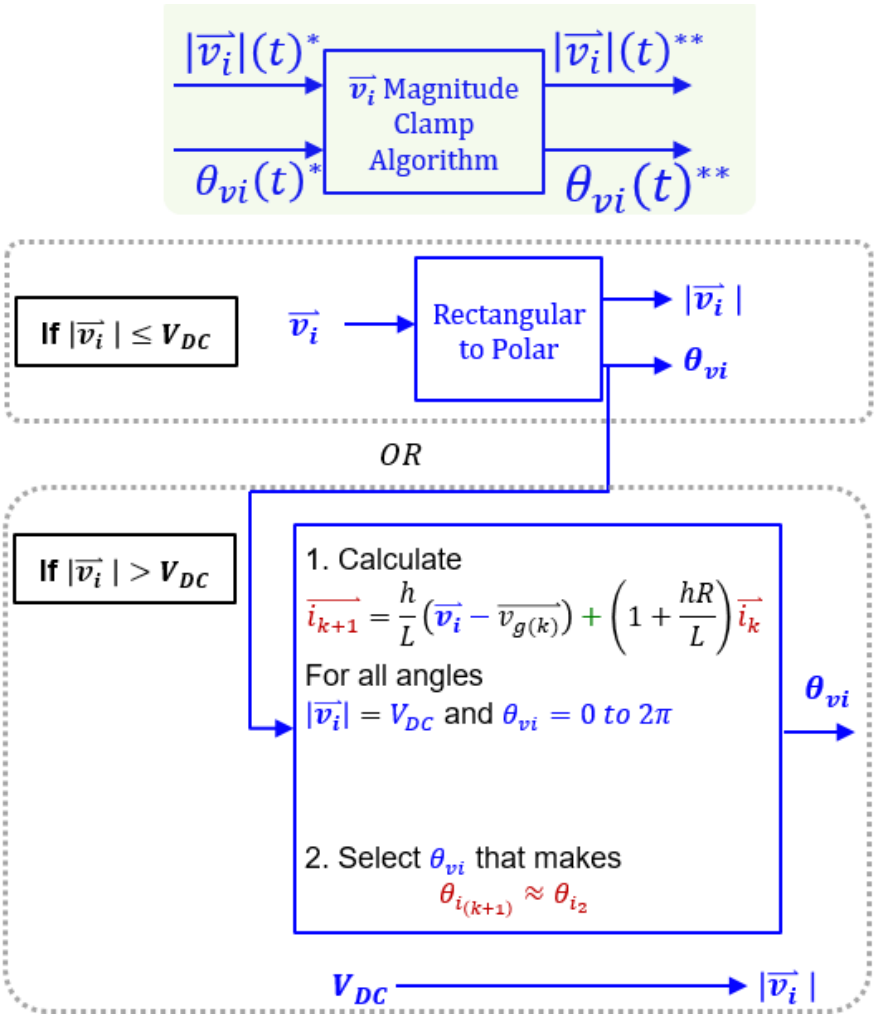

Figure 71: Calculation for inverter output voltage vector optimizing for least error in current vector due to DC link voltage constraints

8.3.5 Simulation with a simple two-source system

A simulation is set up with the same simple system with two sources, as previously described in Figure 56. Using the implementation scheme explained above, the active power setpoint P_{set} is changed from a steady state value of 15 MW to 30 MW at time $t = a$. Figure 72 shows the simulated waveforms for the voltages v_g and v_i, currents i_{abc}, and active power P.

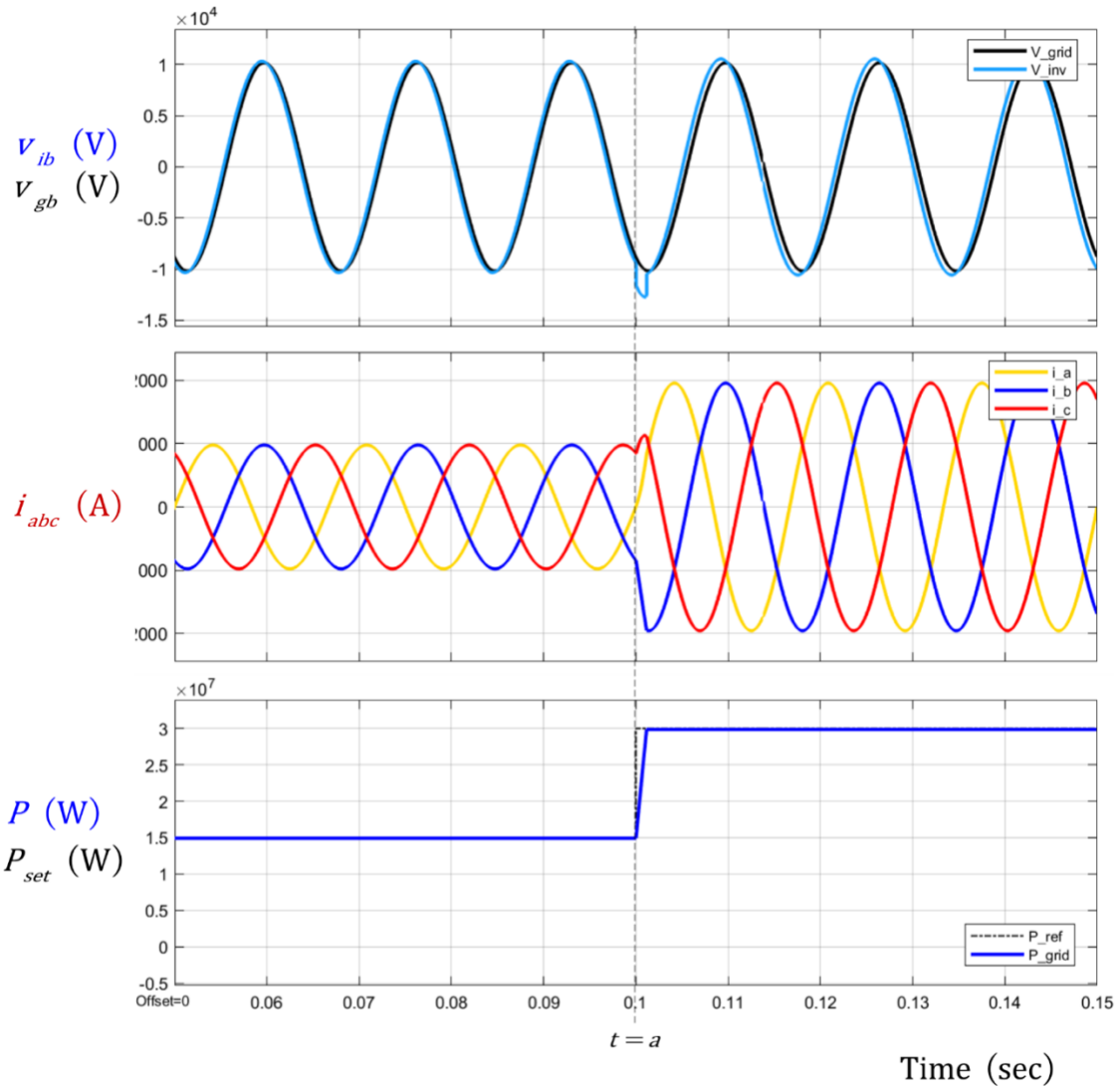

Figure 72: Waveforms for voltages, currents, and power demonstrating the response of vector-based control to a step change in power setpoint

Figure 73 presents a magnified view of the transition from the old steady state value to the new value. It can be seen that the inverter voltage v_i is adjusted according to the calculated vector, while restricting the magnitude of the voltage below the maximum DC link voltage, as seen in the figure. Active power P is regulated to the P_{set} value in the most optimum way within a fraction of the AC voltage cycle, without any overshoots.

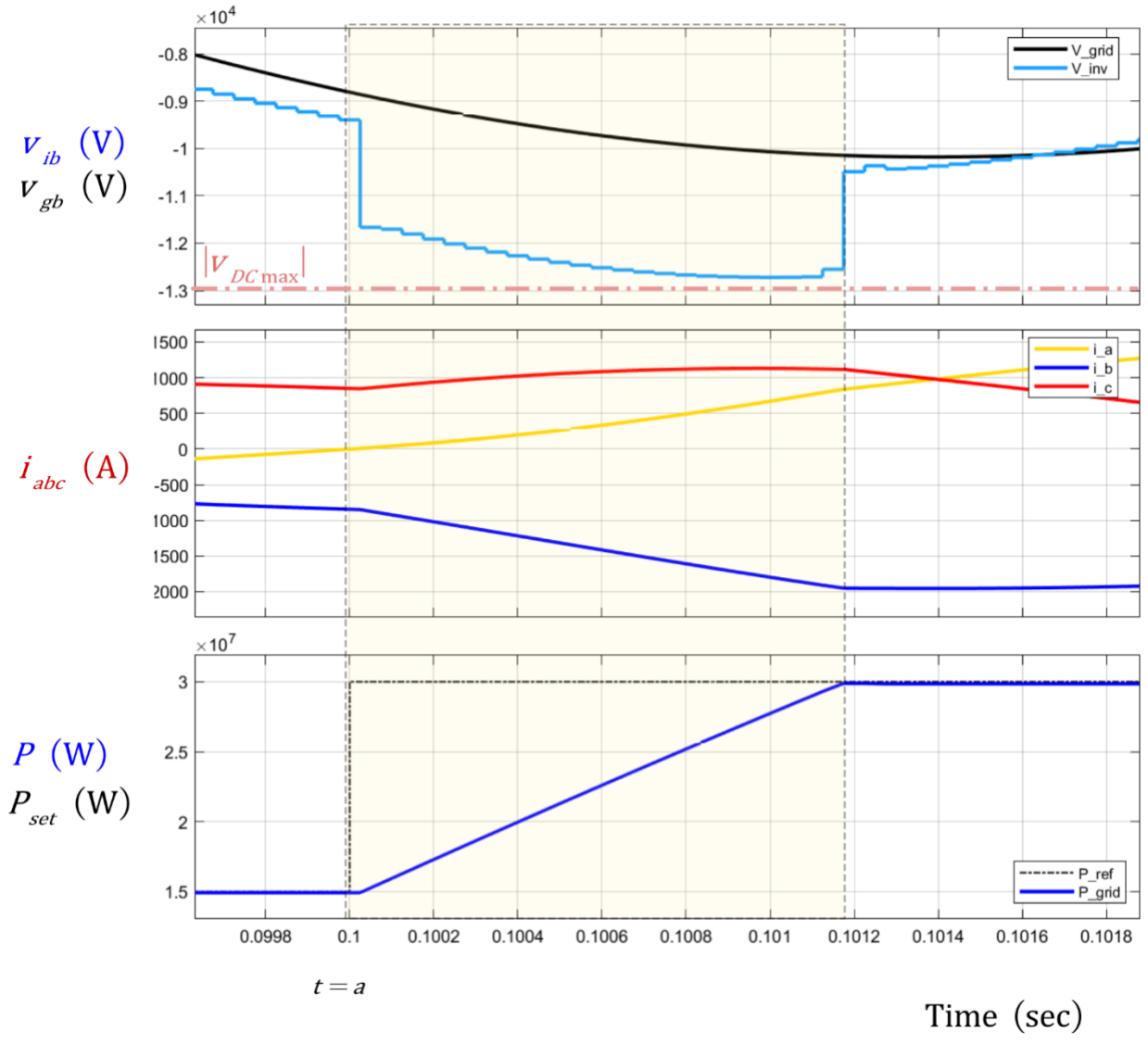

Figure 73: Magnified view showing the transient duration for the waveforms of voltages, currents, and power in vector-based control response to a step change in power setpoint

Figure 74 presents the three phase voltages and currents for this test case, to show that the current i_{abc} is in phase with the grid voltage v_{abc}, since the reactive power setpoint $Q_{set} = 0$.

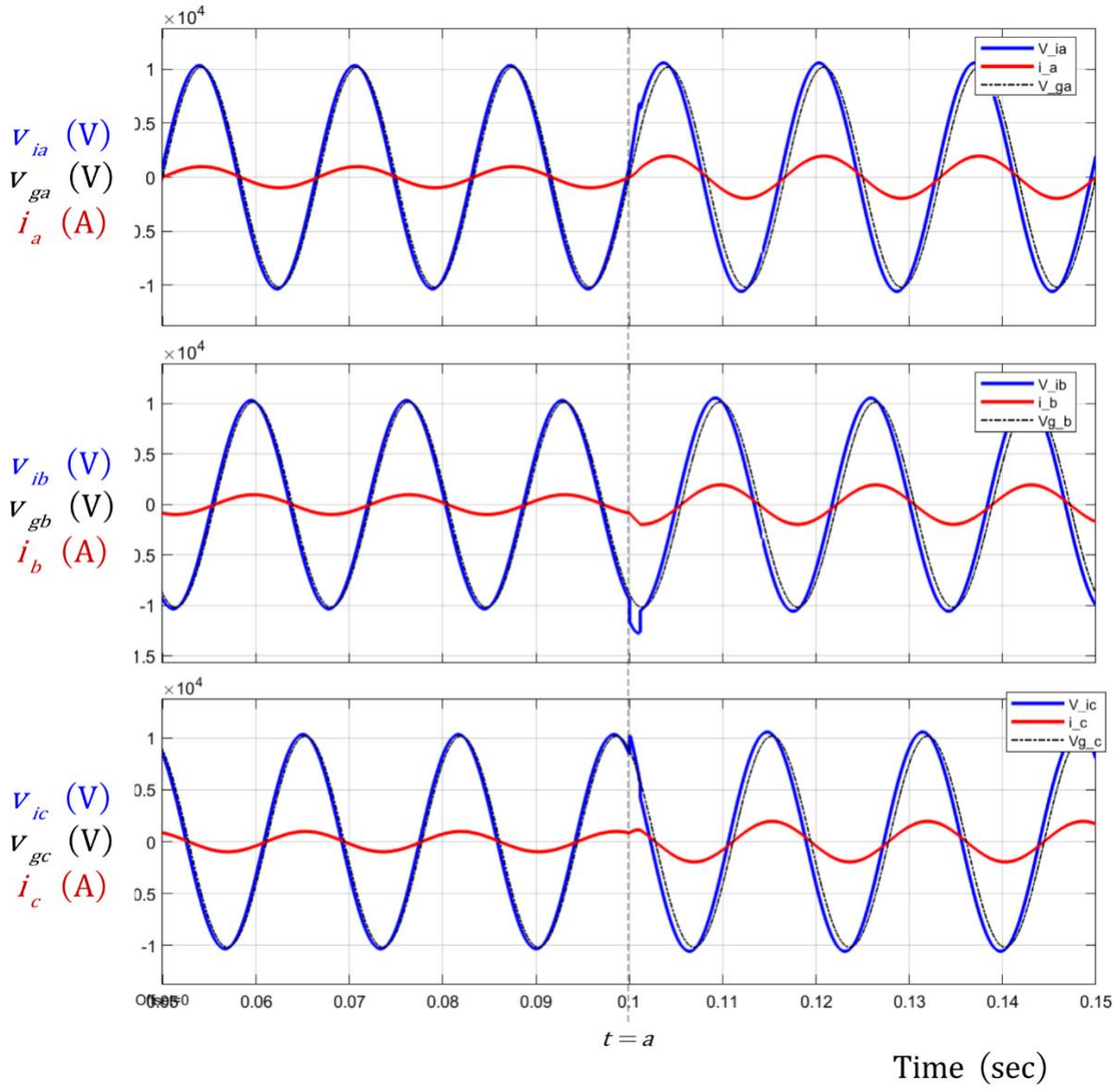

Figure 74: Waveforms for voltages and currents in vector-based controlled system

8.4 Performance Comparisons

The performance of vector-based control can be compared with the other methods to see how well the control objective is fulfilled. The first comparison shows how the system would behave with the proposed control system, as opposed to an open loop system in which power angle δ is changed directly from δ_1 to δ_2. The second comparison shows the system's behavior with several values of $P\omega$ droop coefficients, to evaluate how the system's dynamic response is improved using the proposed vector-based control. As an extreme test case for the comparisons, the active power setpoint P_{set} is changed from 0 to 50 MW at time $t = a$.

8.4.1 Comparison with Open Loop Change in δ

Figure 75 presents the power P setpoint tracking, and v_i for the proposed vector-based control, and the open loop system in which δ is changed abruptly. The abrupt change in δ causes oscillations in P, because the rate of change of current i_{abc} is limited due to the physical property of inductors. This causes a high overshoot and settling time in P. On the other hand, the vector based-control delivers a superior performance because the dynamics of the inductor current i_{abc} are part of the control design. Table 6 provides a summary of the comparison.

Table 6: Performance comparison between vector-based control and open loop change in $\boldsymbol{\delta}$

S. No.	Control Type	Settling Time (As a Factor of fundamental AC Voltage cycles)	Percent Overshoot
1	Vector-Based Control	0.24 cycles	0%
2	Open loop change in δ	5 cycles	74%

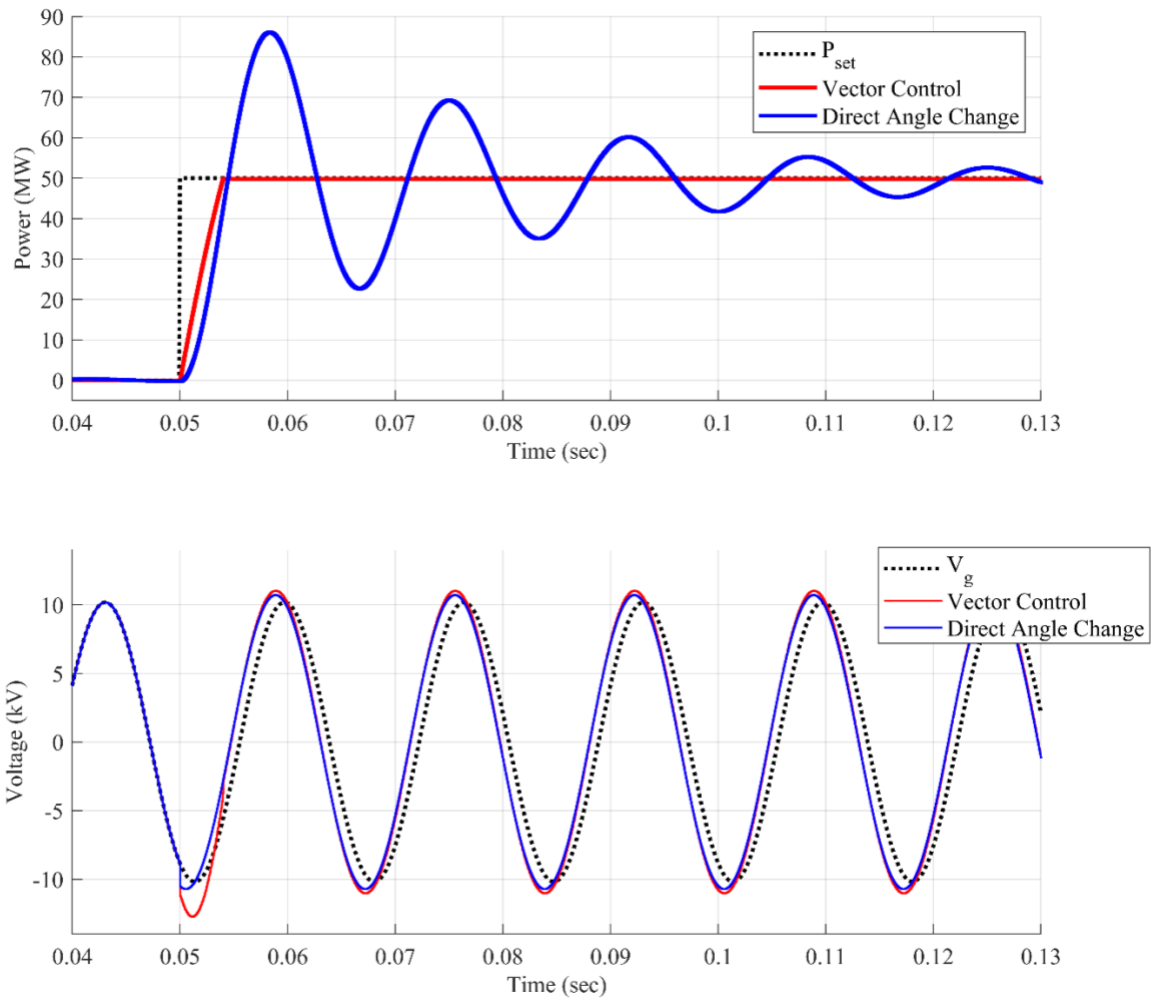

Figure 75: Comparison between instantaneous power and voltage waveforms in vector-based control vs. direct change of power angle

Figure 76 presents a magnified version showing the transient power and voltage. The smooth ramp up of power in the vector-based control clearly contrasts the high overshoot in the case where the power angle is changed abruptly.

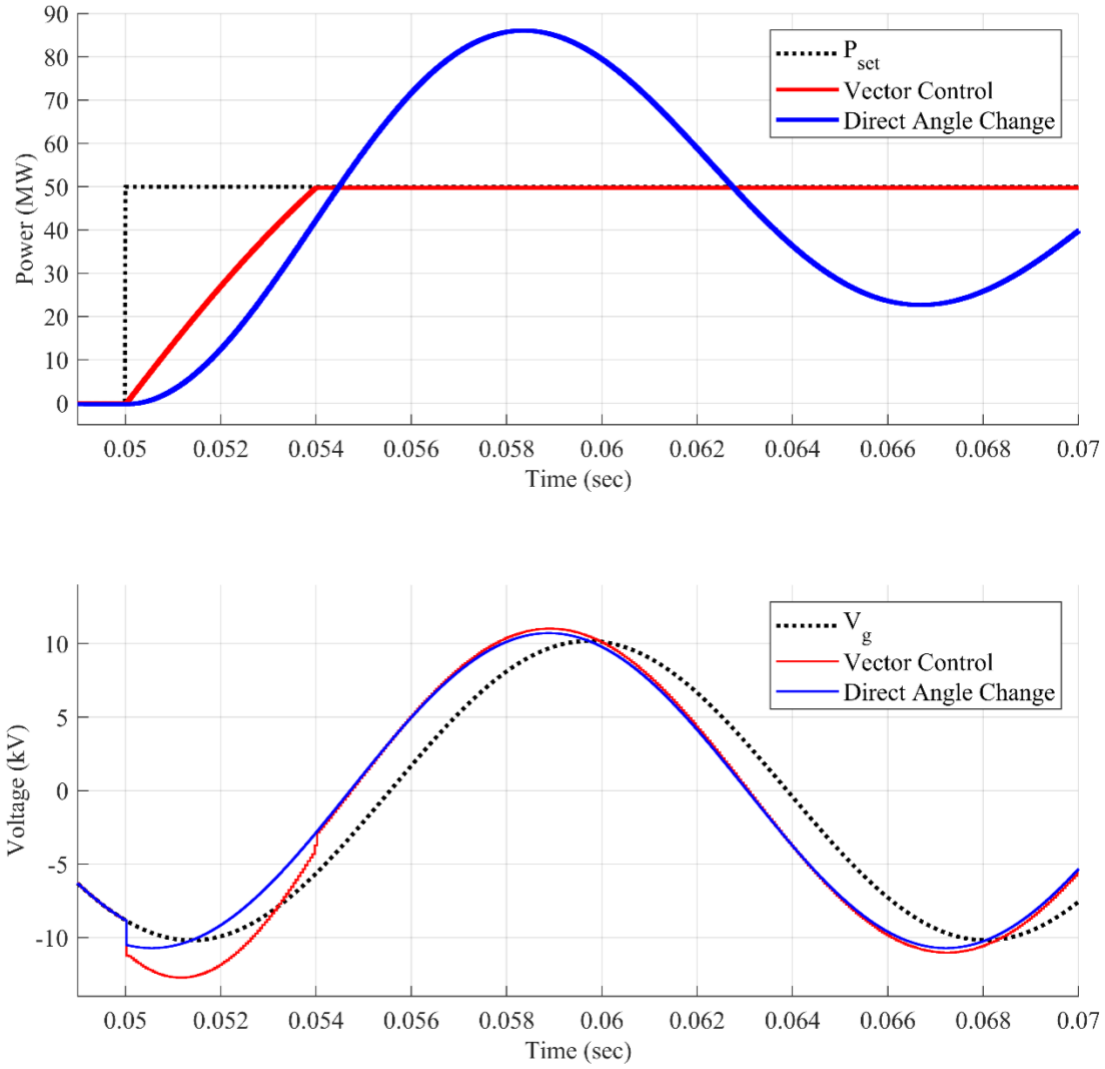

Figure 76: Magnified view of transient duration showing the comparison between instantaneous power and voltage waveforms in vector-based control vs. direct change of power angle

8.4.2 Comparison with Power-Frequency Droop Control

Figure 77 compares the vector-based control with droop control having different droop coefficients. As explained previously, the droop coefficient k_p is selected based on the acceptable deviation in nominal frequency and rated power of the inverter, given by the formula:

$$k_p = \frac{\omega_r - \omega_0}{P_{rated}}$$

It may be possible to increase the droop coefficient and get to the steady state faster. However, this comes at the cost of higher overshoots and even larger oscillations, as seen in Figure 77. The base droop coefficient k_p is multiplied by a factor of 2 and 4 to assess the behavior and check whether it provide a faster response to fulfill the control objective. Table 7 provides a summary of the comparison. This comparison shows that the control objective of regulating power to a reference value P_{set} can be achieved much faster with the proposed vector-based control.

Table 7: Performance comparison between vector-based control and droop control with different droop coefficients

S. No.	**Control Type**	**Settling Time (As a Percentage of fundamental AC Voltage cycle)**	**Percent Overshoot**
1	Vector-Based Control	0.24 cycles	0%
2	Droop Control with k_p	3.3 cycles	16%
3	Droop Control with $2k_p$	3.9 cycles	50%
4	Droop Control with $4k_p$	6.7 cycles	140%

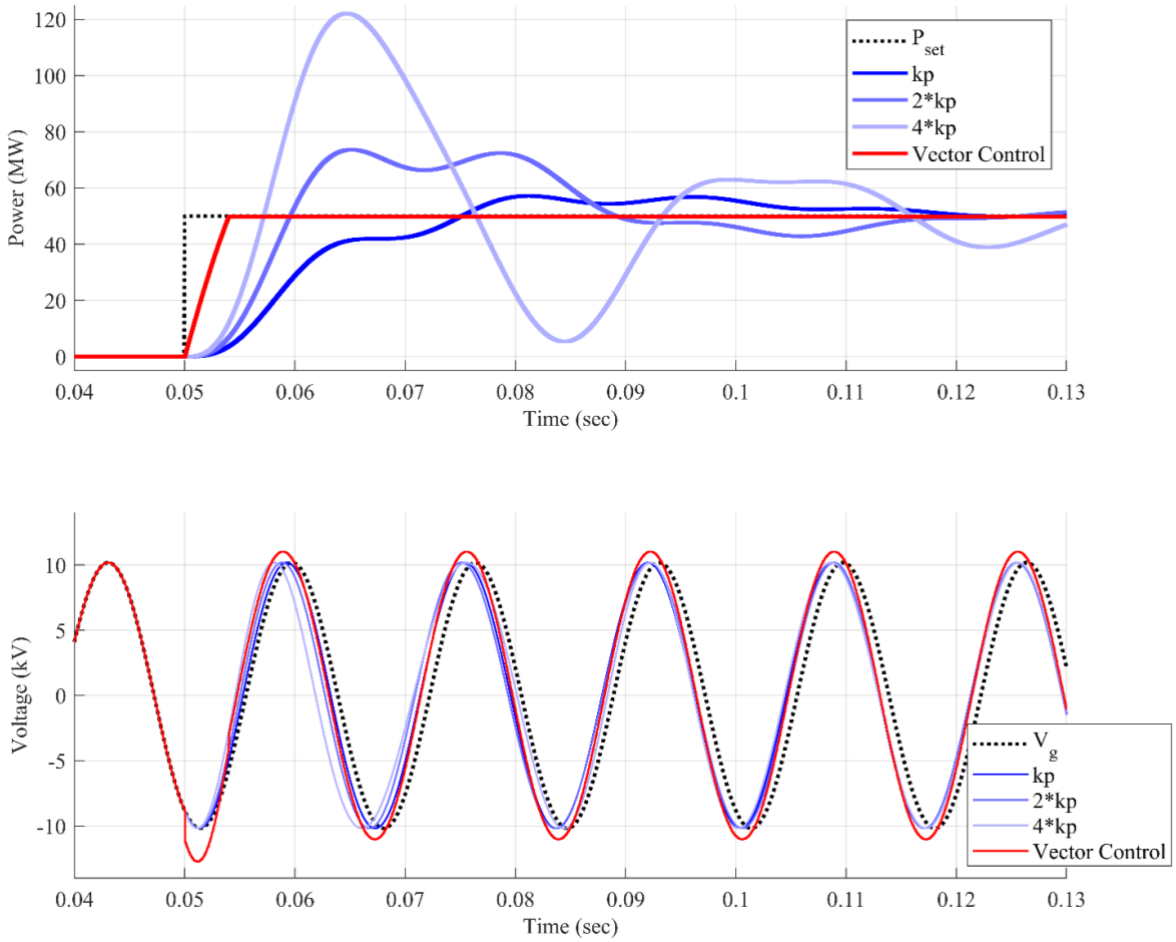

Figure 77: Comparison between instantaneous power and voltage waveforms in vector-based control vs. Droop control with different droop coefficients

8.5 Capabilities of Vector-Based Control for Power Electronics in Power Systems

A control law based on vectors can provide a fast dynamic response to achieve any desired control objectives, as illustrated in this chapter by the initial attempt of regulating setpoints for P and Q. Vector based control can also be used to implement the control objectives of currently

existing GFM methods. These capabilities of vector-based representation and control make it a distinctive and promising choice.

In vector-based control, it is possible to define instantaneous vector references for any voltage and current in the circuit, and develop a control method that generates the required inverter voltage vector to track the defined vector reference. Figure 78 presents a comparison of vector-based control block with existing GFM control block, and control in electrical machines. The output of all these controls is an instantaneous voltage magnitude V and angle θ, as shown in the figure. In electrical machines, the output is dependent on the load demand and droop control. For GFM control in power electronics, it is dependent on the setpoints for P and Q, and internally defined constants such as nominal voltage V_0, nominal frequency ω_0, and inertia constant J. Vector-based control can be used to implement these existing control methods, as well as new methods, as described earlier in this chapter.

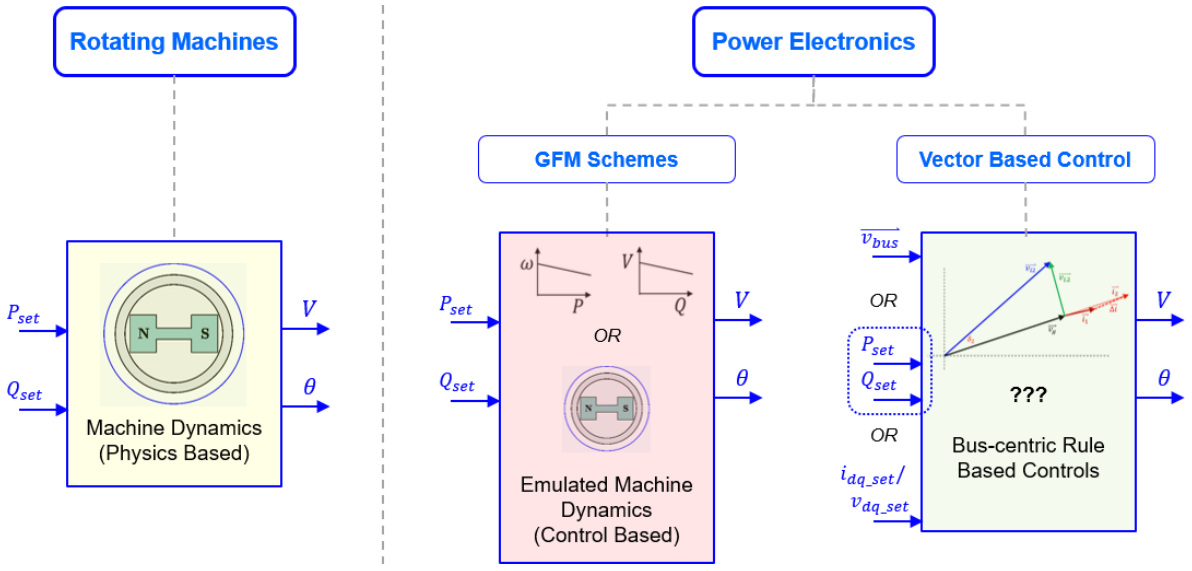

Figure 78: Capabilities of vector-based control for power electronics

8.6 Summary

- In a 100% Power Electronics based grid, power converters will need to collaboratively form the grid. The grid bus voltage and each individual inverter output voltage can be represented as vectors $\overrightarrow{v_{bus}}$ and $\overrightarrow{v_i}$. Using vector representation, a control method can be developed in which all inverter voltage vectors are controlled to maintain the integrity of $\overrightarrow{v_{bus}}$.
- As an initial attempt to show how vectors can be used for control of power electronics in power systems, a control method has been proposed to demonstrate how the inverter voltage vector can be controlled to deliver a setpoint active and reactive power to the bulk grid.
- The proposed vector-based control is able to track the commanded power setpoints within a fraction of the fundamental AC voltage cycle. When compared to droop control and open loop angle change, the required steady state is achieved at least 13 times faster for the example system presented.
- Similar to the proposed control method, the individual inverter voltage vectors can be programmed to fulfill any control objectives. Vector based control can implement all state-of-the-art GFM schemes by specifying the reference setpoint voltage and/or current vectors in the circuit. Furthermore, vector-based control also provides a framework to develop new control methods, such as controlling $\overrightarrow{v_i}$ to maintain the integrity of $\overrightarrow{v_{bus}}$.

Chapter 9: Conclusion and Future Work

9.1 Conclusions

This thesis presents the fundamental issues of phasor-based control methods for power electronics in grid applications, and introduces vector-based control as a potential solution of the highlighted issues. The salient conclusions from this thesis are listed as follows:

- For a 100% Power Electronics Grid, the design considerations for power converter control need to include energy balance, establishing voltage/frequency, small signal stability, dynamic performance in large signal transients, and protection.
- Current GFM schemes are based on making the 'new' PE systems act like 'old' electrical machines. Fundamental differences between PE and electrical machines lead to some assumptions which are not always true (small power angle, constant frequency). This leads to unexpected control behavior when the assumptions are invalid.
- By emulating the behavior of electrical machines, the strength of power electronics (fast control bandwidth) is not being utilized and its weakness (limited overcurrent capability) is being exposed.
- Phasor-based control methods are based on steady state relationships only, considering the frequency to be constant within a cycle. To fully utilize the fast controls of Power Electronics, a new control law based on instantaneous and dynamic characteristics should be advantageous.

- Vector-based representation and control design is introduced that provides truly instantaneous representation and has the potential to be used for new dynamic control law design.
- As an example to show the instantaneous control of vectors, a control loop is designed using vectors to generate the inverter output voltage vector that fulfills the control objective of regulating the active and reactive power setpoints within a fraction of the fundamental AC voltage cycle.
- Vector-based control can be used to collaboratively form a Power Electronics grid by generating each inverter's output voltage vector with the control objective of maintaining the integrity of the grid bus voltage vector.

9.2 Future Work

This thesis serves as the initial step towards a much larger and ambitious goal of creating a 100% power electronics-based grid. Vector-based control is introduced as a possible solution in which the voltage vectors of all inverters forming the grid could be controlled to form the grid bus voltage vector. These goals warrant further research along the following directions:

- **State-of-the-art GFM Control Methods:**
    - A list of myths related to GFM and GFL control will be compiled and analyzed to determine the technical validity of commonly accepted perceptions. One example is the notion that GFM is appropriate for weak grids, while GFL is better suited for strong grids.

- The relationship and issues of reactive power and voltage magnitude need to be investigated further, similar to the issues highlight with the steady state power flow formula that relates active power and frequency
- The current limiting mode due to VSM will be evaluated to determine the cases/faults that cause current to exceed the limit, the implications of exceeding current limit, and how VSM control loop responds in this scenario.
- The power sharing and synchronization mechanism of the virtual oscillator control also needs to be analyzed to determine the strengths and weaknesses of this method.

- **Vector-based Control:**
  - Circuit parameters such as active and reactive power need to be defined using vectors, and quantitatively compared with the conventional definition.
  - An example grid based on 100% power electronics with sufficient complexity needs to be defined to determine the mathematical relationship between each individual inverter voltage vector, and the grid bus voltage vector.
  - Generic rules need to be developed for controlling inverter voltage vectors to collaboratively form a power electronics-based grid.
  - The control method proposed in this thesis does not include zero sequence. For inverters with zero sequence, the representation and calculation of vectors will require three-dimensional vector algebra using spherical coordinates.

- Vector based control relies on the reference grid bus voltage vector. It will be a challenge to have this reference voltage vector at every node. Possible solutions could be to take measurements either at local nodes, or one centralized node could transmit the reference vector over a communication link.

- **Hardware Testing:**
  - The issues highlighted in phasor-based control methods need to be demonstrated in a hardware setup using Power-Hardware-In-the-Loop (PHIL).
  - The proposed vector-based control method also needs to be validated using a testbed with PHIL.

Bibliography

[1] P. F. Schewe, *The Grid: A Journey Through the Heart of Our Electrified World*. National Academies Press, 2007.

[2] G. Constable and B. Somerville, *A Century of Innovation: Twenty Engineering Achievements that Transformed Our Lives*. Joseph Henry Press, 2003.

[3] R. Zhang, "Role of power electronics in Grid 3.0," *iEnergy*, vol. 1, no. 4, pp. 387–390, Dec. 2022, doi: 10.23919/IEN.2022.0052.

[4] "Power Electronics: Revolutionizing the world's future energy systems | Hitachi Energy." Accessed: Nov. 22, 2023. [Online]. Available: https://www.hitachienergy.com/us/en/news/perspectives/2021/08/power-electronics-revolutionizing-the-world-s-future-energy-systems

[5] O. US EPA, "Climate Change Science." Accessed: Nov. 22, 2023. [Online]. Available: https://www.epa.gov/climatechange-science

[6] "Office of Energy Efficiency & Renewable Energy," Energy.gov. Accessed: Nov. 22, 2023. [Online]. Available: https://www.energy.gov/eere/office-energy-efficiency-renewable-energy

[7] "Our 10-Year Utilities Forecast: Renewable Energy to Triple by 2032," Morningstar, Inc. Accessed: Jan. 10, 2024. [Online]. Available: https://www.morningstar.com/stocks/our-10-year-utilities-forecast-renewable-energy-triple-by-2032

[8] "ERCOT Blackout 2021 | Energy Institute." Accessed: Nov. 22, 2023. [Online]. Available: https://energy.utexas.edu/research/ercot-blackout-2021

[9] B. Kroposki and F. PE, "Summarizing the Technical Challenges of High Levels of Inverter-based Resources in Power Grids," 2019, Accessed: Nov. 22, 2023. [Online]. Available: https://www.nrel.gov/docs/fy19osti/73869.pdf

[10] C. L. Sulzberger, “Triumph of AC - from Pearl Street to Niagara,” *IEEE Power and Energy Magazine*, vol. 1, no. 3, pp. 64–67, May 2003, doi: 10.1109/MPAE.2003.1197918.

[11] D. T. Ton and M. A. Smith, “The US department of energy’s microgrid initiative,” *The Electricity Journal*, vol. 25, no. 8, pp. 84–94, 2012.

[12] B. Chen, J. Wang, X. Lu, C. Chen, and S. Zhao, “Networked Microgrids for Grid Resilience, Robustness, and Efficiency: A Review,” *IEEE Trans. Smart Grid*, vol. 12, no. 1, pp. 18–32, Jan. 2021, doi: 10.1109/TSG.2020.3010570.

[13] D. Boroyevich, I. Cvetković, D. Dong, R. Burgos, F. Wang, and F. Lee, “Future electronic power distribution systems a contemplative view,” in *2010 12th International Conference on Optimization of Electrical and Electronic Equipment*, May 2010, pp. 1369–1380. doi: 10.1109/OPTIM.2010.5510477.

[14] A. Ellis and J. D. Johnson, “Lanai grid-connected PV-battery system analysis,” Sandia National Lab.(SNL-NM), Albuquerque, NM (United States), 2012. Accessed: Nov. 12, 2023. [Online]. Available: https://www.osti.gov/servlets/purl/1294245

[15] “IEEE Application Guide for AC High-Voltage Circuit Breakers > 1000 Vac Rated on a Symmetrical Current Basis,” *IEEE Std C37.010-2016 (Revision of IEEE Std C37.010-1999)*, pp. 1–123, Apr. 2017, doi: 10.1109/IEEESTD.2017.7906465.

[16] J. J. LaForest, “Transmission-line reference book. 345 kV and above. Second edition,” General Electric Co., Pittsfield, MA (USA). Large Transformer Div.; General Electric Co., Schenectady, NY (USA). Electric Utility Systems Engineering Dept., EPRI-EL-2500, Jan. 1981. Accessed: Nov. 22, 2023. [Online]. Available: https://www.osti.gov/biblio/5278767

[17] B. Kroposki *et al.*, "Unifi specifications for grid-forming inverter-based resources—version 1," *Universal Interoperability for Grid-Forming Inverters (UNIFI) Consortium, Tech. Rep. UNIFI-2022-2-1,* 2022.

[18] J. Sun, "Impedance-Based Stability Criterion for Grid-Connected Inverters," *IEEE Transactions on Power Electronics*, vol. 26, no. 11, pp. 3075–3078, Nov. 2011, doi: 10.1109/TPEL.2011.2136439.

[19] "TF-77 VSC HVDC Converters as Virtual Synchronous Machine?," CIGRE. Accessed: Nov. 01, 2023. [Online]. Available: https://www.cigre.org/article//tf-77-vsc-hvdc-converters-as-virtual-synchronous-machine

[20] Y. Lin *et al.*, "Research Roadmap on Grid-Forming Inverters," National Renewable Energy Lab. (NREL), Golden, CO (United States), NREL/TP-5D00-73476, Nov. 2020. doi: 10.2172/1721727.

[21] "Grid-Forming Technology in Energy Systems Integration," ESIG. Accessed: Nov. 01, 2023. [Online]. Available: https://www.esig.energy/grid-forming-technology-in-energy-systems-integration/

[22] "IEEE Standard for Interconnection and Interoperability of Inverter-Based Resources (IBRs) Interconnecting with Associated Transmission Electric Power Systems," *IEEE Std 2800-2022*, pp. 1–180, Apr. 2022, doi: 10.1109/IEEESTD.2022.9762253.

[23] A. Jalali, "Voluntary Specification for Grid-forming Inverters-May 2023-A statement of voluntary threshold," 2023, Accessed: Nov. 22, 2023. [Online]. Available: https://policycommons.net/artifacts/4463736/voluntary-specification-for-grid-forming-inverters/5261003/

[24] Y. Li, Y. Gu, and T. C. Green, “Revisiting Grid-Forming and Grid-Following Inverters: A Duality Theory,” *IEEE Transactions on Power Systems*, vol. 37, no. 6, pp. 4541–4554, Nov. 2022, doi: 10.1109/TPWRS.2022.3151851.

[25] E. P. R. Institute, “Grid Forming Inverters: EPRI Tutorial.” EPRI Palo Alto, CA, 2020.

[26] M. C. Chandorkar, D. M. Divan, and R. Adapa, “Control of parallel connected inverters in standalone AC supply systems,” *IEEE Transactions on Industry Applications*, vol. 29, no. 1, pp. 136–143, Jan. 1993, doi: 10.1109/28.195899.

[27] H.-P. Beck and R. Hesse, “Virtual synchronous machine,” in *2007 9th International Conference on Electrical Power Quality and Utilisation*, Oct. 2007, pp. 1–6. doi: 10.1109/EPQU.2007.4424220.

[28] B. B. Johnson, S. V. Dhople, A. O. Hamadeh, and P. T. Krein, “Synchronization of Parallel Single-Phase Inverters With Virtual Oscillator Control,” *IEEE Transactions on Power Electronics*, vol. 29, no. 11, pp. 6124–6138, Nov. 2014, doi: 10.1109/TPEL.2013.2296292.

[29] R. M. Wright, “Understanding modern generator control,” *IEEE Transactions on Energy Conversion*, vol. 4, no. 3, pp. 453–458, Sep. 1989, doi: 10.1109/60.43248.

[30] H. D. Vu and J. C. Agee, “WECC tutorial on speed governors,” *WECC Control Work Group*, 1998.

[31] “Control of Power Electronic Converters and Systems - 1st Edition.” Accessed: Nov. 22, 2023. [Online]. Available: https://shop.elsevier.com/books/control-of-power-electronic-converters-and-systems/blaabjerg/978-0-12-816136-4

[32] “IEEE Guide for Using IEEE Std 1547 for Interconnection of Energy Storage Distributed Energy Resources with Electric Power Systems,” *IEEE Std 1547.9-2022*, pp. 1–87, Aug. 2022, doi: 10.1109/IEEESTD.2022.9849493.

[33] “Textbook of Electrical Technology: B.L. Theraja: 9788121924412: Amazon.com: Books.” Accessed: Nov. 22, 2023. [Online]. Available: https://www.amazon.com/Textbook-Electrical-Technology-B-L-Theraja/dp/8121924413

[34] Q.-C. Zhong and T. Hornik, *Control of power inverters in renewable energy and smart grid integration*. John Wiley & Sons, 2012. Accessed: Nov. 22, 2023. [Online]. Available: https://books.google.com/books?hl=en&lr=&id=m5kWmDIiuxQC&oi=fnd&pg=PT9&dq=+Control+of+Power+Inverters+in+Renewable+Energy+and+Smart+Grid+Integration&ots=9aKYotdSB6&sig=k_CKT5iXWTqVBRxju4PN9ACuEgU

[35] S. D’Arco and J. A. Suul, “Equivalence of Virtual Synchronous Machines and Frequency-Droops for Converter-Based MicroGrids,” *IEEE Transactions on Smart Grid*, vol. 5, no. 1, pp. 394–395, Jan. 2014, doi: 10.1109/TSG.2013.2288000.

[36] P. Denholm, T. Mai, R. W. Kenyon, B. Kroposki, and M. O’Malley, “Inertia and the power grid: A guide without the spin,” National Renewable Energy Lab.(NREL), Golden, CO (United States), 2020. Accessed: Nov. 22, 2023. [Online]. Available: https://www.osti.gov/biblio/1659820

[37] D. B. Grainger, “Virtual Inertia: Designing Power Electronic Systems to Behave like Synchronous Machines”.

[38] “Understanding Power Quality Problems: Voltage Sags and Interruptions | IEEE eBooks | IEEE Xplore.” Accessed: Jan. 16, 2024. [Online]. Available: https://ieeexplore-ieee-org.ezproxy.lib.vt.edu/book/5270869

[39] J. D. Glover, M. S. Sarma, and T. Overbye, “Power System Analysis and Design: Si Edition,” *Thomson Engineering,* 2011.

[40] D. B. Rathnayake *et al.*, "Grid forming inverter modeling, control, and applications," *IEEE Access*, vol. 9, pp. 114781–114807, 2021.

[41] J. Matevosyan *et al.*, "Grid-forming inverters: Are they the key for high renewable penetration?," *IEEE Power and Energy magazine*, vol. 17, no. 6, pp. 89–98, 2019.

[42] C. P. Steinmetz, "Complex quantities and their use in electrical engineering," in *Proceedings of the International Electrical Congress*, 1893, pp. 33–74.

[43] S. R. Sanders, J. M. Noworolski, X. Z. Liu, and G. C. Verghese, "Generalized averaging method for power conversion circuits," *IEEE Transactions on Power Electronics*, vol. 6, no. 2, pp. 251–259, Apr. 1991, doi: 10.1109/63.76811.

[44] A. Nazari, Y. Xue, J. K. Motwani, I. Cvetkovic, D. Dong, and D. Boroyevich, "Dynamic Phasor Modeling of Three Phase Voltage Source Inverters," in *2021 6th IEEE Workshop on the Electronic Grid (eGRID)*, Nov. 2021, pp. 1–6. doi: 10.1109/eGRID52793.2021.9712467.

[45] R. Zhang, "Vector Representation of Electrical Quantities (unpublished)." 2023.

[46] K. Abe, *The Clark and Park transformations: Coordinate transformations for Brushless DC motor in field-oriented control.*

[47] J. C. Butcher, *Numerical Methods for Ordinary Differential Equations*, 2nd edition. Chichester, England ; Hoboken, NJ: Wiley, 2008.